

8-2019

## Nonlinear Estimation and Control Methods for Mechanical and Aerospace Systems under Actuator Uncertainty

Krishna Bhavithavya Kidambi

Follow this and additional works at: <https://commons.erau.edu/edt>



Part of the [Aerospace Engineering Commons](#), and the [Engineering Physics Commons](#)

---

### Scholarly Commons Citation

Kidambi, Krishna Bhavithavya, "Nonlinear Estimation and Control Methods for Mechanical and Aerospace Systems under Actuator Uncertainty" (2019). *Dissertations and Theses*. 466.  
<https://commons.erau.edu/edt/466>

This Dissertation - Open Access is brought to you for free and open access by Scholarly Commons. It has been accepted for inclusion in Dissertations and Theses by an authorized administrator of Scholarly Commons. For more information, please contact [commons@erau.edu](mailto:commons@erau.edu).

NONLINEAR ESTIMATION AND CONTROL METHODS  
FOR MECHANICAL AND AEROSPACE SYSTEMS  
UNDER ACTUATOR UNCERTAINTY

By

Krishna Bhavithavya Kidambi

A Dissertation submitted to the department of Physical Sciences in partial  
fulfillment of the requirements for the degree of

**DOCTOR OF PHILOSOPHY**

**(Engineering Physics)**

August 2019

Embry-Riddle Aeronautical University

Daytona Beach, Florida

Copyright by Krishna Bhavithavya Kidambi 2019

All Rights Reserved

NONLINEAR ESTIMATION AND CONTROL METHODS FOR  
MECHANICAL AND AEROSPACE SYSTEMS UNDER ACTUATOR  
UNCERTAINTY

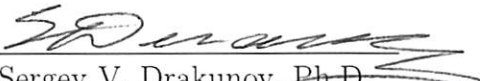
By

Krishna Bhavithavya Kidambi

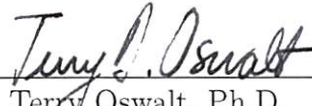
This Dissertation was prepared under the direction of the candidate's Dissertation Committee Chair, Dr. William MacKunis and has been approved by the members of the Dissertation committee. It was submitted to the College of Arts and Sciences and was accepted in partial fulfillment of the requirements for the  
Degree of  
Doctor of Philosophy in Engineering Physics



Dr. William MacKunis, Ph.D.  
Committee Chair



Dr. Sergey V. Drakunov, Ph.D.  
Committee Member



Dr. Terry Oswalt, Ph.D.  
Department Chair, Physical Sciences



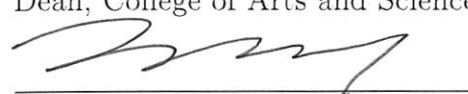
Dr. Mahmut Reyhanoglu, Ph.D.  
Committee Member



Dr. Karen Frances Gaines, Ph.D.  
Dean, College of Arts and Sciences



Dr. Vladimir Golubev, Ph.D.  
Committee Member



Lon D. Moeller  
Senior Vice President for Academic Affairs  
and Provost

8/8/2019

Date

## Abstract

Air flow velocity field control is of crucial importance in aerospace applications to prevent the potentially destabilizing effects of phenomena such as cavity flow oscillations, flow separation, flow-induced limit cycle oscillations (LCO) (flutter), vorticity, and acoustic instabilities. Flow control is also important in aircraft applications to reduce drag in aircraft wings for improved flight performance. Although passive flow control approaches are often utilized due to their simplicity, active flow control (AFC) methods can achieve improved flight performance over a wider range of time-varying operating conditions by automatically adjusting their level of control actuation in response to real-time sensor measurements. Although several methods for AFC have been presented in recent literature, there remain numerous challenges to be overcome in closed-loop nonlinear AFC design. Additional challenges arise in control design for practical systems with limited onboard sensor measurements and uncertain actuator dynamics.

In this thesis, robust nonlinear control methods are developed, which are rigorously proven to achieve reliable control of fluid flow systems under uncertain, time-varying operating conditions and actuator model uncertainty. Further, to address the practical control design challenges resulting from sensor limitations, this thesis research will investigate and develop new methods of sliding mode estimation, which are shown to achieve finite-time state estimation for systems with limited onboard sensing capabilities. The specific contributions presented in this thesis include: 1) the application of proper orthogonal decomposition (POD)-based model order reduction techniques to develop simplified, control-oriented mathematical models of actuated fluid flow dynamic systems; 2) the rigorous development of nonlinear closed-loop active flow control techniques to achieve asymptotic regulation of fluid flow velocity fields; 3) the design of novel sliding mode estimation and control methods to regulate fluid flow velocity fields in the presence of actuator uncertainty; 4) the design of a nonlinear control method that achieves simultaneous fluid flow velocity control and LCO suppression in a flexible airfoil; and 5) the analysis of a discontinuous hierarchical sliding mode estimation method using a differential inclusions-based technique.

## Acknowledgments

First, I would like to give my thanks and deepest gratitude to Dr. William MacKunis for his knowledge, patience, guidance, support, and dedication. I will be forever grateful for what you have taught me and I will always cherish your input. I would like to thank my committee members Dr. Sergey Drakunov, Dr. Mahmut Reyhanoglu and Dr. Vladimir Golubev for their valuable inputs and suggestions. The knowledge, insight and your classes have been invaluable and greatly appreciated.

I would like to thank all my friends in the EP program, specially Chris, Andrea, Niloofar and my academic sister Natalie. I am grateful for her help during the course of my Ph.D. My life as an international student in a new country would not have been so smooth without the help of these people and I'll cherish all those lunch discussions we had. I also would like to thank my friend Irfan and my brother Sriram for their constant feedback and support.

I would like to thank my mom Jayasree, dad Muralidhar and my family for making me a person who I am today. Finally my wife Anu, a simple thank you would not suffice the profound gratitude and love for her, I would not have accomplished this challenging endeavor without her.

# Contents

<b>Abstract</b>	<b>iv</b>
<b>Acknowledgements</b>	<b>v</b>
<b>List of Tables</b>	<b>x</b>
<b>List of Figures</b>	<b>xi</b>
<b>1 Introduction</b>	<b>1</b>
1.1 Motivation . . . . .	1
1.2 Dissertation Organization . . . . .	7
<b>2 Mathematical Definitions</b>	<b>9</b>
2.1 Nonlinear System and Stability . . . . .	9
2.2 Lyapunov Stability Theory . . . . .	10
2.2.1 Lyapunov’s First Stability Theorem . . . . .	10
2.2.2 Lyapunov’s Second Stability Theorem . . . . .	11
2.3 Sliding Mode Estimation . . . . .	12
2.4 Robust Control . . . . .	15
2.4.1 Nonlinear Damping . . . . .	16
2.5 Synthetic Jet Actuators . . . . .	18
2.5.1 Virtual Surface Deflection using SJA . . . . .	18
2.6 Proper Orthogonal Decomposition . . . . .	21
2.6.1 POD based ROM for Unactuated Systems . . . . .	21
2.6.2 POD based ROM for Actuated Flow . . . . .	23

<b>3</b>	<b>A Closed-loop Nonlinear Control and Sliding Mode Estimation Strategy for Fluid Flow Regulation</b>	<b>28</b>
3.1	Flow Dynamics Reduced-order Model . . . . .	29
3.1.1	Unactuated Flow Dynamics Reduced-order Model . . . . .	30
3.1.2	Reduced-order Model for the Actuated Flow . . . . .	32
3.1.2.1	Actuation Modes . . . . .	32
3.1.2.2	Actuated Dynamic Model . . . . .	34
3.2	Sliding Mode Observer Design . . . . .	35
3.2.1	Observer Design 1 . . . . .	37
3.2.2	Observer Design 2 . . . . .	39
3.3	Control Development . . . . .	40
3.3.1	Open Loop Error System . . . . .	41
3.3.2	Closed-Loop Error System . . . . .	42
3.4	Stability Analysis . . . . .	43
3.5	Simulation Results . . . . .	48
3.6	Conclusion . . . . .	51
<b>4</b>	<b>Sliding Mode Estimation Strategy for Synthetic Jet Actuator-based Flow Control Under Actuator Uncertainty</b>	<b>53</b>
4.1	POD-based Reduced-order Model . . . . .	54
4.1.1	Reduced-order Model for the Actuated Flow Dynamics . . . . .	54
4.1.1.1	Actuated Dynamic Model . . . . .	55
4.2	SJA-based Control Model Derivation . . . . .	56
4.2.1	SJA Actuator Model . . . . .	56
4.3	Observer Design . . . . .	59
4.4	Control Development . . . . .	64
4.4.1	Control Objective . . . . .	64
4.4.2	Open Loop Error System . . . . .	65
4.4.3	Closed-Loop Error System . . . . .	67
4.5	Stability Analysis . . . . .	67
4.6	Simulation Results . . . . .	70
4.7	Conclusion . . . . .	77



<b>5</b>	<b>Limit Cycle Oscillation Suppression using a Closed-loop Nonlinear Active Flow Control Technique</b>	<b>79</b>
5.1	Mathematical Model . . . . .	80
5.1.1	LCO Dynamic Model . . . . .	80
5.1.2	Flow Dynamics Reduced-order Model . . . . .	82
5.1.3	Reduced-order Model for the Actuated Flow . . . . .	84
5.2	SJA-based Control Model Derivation . . . . .	85
5.3	Control Development . . . . .	86
5.3.1	Open Loop Error System . . . . .	87
5.3.2	Closed-Loop Error System . . . . .	89
5.4	Stability Analysis . . . . .	89
5.5	Simulation Results . . . . .	92
5.5.1	Flow parameters . . . . .	92
5.5.2	LCO parameters . . . . .	92
5.6	Conclusion . . . . .	95
<b>6</b>	<b>A Hierarchical Sliding Mode Estimation Method Using a Differential Inclusions-based Analysis</b>	<b>96</b>
6.1	Preliminaries . . . . .	97
6.1.1	Mathematical Definitions . . . . .	97
6.1.2	Simple Example of Differential Inclusion . . . . .	100
6.2	Observer Design . . . . .	101
6.2.1	Dynamic Model and Properties . . . . .	101
6.2.2	Observer Design . . . . .	103
6.3	SMO Estimation Error Dynamics . . . . .	105
6.3.1	Objective . . . . .	105
6.3.2	Estimation Error Dynamics . . . . .	106
6.3.3	Hierarchical Analysis of Estimation Error Dynamics . . . . .	107
6.4	Stability Analysis . . . . .	108
6.5	Simulation Study: Flow Field Velocity Estimation . . . . .	112
6.5.1	Reduced-order Model Derivation . . . . .	112
6.5.2	Simulation Results . . . . .	115

6.6	Conclusion . . . . .	118
<b>7</b>	<b>Conclusion and Future Work</b>	<b>119</b>
7.1	Future Work . . . . .	120
<b>A</b>	<b>Proof of Lemma 1</b>	<b>121</b>
<b>B</b>	<b>Proof of Theorem 10</b>	<b>123</b>
	<b>References</b>	<b>125</b>

# List of Tables

4.1	SJA parameters and their estimates for all three cases . . . . .	71
4.2	Initial Conditions of the states and Estimates . . . . .	72
4.3	Parameters Used in the Simulation Plant Model . . . . .	72
4.4	Observer gains used in the simulation . . . . .	72
5.1	Dynamic parameters and geometric dimensions of the LCO Model . .	93
6.1	Parameters Used in the Simulation Plant Model . . . . .	116

4

# List of Figures

2.1	Schematic layout of a synthetic jet actuator . . . . .	19
2.2	Example of synthetic jet actuators and their installation in airfoil (wing) model. . . . .	19
2.3	Variation of virtual surface deflection with the voltage from the synthetic jet actuator . . . . .	20
3.1	Zoomed plots magnifying the initial closed-loop transient response of the states $x_1(t)$ , $x_2(t)$ and the error $e_1(t)$ , $e_2(t)$ using the observers in (3.15) (left) and (3.18) (right). . . . .	49
3.2	Closed-loop response of the states $x_1(t)$ , $x_2(t)$ and the error $e_1(t)$ , $e_2(t)$ for the total simulation time using the observers in (3.15) (left) and (3.18) (right). . . . .	50
3.3	Commanded control inputs during the initial transient period of closed-loop controller operation using the observers in (3.15) (left) and (3.18) (right). . . . .	51
4.1	Time Evolution of the states for open-loop (uncontrolled) configuration	74

4.2	Zoomed-in plots showing the initial convergence phase of the states (blue) and the estimates (red) using the observer in (4.14). . . . .	74
4.3	Closed-loop response of true states with and without compensation for uncertainty . . . . .	75
4.4	Zoomed-in plots showing the initial transient response of the closed-loop system for case 1, with (red) and without (blue) compensation for uncertainty . . . . .	75
4.5	Closed-loop response of the control signal $\gamma(t)$ . . . . .	76
4.6	Monte Carlo-Type simulation results for three different sets of uncertain SJA parameters for actual states . . . . .	76
4.7	Monte Carlo-Type simulation results for three different sets of uncertain SJA parameters for estimated states . . . . .	77
5.1	A block diagram illustrating the proposed nonlinear control method for simultaneous flow control and LCO suppression . . . . .	81
5.2	Open-loop plunging time response of the LCO simulated system . . .	93
5.3	Closed-loop time response of LCO plunging with different initial conditions . . . . .	94
5.4	Control magnitude during closed-loop operation . . . . .	94
6.1	Time evolution of the states (blue) and the estimates (red) using the observer in (6.19) . . . . .	116
6.2	Zoomed plots showing the initial convergence phase of the states (blue) and the estimates (red) using the observer in (6.19) . . . . .	117
6.3	Time evolution of the error in each state over the entire simulation time	117

# Chapter 1

## Introduction

### 1.1 Motivation

Fluid flow can be defined as the motion of liquids or gases, which is a phenomenon that one encounters continuously in everyday life. The flow of air around the body of a car or the wing of an aircraft, flow of water in oceans and the motion of air in the atmosphere carrying the clouds are only a few examples of fluid flows. Flow control refers to the ability to manipulate fluid flow so as to achieve a desired change in its behavior. Flow control is of crucial importance in aerospace applications to prevent the potentially destabilizing effects of phenomena such as cavity flow oscillations, flow separation, flow-induced LCO (flutter), vorticity, and acoustic instabilities (Ito & Ravindran, 1998; Rowley & Williams, 2006; M. Balajewicz & Dowell, 2012). Significant progress has been made in developing various control strategies; however, the control of fluid flow remains an active field of research.

Flow control methods are broadly classified into two categories, passive and active.

Although passive flow control approaches are often utilized due to their simplicity, they can not adapt to flow changes, they might lose their efficiency during the process (Heller & Bliss, 1976; Shaw, 1979; Lin, Howard, & Selby, 1989). Active flow control (AFC) have gained lot of interest, as the technological advancement in computing, sensors and actuation. Moreover AFC methods can achieve improved flight performance over a wider range of time-varying operating conditions by automatically adjusting their level of control actuation in response to sensor measurements. Although several methods for AFC have been presented in recent literature (e.g., (Singh, Myatt, Addington, Banda, & Hall, 2001; Debiasi & Samimy, 2004; Gad-el Hak, 2006; Pinier, Ausseur, Glauser, & Higuchi, 2007; Cadirci, Gunes, & Rist, 2013; Couchot, Deschinkel, & Salomon, 2013)). In (Singh et al., 2001), a feedback linear control law is presented to control two-dimensional incompressible, unsteady wake flow past a circular cylinder. (Debiasi & Samimy, 2004) presents an experimental investigation for controlling a shallow cavity flow using closed-loop control techniques. An efficient proportional feedback loop is presented in (Pinier et al., 2007), to delay the separation of flow over NACA-4412 airfoil at high angle of attacks. Other recently developed AFC methods utilize intelligent control techniques, such as fuzzy logic rules or neural networks (NN). For example, a NN-based AFC method is presented in (Couchot et al., 2013), in which an artificial NN is trained to predict the evolution of the flow dynamics resulting from the actuation effects of an array of micro-electromechanical systems (MEMS) actuators. The AFC strategy in (Couchot et al., 2013) then utilizes the NN-based prediction to optimize the flow according to a pre-defined numerical criterion.

Popular approaches to AFC design often utilize experimental or numerical tech-



niques (Andino et al., 2011; Sohankar, Khodadadi, & Rangraz, 2015; Zhao, Zhao, Gu, & Chen, 2016a). (Andino et al., 2011) presents experimental results of using proportional feedback controller to control flow over a cylindrical turret. (Sohankar et al., 2015) analyzes the effects of uniform suction and blowing through the surface of a square cylinder on vortex shedding. Numerical simulations show a reduction in drag and vortex shedding. Numerical methods to analyze flow systems can be very computationally expensive (M. J. Balajewicz, Dowell, & Noack, 2013). Experimental and computational approaches have been shown to achieve good AFC performance, where the focus is typically on the analysis of numerical or experimental data. However, rigorous mathematical tools of nonlinear control are not often utilized to analyze the performance of closed-loop AFC systems. The motivation for the closed-loop AFC design in this thesis is based on the desire to achieve closed-loop flow control using a computationally inexpensive approach, which can automatically adapt to time-varying operating conditions.

A challenge in nonlinear flow control design is that fluid flow dynamics are governed by complex models such as the Burgers' equations or Navier-Stokes equations, due to their inherent nonlinearity and complexity of infinite-dimensional flow dynamics. Control system design for these class of systems remains a challenging task. POD-based model reduction is a popular technique that is utilized to recast the infinite-dimensional flow dynamic model into finite set of ordinary differential equations (ODEs). The POD method uses Galerkin projection to project the Navier-Stokes (or Burgers') PDEs onto a finite-dimensional subspace such that the projection error is minimized. The reduced-order model (ROM) resulting from POD and the Galerkin projection is a finite set of nonlinear ODEs in terms of the time-varying

coefficients resulting from Galerkin projection. The ROM are capable of approximating the dynamic of the flow field using only a few states (i.e., Galerkin coefficients) (H. Park & Lee, 1998; Rowley, Colonius, & Murray, 2004; Lall, Marsden, & Glavaški, 2002; Chaturantabut, Sep., 2017; Annoni & Seiler, 2017). The ROM resulting from these decomposition techniques enable one to accurately approximate the underlying flow dynamics in a form amenable to control design. However, a key challenge in control design using the ROM is that the state variables of the ROM are not directly measurable, thus they are not available for feedback control design. To address this challenge, closed-loop AFC systems based on ROM must incorporate observers (or estimators), which are capable of generating estimates of the unmeasurable states using direct sensor measurements (D. Park & Guay, 2015; MacKunis, Drakunov, Reyhanoglu, & Ukeiley, 2011; Guay & Hariharan, June 11-13, 2008; John, Guay, & Hariharan, June 10-12, 2009).

Sliding mode observers have been extensively studied over the past two decades to estimate the states (S. Drakunov & Utkin, 1992; Utkin, 2013) of uncertain system dynamics (Zhang & Xu, 2015; Jiang, Huang, & Guo, 2015; Dinh, Kamalapurkar, Bhasin, & Dixon, 2014). Linear observers for flow problems have been implemented over the years due to their simplicity and ease of estimation (Rowley & Juttijudata, 2005; Ahuja & Rowley, 2010; Nagarajan, Cordier, & Airiau, 2013). (Rowley & Juttijudata, 2005) a Kalman filter is designed to estimate the states of a linearized ROM flow system and feedback control was designed to suppress cavity oscillations. In (Ahuja & Rowley, 2010), a feedback control of two-dimensional flow over a flat plat at a low Reynolds number and a reduced-order Kalman filter was developed to accurately reconstruct the flow field from sensor measurement. (Nagarajan et al.,

2013) proposed a feedback control law and a linear observer to control self-sustained instabilities in cavity flows. But the problem of nonlinear estimation has not been looked into relating to closed-loop flow problems. A DNN based robust observer and dynamic filter are designed to estimate the system dynamics and the unmeasurable states respectively in (Dinh et al., 2014), however the use of neural network based estimation and control strategy for flow control incurs a high level of complexity which makes the real time implementation unsuitable. The theoretical design of nonlinear observers for flow systems is further complicated by the fact that the mathematical form of the sensor measurement equation is in a non-standard form.

Actuators play an important role in closed loop feedback control of flow system. A detailed review of recent flow control actuators is presented in (Cattafesta III & Sheplak, 2011; Wang, Luo, Xia, Liu, & Deng, 2012). The use of synthetic jet actuators (SJAs) have emerged a popular tool for flow separation control, trajectory tracking control, LCO suppression (Mohseni & Mittal, 2014; Fisher, Nishino, & Savill, 2017; Ramos-Pedroza, MacKunis, & Golubev, 2017). A detailed review about different actuators used in closed-loop flow control is discussed in (Rowley & Williams, 2006). The application of SJAs in aerospace and active flow control applications are becoming popular due to their small size, cost-effectiveness and they achieve the momentum transfer with zero-net mass-flux (Amitay, Smith, Kibens, Parekh, & Glezer, 2001; Kurowski, 2017; Ramos-Pedroza et al., 2017; Tang, Salunkhe, Zheng, Du, & Wu, 2014; De Giorgi, De Luca, Ficarella, & Marra, 2015; Broglia, Choi, Houston, Pasquale, & Zanchetta, 2018). (Amitay et al., 2001) shows improvements in the aerodynamic performance of a thick, blunt airfoil using sythetic jet fluidic control near the airfoil leading edge. In (Kurowski, 2017), numerical simulation of SJAs for active

flow control has been investigated. In (Ramos-Pedroza et al., 2017), a SJA based output feedback control method is presented that proves asymptotic regulation of LCO in small UAV's. (Tang et al., 2014) demonstrates the use of SJAs in delaying the flow separation and improving the aerodynamics performance on a UAV. A numerical investigation is performed to analyze the suppression of the boundary layer separation on a NACA 0015 airfoil using two different active flow control techniques in (De Giorgi et al., 2015). In (Broglia et al., 2018), a set-point tracking control problem of unsteady flow separation over an airfoil using plasma actuators is presented. However, the major challenge in using SJAs in flow control design is the presence of parametric uncertainty inherent in the SJA actuator model. The parametric uncertainty in the SJA actuator model creates further challenges in observer design for SJA-based systems. These challenges were mitigated through innovative algebraic manipulation in the estimator error system derivation along with a Lyapunov-based adaptive control law.

Relying on the closed-loop active flow control technique proposed in this thesis, a nonlinear control method, which achieves simultaneous fluid flow velocity control and LCO suppression in a flexible airfoil. The proposed control design is based on a dynamic model that incorporates the fluid structure interactions (FSI) in the airfoil. The FSI describe how the flow field velocity at the surface of a flexible structure gives rise to fluid forces acting on the structure. The LCO are controlled via control of the flow field velocity near the surface of the airfoil using surface-embedded SJAs. A Lyapunov-based stability analysis is used to prove that the active flow control system asymptotically converges to the LCO-stabilizing forcing function that suppresses the LCO. The inherent discontinuities typically associated with SMO create significant

theoretical challenges in analyzing the performance of SMO.

To cope with the discontinuities that can arise in the SMO dynamic models, the dissertation also provides a detailed analysis of SMO estimation error dynamics using differential inclusions to rigorously analyze the convergence performance of SMO. The following specific theoretical contributions are presented in detail, A differential inclusions-based analysis of the SMO, which incorporates the set-valued definition of the discontinuous signum function and an expanded derivation of the estimation error dynamics, which emphasizes advantageous properties particular to the SMO structure. Finally, a Lyapunov-based stability analysis of the SMO that rigorously incorporates the multiple discontinuities in the estimation error dynamics and proves that the SMO achieves finite-time estimation of the complete state vector, where the output equation is in a nonstandard mathematical form.

## 1.2 Dissertation Organization

This thesis is organized as follows: Chapter 2 provides various preliminary stability concepts, sliding mode estimation techniques and mathematical analysis of POD based model order reduction with the effects of actuator dynamics embedded in the flow model. Chapter 3 presents preliminary development of sliding mode estimator and closed-loop active flow control technique for fluid flow regulation. This chapter also provides Lyapunov-based stability analysis to achieve asymptotic regulation of the fluid flow system. Chapter 4 presents a novel sliding mode estimation strategy for SJA-based flow control under actuator uncertainty. This is the first closed-loop active flow control result that combines a finite-time sliding mode estimation strategy

with a robust control method under actuator uncertainty. Chapter 5 provides a proof of concept nonlinear control method, that achieves simultaneous fluid flow velocity control and LCO suppression in a flexible airfoil. Finally, Chapter 6 describes a differential inclusions-based analysis of the SMO and a Lyapunov-based analysis that proves that the sliding mode estimator achieves finite-time estimation in the presence of multiple discontinuities in the estimator dynamics.

# Chapter 2

## Mathematical Definitions

This chapter presents the key mathematical concepts involved in the development of closed-loop control design presented in this dissertation. This chapter describes Lyapunov's first and second stability theorem, sliding mode estimation technique based on equivalent control, robust control design structure, SJA dynamics and concludes with POD-based reduced-order modeling.

### 2.1 Nonlinear System and Stability

A nonlinear dynamic system can be represented by a set of nonlinear differential equations of the form

$$\dot{x} = f(x, t) \tag{2.1}$$

where  $f : \mathcal{D} \times [0, \infty) \rightarrow \mathbb{R}^n$  is a nonlinear vector function and  $x(t) \in \mathcal{D} \subset \mathbb{R}^n$  denotes the state vector. The number of states  $n$  is called the order of the system. A solution of (2.1) usually corresponds to a curve in state space as  $t$  varies from  $[0, \infty)$ . The

system defined in (2.1) is called non-autonomous system due to the explicit time dependence (Slotine & Li, 1991).

## 2.2 Lyapunov Stability Theory

Aleksandr Mikhailovich Lyapunov, a Russian mathematician developed a global approach to the analysis of the stability of the nonlinear dynamic systems (Lyapunov, 1992). This section presents some of the important Lyapunov theorems that are used in the control design and stability analysis of the closed-loop system in this dissertation.

**Definition 1. *Stability in the sense of Lyapunov:*** *The equilibrium point  $x^* = 0$  of (2.1) is stable (in the sense of Lyapunov) at  $t = t_0$  for any  $\epsilon > 0$  there exists a  $\delta(t_0, \epsilon) > 0$  such that*

$$\|x(t_0)\| < \delta \Rightarrow \|x(t)\| < \epsilon, \forall t \geq t_0. \quad (2.2)$$

### 2.2.1 Lyapunov's First Stability Theorem

Lyapunov's first stability theorem is often referred to as indirect method of Lyapunov and is important for determining the stability of a nonlinear system around an equilibrium point  $x^*$  from the stability of its linearized system (Gantmakher, 2000)

**Theorem 1.** *If the linearized system is strictly stable around the equilibrium point  $x^* = 0$ , then the equilibrium point is asymptotically stable for the nonlinear system.*

- *If the linearized system is unstable around the equilibrium point  $x^* = 0$ , then the equilibrium point is unstable for the nonlinear system.*



- *If the linearized system is marginally stable around the equilibrium point  $x^* = 0$ , then one cannot conclude anything from the linear approximation for the nonlinear system*

### 2.2.2 Lyapunov's Second Stability Theorem

The basic philosophy of Lyapunov's second (direct) stability theorem is from fundamental physical observation. If the total energy of a system is continuously dissipated then the system must eventually settle down to an equilibrium point (whether linear or nonlinear). Let  $V : \mathbb{R}^n \rightarrow \mathbb{R}$  be a continuously differentiable Lyapunov function.

**Theorem 2.** *Consider the dynamic system in (2.1), where  $x^*$  is the equilibrium point of the system. Then the equilibrium point is*

- *Stable if,*

$$V(x^*) = 0 \quad \text{and} \quad V(x) > 0 \text{ in } \mathbb{D} - \{x^*\} \quad \forall t \quad (2.3)$$

*and its time derivative along the trajectories of the system is negative semi-definite in the sense that*

$$\dot{V}(x) \leq 0. \quad (2.4)$$

- *Asymptotically stable if, (2.3) is satisfied and  $\dot{V}(x)$  is negative definite in the sense that*

$$\dot{V}(x) < 0 \text{ in } \mathbb{D} - \{x^*\}. \quad (2.5)$$

- *Globally asymptotically stable if, (2.3) is satisfied for any initial state  $x(t_0)$  along*

with (2.4) and the function  $V(x)$  is radially bounded

$$\|x(t)\| \Rightarrow \infty \quad V(x) \rightarrow \infty. \quad (2.6)$$

- Unstable if,

$$\dot{V}(x) > 0 \quad \forall x \neq x^* \quad (2.7)$$

$$\dot{V}(x^*) = 0 \quad \forall t. \quad (2.8)$$

## 2.3 Sliding Mode Estimation

This section summarizes a sliding mode estimator (or observer) design, which can be utilized to generate state estimates using only available sensor measurements. The sliding mode estimator described here can be applied to linear systems or nonlinear systems (S. V. Drakunov, 1992; S. Drakunov & Utkin, 1992; S. V. Drakunov & Reyhanoglu, 2011), where the dynamic model is not completely known.

Consider a nonlinear system

$$\dot{x} = f(x) + g(x)u \quad (2.9)$$

$$y = h(x) \quad (2.10)$$

where  $x \in \mathbb{R}^n$ ,  $f(x) \in \mathbb{R}^n$ ,  $y \in \mathbb{R}^m$  denote sufficiently differentiable vector functions,  $g(x) \in \mathbb{R}^{n \times m}$  denotes a sufficiently differentiable input gain matrix and  $u(t) \in \mathbb{R}^m$  denotes the control input.

**Assumption 1.** *If  $x(t) \in \mathcal{L}_\infty$ , the first and second partial derivatives of  $f(x)$ ,  $g(x)$ , and  $h(x)$  with respect to  $x(t)$  exist and are bounded.*

An observer that estimates the full state  $x(t)$  of the system in (2.9) using only measurements of  $y(t)$  can be designed as

$$\dot{\hat{x}} = \left( \frac{\partial H(\hat{x})}{\partial x} \right)^{-1} M(\hat{x}) \{ \text{sgn}(V(t) - H(\hat{x})) \}_{eq} + g(\hat{x})u(\hat{x}) \quad (2.11)$$

where  $\{ \text{sgn}(\cdot) \}_{eq}$  represents a smooth continuous value operator of the discontinuous signum function (S. V. Drakunov, 1992),  $M(\hat{x}) \in \mathbb{R}^{n \times n}$  is the sliding gain diagonal matrix as previously mentioned of the form

$$M(\hat{x}) = \text{diag} \left[ m_1(\hat{x}) \quad \cdots \quad m_n(\hat{x}) \right], \quad (2.12)$$

$H(\hat{x}) \in \mathbb{R}^n$  is a vector of the output derivatives (S. V. Drakunov, 1992; MacKunis et al., 2011; S. V. Drakunov & Reyhanoglu, 2011) of the form

$$H(x) \triangleq \begin{bmatrix} h_1(x) & h_2(x) & \cdots & h_n(x) \end{bmatrix}^T \quad (2.13)$$

$$= \begin{bmatrix} h(x) & L_f h(x) & \cdots & L_f^{n-1} h(x) \end{bmatrix}^T \quad (2.14)$$

where  $L_f = \frac{\partial h}{\partial x} f(x)$  denotes the Lie derivative of the output function,  $h(x)$ , along the direction of the vector field. If  $x(t)$  is a solution to the system described in (2.9), then

$$\frac{d}{dt} h_i(x(t)) = h_{i+1}(x(t)), \quad i = 1, \dots, n-1. \quad (2.15)$$

Lastly,  $V(t) \in \mathbb{R}^n$  is the observer vector in the form of

$$V(t) = \begin{bmatrix} v_1(t) & \cdots & v_n(t) \end{bmatrix}^T \quad (2.16)$$

$$= \begin{bmatrix} h_1(x) & \cdots & m_i \{\text{sgn}(v_i(t) - h_i(\hat{x}))\}_{eq} \end{bmatrix}^T \quad (2.17)$$

for  $i = 1, \dots, n$ .

**Definition 2.**  $\mathcal{L}_\infty$  is a function space, in which for a function  $f$  in this set, its essential supremum serves as an norm:

$$\|f(x)\|_\infty \equiv \inf\{\mathcal{C} \geq 0 : |f(x)| \leq \mathcal{C} \quad \forall x\} \quad (2.18)$$

**Condition 1** (Observability). *The system given in (2.9) and (2.10) must satisfy the observability condition*

$$\text{rank}(\mathcal{O}(x, \mu)) = n, \quad \forall x \in \mathbb{R}^n, \quad (2.19)$$

where the observability matrix  $\mathcal{O}(x, \mu) \triangleq \frac{\partial H(x, \mu)}{\partial x} \in \mathbb{R}^{n \times n}$ .

**Theorem 3.** *Provided the observability Condition 1 and Assumption 1 are satisfied, the sliding mode observer in (2.11) achieves finite-time estimation of the state  $x(t)$  in the sense that  $\hat{x}(t) \equiv x(t)$  for  $t \geq t_n$ , where  $t_n \in \mathcal{L}_\infty$*

*Proof.* Based on Condition 1, the observability matrix is full rank, and  $\left| \det \left( \frac{\partial H(x)}{\partial x} \right) \right| \geq \epsilon > 0$ . It thus follows that the map  $H(x)$  is a diffeomorphism (i.e., there is a one to one correspondence between  $x(t)$  and  $H(x)$ ). Since  $H(x)$  is a diffeomorphism, it is sufficient to prove that  $e(t) = H(x) - H(\hat{x}) = 0$  for  $t \geq t_n$ .

The estimation error dynamics can be obtained by taking the time derivative of

$e(t) = [e_1(t), \dots, e_n(t)]^T$  as

$$\dot{e}(t) = \frac{\partial H(x)}{\partial x} \dot{x} - \frac{\partial H(\hat{x})}{\partial x} \dot{\hat{x}}. \quad (2.20)$$

By using (2.9), (2.11), (2.13) and (2.12) the estimation error dynamics can be expressed as

$$\dot{e}(t) = \frac{\partial H(x)}{\partial x} \dot{x} - M(\hat{x}) \{ \text{sgn}(V(t) - H(\hat{x})) \}_{eq} - \frac{\partial H(\hat{x})}{\partial x} g(\hat{x}) u(t). \quad (2.21)$$

Therefore from (2.15),

$$\dot{e}_i(t) = h_{i+1}(t) - m_i(\hat{x}) \{ \text{sgn}(v_i(t) - h_i(\hat{x})) \} - \sum_{i=1}^n \frac{\partial h_i(\hat{x})}{\partial x} \sum_{j=1}^m g_{ij} u_j(t) \quad (2.22)$$

for  $i = 1, \dots, n$  and for  $j = 1, \dots, m$ . The convergence of  $e_i(t)$  to the corresponding sliding manifolds can be achieved by selecting the sliding gain terms  $m_i(\hat{x})$  to satisfy

$$m_i(\hat{x}) > h_{i+1} - \sum_{i=1}^n \frac{\partial h_i(\hat{x})}{\partial x} \sum_{j=1}^m g_{ij} u_j(t) \quad (2.23)$$

for  $i = 1, \dots, n$  and for  $j = 1, \dots, m$ . Hence, provided Assumption 1 and Condition 1 and (2.23) are satisfied, it can be shown that the sliding manifolds  $e_i(t) = 0$  are reached in finite time. Hence,  $\hat{x}(t) \equiv x(t)$  in finite time.  $\square$

## 2.4 Robust Control

The control of uncertain nonlinear dynamic systems is a topic that continues to challenge control theoreticians. In many real-world applications, the mathematical

model is poorly known or uncertain. Various robust control techniques have emerged over the last decade to facilitate the uncertainties of nonlinear systems. Among these, RISE (Robust Integral of the Sign of the Error) is advantageous because it is a differentiable control method that can compensate for additive system uncertainties. Due to its advantages, flurry of results have been published in the literature (Xian, Dawson, de Queiroz, Chen, et al., 2004; Patre, MacKunis, Kaiser, & Dixon, 2008; Cai, de Queiroz, & Dawson, 2006). This section presents a stability analysis proof similar to the ones presented in Chapters.

### 2.4.1 Nonlinear Damping

Consider the dynamical system

$$\dot{x} = f(x, t) + u(t) \tag{2.24}$$

where  $x(t) \in \mathbb{R}^n$  is the state space vector,  $u(t) \in \mathbb{R}^n$  is the control input vector, and  $f : \mathcal{D} \times [0, \infty) \rightarrow \mathbb{R}^n$  is an unknown disturbance that is bounded and sufficiently smooth in the sense that

$$|f(x, t)| \leq \zeta \quad |\dot{f}(x, t)| \leq \zeta_0 \tag{2.25}$$

where  $\zeta, \zeta_0 \in \mathbb{R}^+$  are known constants. A control law design,  $u(t)$ , is utilized to drive the state vector,  $x(t)$ , to the desired equilibrium point,  $x^*$ , as

$$u = -(k_s + 1)x \tag{2.26}$$

where  $k_s \in \mathbb{R}^+$  is the nonlinear damping gain ( $k_s$  could also be defined as a positive definite diagonal gain matrix). The closed loop dynamics are obtained when (2.26) is substituted into (2.24) as

$$\dot{x} = f(x, t) - (k_s + 1)x \quad (2.27)$$

To analyze the stability of (2.27), consider the following positive definite Lyapunov function and its derivative

$$V = \frac{1}{2}x^2 \quad (2.28)$$

$$\dot{V} = x\dot{x} \quad (2.29)$$

Substituting (2.27) into (2.29) results in

$$\dot{V} = xf(x, t) - (k_s + 1)x^2 \quad (2.30)$$

After completing the squares, the Lyapunov derivative can be expressed as

$$\dot{V} \leq -x^2 - k_s \left( |x|^2 - \frac{\zeta}{k_s}|x| \right) \quad (2.31)$$

$$\dot{V} \leq -x^2 + \frac{\zeta^2}{4k_s} \leq -2V + \frac{\zeta^2}{4k_s} \quad (2.32)$$

Based on the expression in (2.32),  $x(t)$  is bounded and converges to the compact set described as

$$\mathcal{S} = \left\{ x \mid |x| \leq \frac{\zeta}{2\sqrt{k_s}} \right\}. \quad (2.33)$$

Note that the size of the ultimate bound on the tracking error can be made arbitrarily small by increasing the control gain  $k_s$ .

## 2.5 Synthetic Jet Actuators

The use of SJAs have emerged a popular tool for flow separation control, trajectory tracking control, LCO suppression (Mohseni & Mittal, 2014; Fisher et al., 2017; Ramos-Pedroza et al., 2017).

The most common SJA assemblies are piston cylinder, voice-coil magnet, or piezoelectric disk type actuators. These SJAs transfer linear momentum to a flow system using a piezoelectric membrane inside a cavity, which creates a train of vortices through the alternating suction and ejection of the air around it through a small orifice as seen in Figure 2.5. This means that SJAs achieve momentum transfer with zero net mass flux across the flow boundary. Figure 2.2 illustrates an example of the installation of these SJAs in an airfoil.

### 2.5.1 Virtual Surface Deflection using SJA

The control actuation in SJA is generated by a given  $m$  number of SJA arrays and the control input  $u(t)$  represents the *virtual surface deflection angle* resulting from the cumulative effect of these the SJA arrays. The key challenge in SJA-based control design is that the virtual deflection angle due to the  $i^{th}$  SJA array is an uncertain nonlinear function of the input voltage applied to the array. Specifically, the dynamics of the virtual surface deflection due to the  $i^{th}$  SJA array can be expressed using the empirically determined model (Deb, Tao, Burkholder, & Smith, 2007), (Deb, Tao,



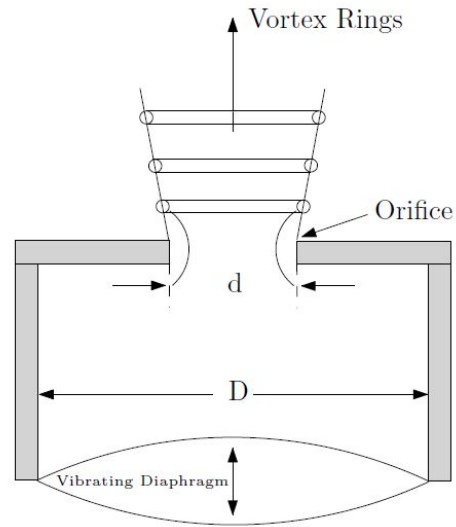


Figure 2.1: Schematic layout of a synthetic jet actuator (Pedroza, 2018).

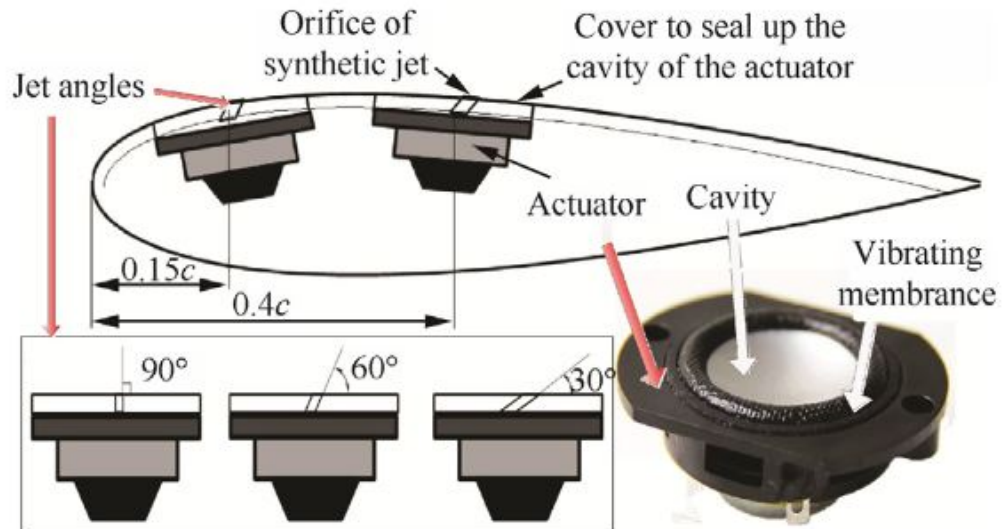


Figure 2.2: Example of synthetic jet actuators and their installation in an airfoil (wing) model (Zhao et al., 2016b).

Burkholder, & Smith, 2008)

$$u_i(t) = \theta_{2i}^* - \frac{\theta_{1i}^*}{v_i(t)}, \quad i = 1, \dots, m \quad (2.34)$$

where  $u_i(t) \in \mathbb{R}$  denotes the virtual deflection angle due to the  $i^{\text{th}}$  SJA array;  $v_i(t) = A_{ppi}^2(t) \in \mathbb{R}$  denotes the peak-to-peak voltage applied to the  $i^{\text{th}}$  SJA array in [Volts]; and  $\theta_{1i}^*, \theta_{2i}^* \in \mathbb{R}$  are uncertain constant physical parameters in [Volt–deg] and [deg], respectively, for the  $i^{\text{th}}$  SJA array. The parameter  $\theta_{2i}^*$  physically represents the maximum surface deflection angle achievable using the  $i^{\text{th}}$  SJA array. Figure 2.3 shows the different variation of the virtual surface deflection with the voltage provided from the SJA for four different values of the constant physical parameter  $\theta_1^*$ .

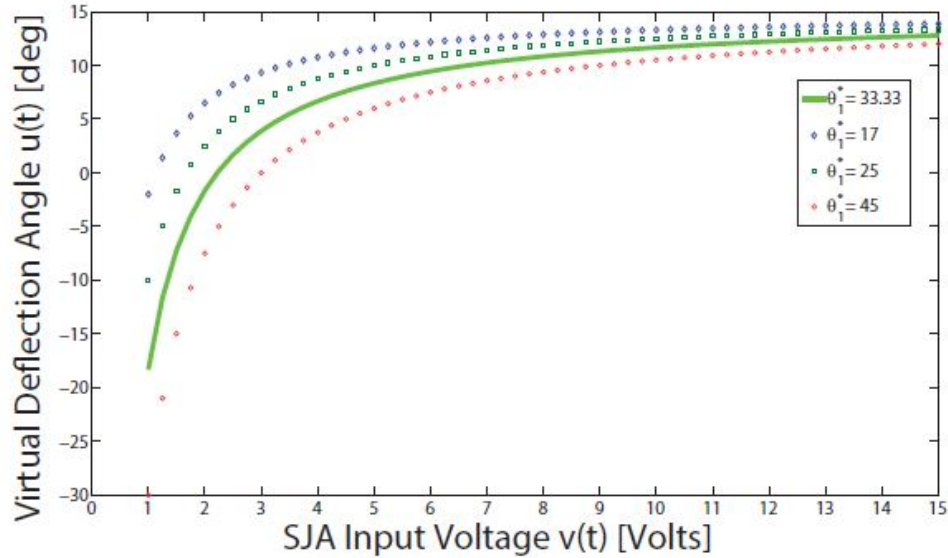


Figure 2.3: Variation of virtual surface deflection with the voltage from the synthetic jet actuator (Ramos-Pedroza et al., 2017).

To compensate for the SJA nonlinearity and input parametric uncertainty in

(2.34), a robust-inverse control structure will be utilized (MacKunis et al., 10-13 Dec., 2013), which employs constant, “best-guess” estimates of the uncertain SJA parameters  $\theta_{1i}^*$ ,  $\theta_{2i}^*$ . The robust-inverse control law can be expressed as

$$v_i(t) = \frac{\hat{\theta}_{1i}}{\hat{\theta}_{2i} - u_{di}(t)}, \quad i = 1, \dots, m \quad (2.35)$$

where  $\hat{\theta}_{1i}$ ,  $\hat{\theta}_{2i} \in \mathbb{R}^+$  are constant feedforward estimates of  $\theta_{1i}^*$  and  $\theta_{2i}^*$ , respectively; and  $u_{di}(t) \in \mathbb{R}$ , for  $i = 1, \dots, m$ , are the auxiliary control terms. These auxiliary control terms are defined in the subsequent chapters.

## 2.6 Proper Orthogonal Decomposition

POD, was introduced by Lumley (Bakewell Jr & Lumley, 1967) to identify coherent structures in flow. Since then it has been successfully applied to many scientific and engineering applications for low-dimensional dynamic modeling, image compression (Richards John & Xiuping, 1999). In this section, a POD based model order reduction for Incompressible Navier-Stokes is presented. For more detailed analysis on POD the reader is referred to (Holmes, 2012).

### 2.6.1 POD based ROM for Unactuated Systems

The incompressible Navier-Stokes equations are given as (Batchelor, 2000)

$$\nabla \cdot u = 0, \quad \frac{\partial u}{\partial t} = -(u \cdot \nabla)u + \nu \nabla^2(u) - \nabla p, \quad (2.36)$$

where  $u(s, t) : \Omega \times [0, \infty) \in \mathbb{R}^3$  denotes the velocity of the flow field over a spatial domain  $s \in \Omega \subset \mathbb{R}^3$ ;  $p(s, t) \in \mathbb{R}^3$  is the space- and time-dependent pressure of the flow field over  $\Omega$ ; and  $v \triangleq 1/\text{Re}$ , where  $\text{Re}$  denotes the Reynolds number. In the POD modal decomposition technique, the flow velocity field  $u(s, t)$  is expanded as a weighted sum of POD modes defined in the spatial domain  $\Omega$  as

$$u(s, t) = u_0 + \sum_{i=1}^n x_i(t) \phi_i(s). \quad (2.37)$$

In (2.37),  $\phi_i(s) \in \mathbb{R}^3$ , denote the POD modes and  $x_i(t)$ ,  $i = 1, \dots, n$ , denote unknown, time-varying coefficients resulting from the modal decomposition, respectively; and  $u_0 \in \mathbb{R}^3$  denotes the mean flow velocity over  $\Omega$ . By substituting the velocity field expansion (2.37) into (2.36), the POD-based reduced-order model of the Navier-Stokes equations is obtained as (MacKunis et al., 2011; Guay & Hariharan, June 11-13, 2008; John et al., June 10-12, 2009)

$$\begin{aligned} \frac{\partial}{\partial t} \sum_{j=1}^n x_j(t) \phi_j(s) = & - \left[ u_0 + \sum_{i=1}^n x_i(t) \phi_i(s) \right] \cdot \nabla \left[ u_0 + \sum_{k=1}^n x_k(t) \phi_k(x) \right] + \\ & v \nabla^2 \left[ u_0 + \sum_{j=1}^n x_j(t) \phi_j(x) \right] - \nabla p. \end{aligned} \quad (2.38)$$

$$\begin{aligned} \dot{x}_k(t) = & \sum_{j=1}^n x_j(t) \langle (-\phi_j(s) \cdot \nabla) u_0 - (u_0 \cdot \nabla) \phi_j(s) + v \nabla^2 \phi_j(s), \phi_k(s) \rangle \\ & - \sum_{i=1}^n \sum_{j=1}^n x_i(t) x_j(t) \langle (\phi_i(s) \cdot \nabla) \phi_j(s), \phi_k(s) \rangle + \langle -u_0 \cdot \nabla u_0 + v \nabla^2 u_0, \phi_k(s) \rangle \end{aligned} \quad (2.39)$$

where  $\langle \phi_i(s), \phi_j(s) \rangle$  denotes the standard inner product between two vectors in Euclidean space. By orthogonality of modes,  $\langle \phi_i(s), \phi_j(s) \rangle = \delta_{ij}$ , where  $\delta_{ij}$  denotes the Kronecker delta symbol. Note that, since  $\text{div}(\phi_k) = 0$ , it can be shown that  $\phi_k(s) = 0$  on the boundary of  $\Omega$ . Indeed, it follows that

$$\int_{\Omega} \nabla p \cdot \phi_k(s) dV = \int_{\partial\Omega} p \phi_k(s) \cdot n_{\Omega} ds \quad (2.40)$$

where  $n_{\Omega}$  represents the unit vector normal to the spatial domain  $\Omega$ . Thus, the pressure term can be ignored, and the expression in (2.39) can be rewritten in the compact form

$$\dot{x}_k(t) = L_k x(t) + x^T(t) Q_k x(t) + b_k, \quad k = 1, \dots, n. \quad (2.41)$$

The expression in (2.41) represents a system of nonlinear ordinary differential equations resulting from POD-based model reduction. In (2.41),  $L_k(s) \in \mathbb{R}^{1 \times n}$ ,  $Q_k(s) \in \mathbb{R}^{n \times n}$ , and  $b_k \in \mathbb{R}$  are defined as

$$L_{k_i}(s) = \langle -(\phi_j(s) \cdot \nabla) u_0 - (u_0 \cdot \nabla) \phi_j(s) + v \nabla^2 \phi_j(s), \phi_k(s) \rangle, \quad (2.42)$$

$$Q_{k_{ij}}(s) = -\langle (\phi_i(s) \cdot \nabla) \phi_j(s), \phi_k(s) \rangle, \quad (2.43)$$

$$b_k(s) = \langle -u_0 \cdot \nabla u_0 + v \nabla^2 u_0, \phi_k(s) \rangle. \quad (2.44)$$

## 2.6.2 POD based ROM for Actuated Flow

In the POD-based model order reduction method described in Section 2.6.1, the flow field expansion does not include the effects of actuation. This section presents an

extension of the POD based ROM where the flow velocity field  $u(s, t)$  is expanded as a weighted sum of actuated and unactuated POD modes defined in the spatial domain  $\Omega$  (Akhtar, Nayfeh, & Ribbens, 2009; Kasnakoglu, Camphouse, & Serrani, 2009)

$$u(s, t) = u_0 + \sum_{i=1}^n x_i(t)\phi_i(s) + \sum_{i=1}^m \gamma_i(t)\psi_i(s) \quad (2.45)$$

In (2.45),  $\phi_i(s) \in \mathbb{R}^3$  denote the POD modes;  $x_i(t)$ ,  $i = 1, \dots, n$ , are the unknown, unmeasurable time-varying coefficients resulting from the modal decomposition; and  $u_0 \in \mathbb{R}^3$  denotes the mean flow velocity over  $\Omega$ , where  $\psi_i(s) \in \mathbb{R}$  denote the actuation modes, and  $\gamma_i(t) \in \mathbb{R}$  denote actuation values (i.e., control inputs). After substituting (2.45) in (2.36), the individual terms  $\frac{\partial u}{\partial t}$ ,  $(u \cdot \nabla u)$  and  $\nabla^2 u$  are expressed as

$$\begin{aligned} \frac{\partial u}{\partial t} &= \frac{\partial u_0}{\partial t} + \frac{\partial}{\partial t} \sum_{i=1}^n x_i \phi_i + \frac{\partial}{\partial t} \sum_{j=1}^m \gamma_j \psi_j \\ &= \sum_{i=1}^n \dot{x}_i \phi_i + \sum_{j=1}^m \dot{\gamma}_j \psi_j \end{aligned} \quad (2.46)$$

$$\begin{aligned} u \cdot \nabla u &= \left[ u_0 + \sum_{i=1}^n x_i \phi_i + \sum_{i=1}^m \gamma_i \psi_i \right] \cdot \nabla \left[ u_0 + \sum_{j=1}^n x_j \phi_j + \sum_{j=1}^m \gamma_j \psi_j \right] \\ &= u_0 \cdot \nabla u_0 + u_0 \cdot \sum_{j=1}^m x_j \nabla \phi_j + u_0 \cdot \sum_{j=1}^m \gamma_j \nabla \psi_j \\ &\quad + \sum_{i=1}^n x_i \phi_i \cdot \nabla u_0 + \sum_{i=1}^n x_i \phi_i \cdot \sum_{j=1}^n x_j \nabla \phi_j + \sum_{i=1}^n x_i \phi_i \cdot \sum_{j=1}^m \gamma_j \nabla \psi_j \\ &\quad + \sum_{i=1}^m \gamma_i \psi_i \cdot \nabla u_0 + \sum_{i=1}^m \gamma_i \psi_i \cdot \sum_{j=1}^n x_j \nabla \phi_j + \sum_{i=1}^m \gamma_i \psi_i \cdot \sum_{j=1}^m \gamma_j \nabla \psi_j \end{aligned} \quad (2.47)$$

rearranging the terms in (2.47),

$$\begin{aligned}
 u \cdot \nabla u &= u_0 \cdot \nabla u_0 + \sum_{i=1}^n (u_0 \cdot \nabla \phi_i + \phi_i \cdot \nabla u_0) x_i + \sum_{j=1}^m (u_0 \cdot \nabla \psi_j + \psi_j \cdot \nabla u_0) \gamma_j \\
 &+ \sum_{i=1}^n \sum_{j=1}^n (\phi_i \cdot \nabla \phi_j) x_i x_j + \sum_{i=1}^m \sum_{j=1}^m (\psi_i \cdot \nabla \psi_j) \gamma_i \gamma_j \\
 &+ \sum_{i=1}^n \sum_{j=1}^m (\phi_i \cdot \nabla \psi_j + \psi_j \cdot \nabla \phi_i) x_i \gamma_j.
 \end{aligned} \tag{2.48}$$

The diffusion term is expanded as

$$\nabla^2 u = \nabla^2 u_0 + \sum_{i=1}^n x_i \nabla^2 \phi_i + \sum_{j=1}^m \gamma_j \nabla^2 \psi_j \tag{2.49}$$

By utilizing (2.46), (2.48) and (2.49) into (2.36) and project these equations along  $\phi_k$  and obtain

$$\begin{aligned}
 \dot{x}_k(t) &= \mathcal{A}_k + \sum_{i=1}^n \mathcal{B}_{ki} x_i(t) + \sum_{i=1}^n \sum_{j=1}^n \mathcal{C}_{kij} x_j(t) x_i(t) \\
 &+ \sum_{i=1}^m \mathcal{D}_{ki} \dot{\gamma}_i(t) + \sum_{i=1}^n \sum_{j=1}^m \mathcal{E}_{kij} x_i(t) \gamma_j(t) \\
 &+ \sum_{i=1}^m \mathcal{F}_{ki} \gamma_i(t) + \sum_{i=1}^m \sum_{j=1}^m \mathcal{G}_{kij} \gamma_i(t) \gamma_j(t),
 \end{aligned} \tag{2.50}$$

where

$$\begin{aligned}
 \mathcal{A}_k &= -\langle u_0 \cdot \nabla u_0, \phi_k \rangle + \frac{1}{Re} \langle \nabla^2 u_0, \phi_k \rangle \\
 \mathcal{B}_k &= -\langle u_0 \cdot \nabla \phi_i, \phi_k \rangle - \langle \phi_i \cdot \nabla u_0, \phi_k \rangle + \frac{1}{Re} \langle \nabla^2 \phi_i, \phi_k \rangle \\
 \mathcal{C}_k &= -\langle \phi_i \cdot \nabla \phi_j, \phi_k \rangle \\
 \mathcal{D}_k &= -\langle \psi_i, \phi_k \rangle \\
 \mathcal{E}_k &= -\langle \psi_j \cdot \nabla \phi_i, \phi_i \rangle - \langle \phi_i \cdot \nabla \psi_j, \phi_k \rangle \\
 \mathcal{F}_k &= -\langle u_0 \cdot \nabla \psi_i, \phi_k \rangle - \langle \psi_i \cdot \nabla u_0, \phi_k \rangle + \frac{1}{Re} \langle \nabla^2 \psi_i, \phi_k \rangle \\
 \mathcal{G}_k &= -\langle \psi_i \cdot \nabla \psi_j, \phi_k \rangle.
 \end{aligned}$$

The actuated reduced-order flow dynamics model in (2.50) can be expressed in control affine form as

$$\dot{x} = f(x) + g(x)u, \quad y = h(x) \quad (2.51)$$

where  $x(t) \triangleq [x_1(t), x_2(t), \dots, x_n(t)]^T \in \mathbb{R}^n$  contains the unmeasurable coefficients resulting from POD-based model order reduction,  $g(x) \in \mathbb{R}^{n \times m}$  is an input gain matrix,  $u(t) \triangleq [u_1(t), \dots, u_m(t)] \in \mathbb{R}^m$  denotes a subsequently defined virtual control input (e.g., resulting from  $m$  arrays of SJAs), and  $y(t) \in \mathbb{R}$  is the measurable output (e.g., sensor measurements of flow field velocity or pressure). In the subsequent AFC design and analysis, the observer and controller development will be presented using a virtual control signal  $u(t) \in \mathbb{R}^m$ , which is defined via the parameterization

$$g(x)u = Q_{ain}(x, \gamma) + Q_{in}(\gamma, \gamma). \quad (2.52)$$



**Remark 1.** In (2.52),  $\gamma(t) \in \mathbb{R}^m$ , and the terms  $Q_{ain}(x, \gamma)$ ,  $Q_{in}(\gamma, \gamma)$  are quadratic in their respective arguments ((i.e,  $Q_{in}(x, \gamma)$  is a function that includes products of  $x$  and  $\gamma$ ,  $Q_{in}(\gamma, \gamma)$  is quadratic in  $\gamma$ ). Since the  $\gamma(t)$  dependence is quadratic in this case, the mapping between  $\gamma(t)$  and  $u(t)$  will not be unique in general and any ‘desired’ control signal commanded by the actuation signal  $\gamma(t)$  can be realized by the virtual control signal  $u(t)$ .

## Chapter 3

# A Closed-loop Nonlinear Control and Sliding Mode Estimation Strategy for Fluid Flow Regulation

In this chapter, a sliding mode observer and robust nonlinear control method are presented, which are shown to achieve finite-time state estimation and asymptotic regulation of a fluid flow system. To facilitate the design and analysis of the closed-loop active flow control system, POD-based model order reduction is utilized to express the Navier-Stokes partial differential equations as a set of nonlinear ordinary differential equations. The resulting reduced-order model contains a measurement equation that is in a non-standard mathematical form. This challenge is mitigated through the detailed design and analysis of a sliding mode observer. The observer is shown to achieve finite-time estimation of the unmeasurable states of the reduced-order model using direct sensor measurements of the flow field velocity. The estimated states are

utilized as feedback measurements in a closed-loop active flow control system. To address the practical challenge of actuator bandwidth limitations, the control law is designed to be continuous. A rigorous Lyapunov-based stability analysis is presented to prove that the closed-loop flow estimation and control method achieves asymptotic regulation of a fluid flow field to a prescribed state. Numerical simulation results are also provided to demonstrate the performance of the proposed closed-loop active flow control system, comparing two different designs for the sliding mode observer.

### 3.1 Flow Dynamics Reduced-order Model

In this section, a POD-based model reduction technique is utilized to recast the incompressible Navier-Stokes equations as a finite set of nonlinear ODEs. The derivation of the ROM for the unactuated flow dynamics is presented in Section 3.1.1. The additional details involved in deriving the reduced-order Galerkin model for the actuated flow dynamics are then presented in Section 3.1.2. The ROM for the actuated flow dynamics presented in Section 3.1.2 will be utilized to develop the proposed closed-loop AFC system.

**Remark 2. (*Flow Reconstruction vs. Flow Control*)** *POD-based model order reduction can require a large number of modes to achieve resolution high enough to reconstruct highly turbulent flow fields (Saha, Biswas, Mandal, & Sarkar, 2017). However, the focus of the effort presented here is on control of the fluid flow, as opposed to reconstruction of the flow. It has been shown in recent research that ROM accuracy sufficient for flow control can be achieved using only the first few POD modes (Rowley et al., 2004; Wallace, Shea, Glauser, Thirunavukkarasu, & Carlson, 2012;*

*Siegel, Cohen, & McLaughlin, 2006; Kasnakoğlu, Serrani, & Efe, 2008; S. Gordeyev & Thomas, 2013; Caraballo, Little, Debiasi, & Samimy, 2007). For the proof-of-concept of the sliding mode estimation and flow control method presented here, complete flow field reconstruction is not necessary, and it is assumed that the ROM has sufficient accuracy for the flow control objective.*

### 3.1.1 Unactuated Flow Dynamics Reduced-order Model

The incompressible Navier-Stokes equations are given as (Batchelor, 2000)

$$\nabla \cdot u = 0, \quad \frac{\partial u}{\partial t} = -(u \cdot \nabla)u + v\nabla^2(u) - \nabla p, \quad (3.1)$$

where  $u(s, t) : \Omega \times [0, \infty) \in \mathbb{R}^3$  denotes the velocity of the flow field over a spatial domain  $s \in \Omega \subset \mathbb{R}^3$ ;  $p(s, t) \in \mathbb{R}$  is the space- and time-dependent pressure of the flow field over  $\Omega$ ; and  $v \triangleq 1/\text{Re}$ , where  $\text{Re}$  denotes the Reynolds number.

POD, which is often referred to as Karhunen-Loève expansion or principal component analysis, is used to obtain lower-dimensional dynamic models for fluid flow. Specifically, POD is utilized to develop a set of basis functions (POD modes) that approximates the original infinite-dimensional flow dynamic model as a finite-dimensional model in terms of the POD modes. In the POD modal decomposition technique, the flow velocity field  $u(s, t)$  is expanded as a weighted sum of POD modes defined in the spatial domain  $\Omega$  as

$$u(s, t) = u_0 + \sum_{i=1}^n x_i(t)\phi_i(s). \quad (3.2)$$

In (3.2),  $\phi_i(s) \in \mathbb{R}^3$ , denote the POD modes and  $x_i(t)$ ,  $i = 1, \dots, n$ , denote unknown, time-varying coefficients resulting from the modal decomposition, respectively; and

$u_0 \in \mathbb{R}^3$  denotes the mean flow velocity over  $\Omega$ . By substituting the velocity field expansion (3.2) into (3.1), and following the procedure described in Section 2.6.1, the POD-based reduced-order model can be expressed as

$$\dot{x} = A(x)x, \quad A(x) = L + \sum_{i=1}^n x_i P_i, \quad (3.3)$$

where  $x(t) \triangleq [x_1(t), x_2(t), \dots, x_n(t)]^T \in \mathbb{R}^n$ .

The flow field observer design presented here is based on the standard assumption that one or more sensor measurements are available. For a general case where  $q$  velocity field measurements are available at  $q$  predefined locations, the corresponding average velocity measurement can be expressed in terms of the modal decomposition. For example, a sensor velocity measurement at a single location  $s_0$  can be expressed as (John et al., June 10-12, 2009)

$$y(t) = \sum_{i=1}^n x_i(t) (\phi_i^1(s_0) + \phi_i^2(s_0) + \phi_i^3(s_0)), \quad (3.4)$$

where  $\phi_i^j(s) \in \mathbb{R}$  denotes the  $j^{\text{th}}$  element of the  $i^{\text{th}}$  POD mode. Since the POD modes are temporally independent, the output measurement in (3.4) can be expressed as

$$y(t) = Cx(t), \quad (3.5)$$

where  $y(t) \in \mathbb{R}$ , and  $C \in \mathbb{R}^{1 \times n}$  is a vector of known constants, and  $x(t)$  is introduced in (3.3). Physically, the expression in (3.5) can be interpreted as the measured velocity at a predefined location as expressed in terms of the POD modes.

An expression similar to that in (3.5) can be obtained to represent pressure mea-

surements or other physical quantities. The subsequent analysis is based on the assumption that a single velocity sensor measurement is available, without loss of generality.

Further details of the reduced-order model derivation summarized above can be found in (Holmes, 2012; Kalashnikova & Barone, 2012; Rowley, 2005). Note that the derivation of the reduced-order model in this section does not explicitly include the effects of control actuation, since the actuation effects are embedded in the coefficients in the Galerkin model. The details of the ROM derivation for the actuated flow system are summarized in the following section.

### 3.1.2 Reduced-order Model for the Actuated Flow

For the control design presented here, it will be assumed that an input separation method (Kasnaoğlu et al., 2009) is utilized to expand the flow field in terms of baseline (unactuated) POD modes and actuation modes. The baseline POD modes are extracted using a standard POD procedure as described in Section 3.1.1, whereas the actuation modes are built using an optimization algorithm similar to that in (Kasnaoğlu et al., 2009). The following section provide details on the ROM for actuated flow that is being considered in this paper.

#### 3.1.2.1 Actuation Modes

Note that the reduced-order model given in (3.3) - (3.5) does not explicitly include the effects of actuation. The actuation effects are embedded in the coefficients of the Galerkin system. Specifically, the actuation effects can be included in the reduced-order model by redefining the modal decomposition in (3.2) to include *actuation*

modes as

$$u(s, t) = u_0 + \sum_{i=1}^n x_i(t) \phi_i(s) + \gamma_1(t) \psi_1(s) + \gamma_2(t) \psi_2(s), \quad (3.6)$$

where  $\psi_1(s), \psi_2(s) \in \mathbb{R}$  denote the actuation modes, and  $\gamma_1(t), \gamma_2(t) \in \mathbb{R}$  denote actuation values (i.e., control inputs). Physically, the actuation values could represent voltage input signals to SJAs, for example (MacKunis et al., 10-13 Dec., 2013). By following an optimization technique similar to that in (Kasnakoğlu et al., 2009), the actuation modes can be defined as the modes  $\psi_1(x)$  and  $\psi_2(x)$  that minimize the energy not captured in the modal expansion of the actuated flow field. Details of the minimization algorithm can be found in (Kasnakoğlu et al., 2009). The decomposition in (3.6) assumes the presence of two actuation values, but the model can easily be extended to an arbitrary number of actuation values with little modification. Our subsequent numerical simulation results assume two actuation modes and two baseline POD modes in the dynamic model, without loss of generality.

**Remark 3. (*Fully Actuated System*)** *The theoretical estimator and control design presented here can be applied to the general case of  $m \geq n$ . The case where there are fewer control inputs than modes to be controlled (i.e., the underactuated case  $m < n$ ) requires a specialized treatment that is not addressed in the current result. The numerical simulation results presented in this paper test the case of two modes and two control inputs, without loss of generality.*

### 3.1.2.2 Actuated Dynamic Model

By replacing the actuated modal decomposition described in (3.6), the actuated reduced-order flow dynamics can be expressed as (3.3)

$$\dot{x} = A(x)x + Q_{ain}(x, \gamma) + Q_{in}(\gamma, \gamma), \quad (3.7)$$

where  $\gamma(t) \triangleq \begin{bmatrix} \gamma_1(t) & \gamma_2(t) \end{bmatrix}^T \in \mathbb{R}^2$ ,  $x(t)$  is introduced in (3.3), and the terms  $Q_{ain}(x, \gamma)$ ,  $Q_{in}(\gamma, \gamma) \in \mathbb{R}^n$  are quadratic in their respective arguments ((i.e,  $Q_{ain}(x, \gamma)$  is a function that includes products of  $x$  and  $\gamma$ ,  $Q_{in}(\gamma, \gamma)$  is quadratic in  $\gamma$ ). In this preliminary AFC design and analysis, the observer and controller development will be presented using a virtual control signal  $\mu(t) \in \mathbb{R}^2$ , which is defined via

$$g(x)\mu = Q_{ain}(x, \gamma) + Q_{in}(\gamma, \gamma). \quad (3.8)$$

In (3.8),  $g(x) \in \mathbb{R}^{2 \times 2}$  is a measurable input gain matrix, and  $\mu(t)$  represents the control actuation resulting from the cumulative effects of the actuation values  $\gamma_1(t)$  and  $\gamma_2(t)$ . Based on the quadratic structure of the actuation functions  $Q_{ain}(x, \gamma)$  and  $Q_{in}(\gamma, \gamma)$ , it can be shown that any ‘desired’ control signal commanded by the actuation signal  $\gamma(t)$  can be realized by the virtual control signal  $\mu(t)$ . Since the  $\gamma(t)$  dependence is quadratic, the mapping between  $\gamma(t)$  and  $\mu(t)$  will not be unique in general; but the subsequent discussion is based on the assumption that the desired, commanded control input can be delivered by the virtual control signal. Future work will address a formal handling of the non-affine control problem.

**Remark 4. (*Zero-net Mass Flux*)** Note that the control mechanism being consid-



ered here does not add mass to the flow system, since the control actuation is assumed to be generated by means of boundary movement or using SJAs, which transfer momentum with zero net mass injection across the flow boundary.

## 3.2 Sliding Mode Observer Design

This section presents two sliding mode observer designs to estimate the unknown coefficients resulting from POD-based reduced-order dynamic model for an actuated flow velocity field. Our previous result in (MacKunis et al., 2011) presents the design of a sliding mode observer, which is shown to achieve finite-time estimation of the unknown modal coefficients for unactuated flow systems in the form given in (3.3) - (3.5). The current result extends our previous work by designing a closed-loop observer/controller system to estimate the unknown coefficients while simultaneously driving the flow field to a desired velocity profile. This section will describe the non-trivial reworking of the sliding mode observers that is required for the *actuated* flow dynamics in (3.7) and (3.8).

By following a procedure similar to that in Sections 3.1.1 and 3.1.2, a reduced-order (control-oriented) model for the actuated flow system can be obtained as

$$\dot{x} = f(x) + g(x)\mu, \quad (3.9)$$

$$y = h(x). \quad (3.10)$$

where  $\mu(t) \in \mathbb{R}^2$  denotes the control input,  $g(x) \in \mathbb{R}^{n \times 2}$  denotes a sufficiently differentiable input gain matrix, and  $y(t) \in \mathbb{R}$  is the measurable output. In (3.9),  $f(x) \in \mathbb{R}^n$  and  $h(x) \in \mathbb{R}$  denote sufficiently differentiable vector functions. In the flow control

design presented here,  $f(x)$  and  $h(x)$  can be explicitly defined as  $f(x) \triangleq A(x)x$  and  $h(x) \triangleq Cx$  as they are defined for the system in (3.3) - (3.5). The explicit definition for  $g(x)$  can be obtained by following the POD-based model reduction procedure presented in Section 3.1, where the actuated modal decomposition in (3.6) is utilized in place of (3.2).

**Definition 3.**  $\mathcal{L}_\infty$  is a function space, in which for a function  $f$  in this set, its essential supremum serves as a norm:

$$\|f(x)\|_\infty \equiv \inf\{\mathcal{C} \geq 0 : |f(x)| \leq \mathcal{C} \quad \forall x\} \quad (3.11)$$

**Property 1.** If  $x(t) \in \mathcal{L}_\infty$ , the first and second partial derivatives of  $f(x)$ ,  $g(x)$ , and  $h(x)$  with respect to  $x(t)$  exist and are bounded.

To facilitate the subsequent observer design and analysis, a vector  $H(x) \in \mathbb{R}^n$  of output derivatives is defined as (S. V. Drakunov, 1992; MacKunis et al., 2011)

$$\begin{aligned} H(x) &\triangleq \begin{bmatrix} h_1(x) & h_2(x) & \cdots & h_n(x) \end{bmatrix}^T \\ &= \begin{bmatrix} h(x) & L_f h(x) & \cdots & L_f^{n-1} h(x) \end{bmatrix}^T \end{aligned} \quad (3.12)$$

where  $L_f^i h(x)$  denotes  $i^{\text{th}}$  Lie derivative of the output function  $h(x)$  along the direction of the vector field  $f(x)$  (e.g.,  $L_f = \frac{\partial h}{\partial x} f(x)$ ). If  $x(t)$  is a solution to the system described in (3.9), then

$$\frac{d}{dt} h_i(x(t)) = h_{i+1}(x(t)), \quad i = 1, \dots, n-1. \quad (3.13)$$

To design an observer for the actuated system in (3.9) and (3.10), the dynamic model must satisfy the following observability condition and matching condition.

**Remark 5. (*Sufficiently Differentiable Control Input*)** *Based on the definitions in (3.12) and (3.13) and the subsequent analysis, it must be assumed that the functions  $g(x)$ ,  $h(x)$ , and  $f(x)$  in (3.9) and (3.10) have continuous partial derivatives. In addition to this requirement, the control input function  $\mu(t)$  must be sufficiently differentiable. In the subsequent controller development, the choice to include the discontinuous signum function in the control law  $\mu(x)$  is based on the subsequent Lyapunov-based stability analysis only. In numerical implementation of the control law presented here, the discontinuous signum function is replaced with the continuously differentiable  $\tanh(\cdot)$  function. This is a standard approximation, which relates to the well-accepted definition of an “equivalent value operator” of a discontinuous function in sliding mode (S. V. Drakunov, 1992; Sánchez-Torres, Loukianov, Moreno, & Drakunov, 27-29 June, 2012).*

**Condition 2 (Observability).** *The system given in (3.9) and (3.10) must satisfy the observability condition*

$$\text{rank}(\mathcal{O}(x)) = n, \quad \forall x \in \mathbb{R}^n, \quad (3.14)$$

where the observability matrix  $\mathcal{O}(x) \triangleq \frac{\partial H(x)}{\partial x} \in \mathbb{R}^{n \times n}$ .

### 3.2.1 Observer Design 1

Under Condition 2, an observer that estimates the full state  $x(t)$  of the system in (3.9) using only measurements of  $y(t)$  can be designed as (Sánchez-Torres et al., 27-29

June, 2012)

$$\dot{\hat{x}} = \mathcal{O}(\hat{x})^{-1} M(\hat{x}) \{\text{sgn}[V(t) - H(\hat{x})]\} + g(\hat{x}) \mu(\hat{x}), \quad (3.15)$$

where  $\mathcal{O}(\cdot)$  is introduced in (3.14).

**Remark 6. (*Continuous Approximation of the signum Function*)** Note that the theoretical design and stability analysis in this paper is based on the discontinuous signum function (i.e.)

$$\text{sgn}(\zeta) = \begin{cases} 1 & \zeta > 0 \\ 0 & \zeta = 0 \\ -1 & \zeta < 0 \end{cases} \quad \forall \zeta \in \mathbb{R}. \quad (3.16)$$

The subsequent simulation results use a smooth, continuous equivalent operator,  $\{\text{sgn}[\cdot]\}_{eq}$ , to approximate the discontinuous signum function (i.e., the tanh function).

In (3.15),  $V(t) = [v_1(t), \dots, v_n(t)]^T$  is defined via the recursive form

$$v_1(t) = y(t), \quad v_{i+1}(t) = m_i(\hat{x}) \{\text{sgn}[v_i(t) - h_i(\hat{x}(t))]\}_{eq},$$

for  $i = 1, \dots, n-1$ . Also in (3.15),  $M(\hat{x}) \in \mathbb{R}^n$  denotes a diagonal matrix with positive elements defined as

$$M(\hat{x}) = \text{diag}[m_1(\hat{x}), \dots, m_n(\hat{x})], \quad (3.17)$$

where  $m_i(\hat{x}) \in \mathbb{R}$ ,  $i = 1, \dots, n$ , are introduced in (3.17). Through judicious choice of the gain matrix  $M(\hat{x})$ , it can be shown that the observer in (3.15) estimates the state  $x(t)$  in a finite time interval. The convergence of  $\hat{x}(t) \rightarrow x(t)$  is achieved through convergence to the desired sliding manifold  $\sigma = V(t) - H(\hat{x}) = 0$ . The choice of

$M(\hat{x})$  is based on the region of initial conditions for the system (3.9) and the upper bounds of  $h_i(x)$ . The complete proof of convergence of the observer in (3.15) can be found in Section 2.3.

### 3.2.2 Observer Design 2

Motivated by the desire to improve estimation performance, an alternative to the observer design in Section 3.2.1 will also be utilized in the closed-loop flow control system (S. V. Drakunov & Reyhanoglu, 2011). In the second observer design,  $x(t)$  is the state of the actuated flow dynamics in (3.9), and the state estimates  $\hat{x}(t)$  are obtained using the following observer:

$$\dot{\hat{x}} = f(\hat{x}) + \mathcal{O}(\hat{x})^{-1} M(\hat{x}) \{\text{sgn}[V(t) - H(\hat{x})]\} + g(\hat{x}) \mu(\hat{x}) \quad (3.18)$$

Similar to the design in (3.15), it can be shown that the observer design in (3.18) achieves finite-time estimation of the state  $x(t)$ . Specifically, it can be shown that, through judicious selection of the diagonal matrix  $M(\hat{x})$ ,  $\hat{x}(t) \equiv x(t)$  for any  $t \geq t_1$ . By including the additional term  $f(\hat{x})$  in the observer design in (3.18), it follows that, for  $t \geq t_1$ , the system converges to the sliding manifold  $\sigma = V(t) - H(\hat{x}) = 0$ ; and the observer equation (3.18) converges to the flow dynamic system in (3.9). Heuristically, the additional knowledge of the system dynamics used in the second observer in (3.18) should improve the performance of the closed-loop system.

The subsequent Section 3.5 presents numerical simulation results for the closed-loop flow control system using both of the observer designs given in (3.15) and (3.18).

### 3.3 Control Development

The control objective is to design the control signal  $\mu(t)$  to regulate the state vector  $x(t)$  to a desired reference profile  $x_d(t)$ , using only state estimates  $\hat{x}(t)$  as feedback measurements. To quantify the control objective, a tracking error  $e(t) \in \mathbb{R}^n$  and an auxiliary tracking error  $r(t) \in \mathbb{R}^n$  are defined as

$$e(t) = x(t) - x_d(t), \quad r(t) = \dot{e} + \alpha e, \quad (3.19)$$

where  $\alpha \in \mathbb{R}$  is a positive, constant control gain. Thus, the control objective can be stated mathematically as

$$e(t) \rightarrow 0. \quad (3.20)$$

Note that the tracking error signal  $e(t)$  and auxiliary tracking error  $r(t)$  are not directly measurable since they depend on the state  $x(t)$ .

**Assumption 2.** *The desired flow field velocity profile  $x_d(t)$  and its first three time derivatives are bounded in the sense that  $x_d(t), \dot{x}_d(t), \ddot{x}_d(t), \dddot{x}_d(t) \in \mathcal{L}_\infty \forall t \geq 0$ .*

**Assumption 3.** *In this preliminary result, it will be assumed that the energy content of the neglected POD modes is insufficient to cause transition to turbulence resulting from instability in the closed-loop system. Future work will investigate AFC system design to compensate for the neglected higher-order modes.*

### 3.3.1 Open Loop Error System

Taking the time derivative of (3.19) and using the definition of (3.19), the open loop error dynamics can be expressed as

$$\dot{r} = \frac{\partial f(x)}{\partial x} (r - \alpha e + \dot{x}_d) + \dot{g}(x) \mu + g(x) \dot{\mu} - \ddot{x}_d + \alpha(r - \alpha e). \quad (3.21)$$

**Assumption 4.** *In this preliminary closed-loop control design, it is assumed that the matrix  $g(x)$  can be considered constant or slowly varying; and thus,  $\dot{g}(x) \approx 0$ . The analysis can be extended to address a time varying  $g$  by including a compensation term in the form of  $\dot{\mu} = -k\|\mu\|\text{sgn}(\hat{r})$  as in (MacKunis et al., 10-13 Dec., 2013; Wilcox, MacKunis, Bhat, Lind, & Dixon, 2010), but the analysis is not considered here and would be a future extension of this result.*

The error dynamics in Equation (3.21) can be expressed as

$$\dot{r} = \tilde{N}(t) + N_d(t) - e + g\dot{\mu}(t), \quad (3.22)$$

where the unknown, unmeasurable auxiliary functions,  $\tilde{N}(t), N_d(t) \in \mathbb{R}^n$  are defined as

$$\tilde{N} = \frac{\partial f(x)}{\partial x} (r - \alpha e + \dot{x}_d) + \alpha(r - \alpha e) + e, \quad N_d = -\ddot{x}_d \quad (3.23)$$

The motivation for the separation of terms in (3.23) are based on the fact that the following inequalities can be developed

$$\|\tilde{N}\| \leq \rho(\|z\|)\|z\|, \quad \|N_d\| \leq \zeta_{N_d}, \quad \|\dot{N}_d\| \leq \zeta_{N_{d2}} \quad (3.24)$$

where  $\zeta_{N_d}, \zeta_{N_{d2}} \in \mathbb{R}^+$  are known bounding constants;  $\rho(\cdot)$  is a positive, globally invertible, non-decreasing function; and  $z(t) \in \mathbb{R}^{2n}$  is defined as

$$z(t) \triangleq \begin{bmatrix} e^T(t) & r^T(t) \end{bmatrix}^T. \quad (3.25)$$

### 3.3.2 Closed-Loop Error System

Based on the open-loop error system dynamics in (3.22), the control term  $\mu(t)$  is designed as:

$$\begin{aligned} \mu(t) = & g^{-1} \left( - (k_s + 1)\hat{e}(t) + (k_s + 1)\hat{e}(0) - \alpha \int_0^t (k_s + 1)\hat{e}(\tau) d\tau \right. \\ & \left. - \beta \int_0^t \text{sgn}(\hat{e}(\tau)) d\tau \right) \end{aligned} \quad (3.26)$$

where  $k_s, \beta \in \mathbb{R}$  are positive, constant control gains.

In (3.26),  $\hat{e}(t), \hat{r}(t) \in \mathbb{R}^n$  are estimates of the error signals  $e(t)$  and  $r(t)$  defined as

$$\hat{e}(t) \triangleq \hat{x}(t) - x_d(t), \quad \hat{r}(t) \triangleq \dot{\hat{e}} + \alpha \hat{e}. \quad (3.27)$$

Note that the matrix inverse (i.e.,  $g^{-1}$ ) calculation in (3.26) is valid for any constant, square, nonsingular matrix  $g$ . After substituting (3.26) into (3.22), the closed-loop error dynamics is obtained as

$$\dot{r} = \tilde{N} + N_d - e - (k_s + 1)\hat{r} - \beta \text{sgn}(\hat{e}). \quad (3.28)$$

To facilitate the following stability proof, the control gain  $\beta$  in (3.26) is selected to



satisfy the sufficient condition

$$\beta \geq \zeta_{N_d} + \frac{1}{\alpha} \zeta_{N_{d2}}, \quad (3.29)$$

where  $\zeta_{N_d}$  and  $\zeta_{N_{d2}}$  are introduced in (3.24).

### 3.4 Stability Analysis

**Theorem 4** (Observer Convergence). *The observers given in (3.15) and (3.18) achieve finite-time estimation of the state  $x(t)$  in the sense that*

$$V(t) \equiv H(\hat{x}) \Rightarrow \hat{x}(t) \equiv x(t), \quad \text{for } t \geq t_1 > 0. \quad (3.30)$$

*Proof.* By using the observer designs in (3.15) and (3.18), Assumption 4 can be used along with (3.26) to prove that finite-time estimation is achieved under the influence of the proposed control law. The formal proof is similar to that provided in Section 2.3. □

The following definition and lemma will be utilized in the proof of Theorem 4.

**Definition 4.** *To facilitate the Lyapunov-based proof of Theorem 4, an auxiliary function  $P(t) \in \mathbb{R}$  is defined as*

$$P(t) \triangleq \beta |e(0)| - e^T(0) N_d(0) - \int_0^t L(\tau) d\tau \quad (3.31)$$

where the auxiliary function  $L(t) \in \mathbb{R}$  is defined as

$$L(t) = r^T(t) (N_d(t) - \beta \operatorname{sgn}(e(t))). \quad (3.32)$$

**Lemma 1.** *Provided the sufficient condition in (3.29) is satisfied, the following inequality can be obtained:*

$$\int_0^t L(\tau) d\tau \leq \beta |e(0)| - e^T(0) N_d(0). \quad (3.33)$$

Hence, (3.33) can be used to prove that  $P(t) \geq 0$ .

Proof of Lemma 1 can be found in appendix section.

**Theorem 5** (Asymptotic Profile Tracking). *Provided Theorem 4 is satisfied, the robust nonlinear control law given in (3.26) ensures that all system signals remain bounded throughout closed-loop operation, and that the flow field profile tracking error is asymptotically regulated in the sense that*

$$\|e(t)\| \rightarrow 0 \quad \text{as} \quad t \rightarrow \infty, \quad t \geq t_1, \quad (3.34)$$

where  $t_1$  is introduced in (3.30), provided the control gain  $k_s$  introduced in (3.26) is selected sufficiently large, and  $\beta$  is selected to the sufficient condition in (3.29).

**Remark 7. (Stability Analysis for Non-smooth Systems)** *The following Lyapunov-based stability analysis does not include a rigorous treatment to address the discontinuous right hand side of the close-loop error system in (3.28) (i.e., using Filippov Solutions (Filippov, 1988)). Note that this does not invalidate the current result,*

since (Fischer, Kamalapurkar, & Dixon, 2013) provides a detailed Filippov solutions in a Lyapunov-based framework for a closed-loop system in a form similar to that in (3.28). Chapter 6 addresses a Filippov solution-based stability analysis for the proposed estimator design.

*Proof.* (See Theorem 5) Let  $\mathcal{D} \subset \mathbb{R}^{2n+1}$  be a domain containing  $w(t) = 0$ , where  $w(t) \in \mathbb{R}^{2n+1}$  is defined as

$$w(t) \triangleq \begin{bmatrix} z^T(t) & \sqrt{P(t)} \end{bmatrix}^T, \quad (3.35)$$

where  $P(t)$  is defined in (3.31).

Let  $V(w, t) : \mathcal{D} \times [0, \infty) \rightarrow \mathbb{R}$  be a radially unbounded, positive definite function defined as

$$V = \frac{1}{2}e^T e + \frac{1}{2}r^T r + P, \quad (3.36)$$

which satisfies the inequalities

$$U_1(w) \leq V(w, t) \leq U_2(w), \quad (3.37)$$

provided the sufficient condition in (3.29) is satisfied. In (3.37), the continuous positive definite functions  $U_1(w), U_2(w) \in \mathbb{R}$  are defined as

$$U_1(w) \triangleq \frac{1}{2} \|w\|^2, \quad U_2(w) \triangleq \|w\|^2. \quad (3.38)$$

After taking the time derivative of (3.36) and using (3.28),  $\dot{V}(t)$  can be expressed as

$$\dot{V} = e^T (r - \alpha e) + r^T \left( \tilde{N} + N_d - e - (k_s + 1)r - \beta \text{sgn}(e) \right) + \dot{P}, \quad (3.39)$$

where (3.19) and (3.30) were utilized. After canceling common terms, the expression in (3.39) can be rewritten as

$$\dot{V} = -\alpha \|e\|^2 - \|r\|^2 - \left( k_s \|r\|^2 - r^T \tilde{N} \right), \quad (3.40)$$

where (3.31) and (3.32) were utilized. After completing the squares for the parenthetic terms in (3.40) and using inequality (3.24), (3.40) can be upper bounded as follows:

$$\dot{V} \leq -\lambda_0 \|z\|^2 - k_s \left( \|r\| - \frac{\rho(\|z\|)}{2k_s} \|z\| \right)^2 + \frac{\rho^2(\|z\|)}{4k_s} \|z\|^2 \quad (3.41)$$

$$\Rightarrow \dot{V} \leq - \left( \lambda_0 - \frac{\rho^2(\|z\|)}{4k_s} \right) \|z\|^2, \quad (3.42)$$

where  $\lambda_0 \triangleq \min(\alpha, 1)$ . The following expression can be obtained from (3.42):

$$\dot{V} \leq -U(w), \quad (3.43)$$

where  $U(w) = c \|z\|^2$ , for some positive constant  $c \in \mathbb{R}$  is a continuous positive semi-definite function that is defined on the domain

$$\mathcal{D} \triangleq \left\{ w(t) \in \mathbb{R}^{2n+1} \mid \|w\| \leq \rho^{-1} \left( 2\sqrt{k_s \lambda_0} \right) \right\}. \quad (3.44)$$

The expressions in (3.37) and (3.42) can be used to prove that  $V(w, t) \in \mathcal{L}_\infty$  in  $\mathcal{D}$ ; hence,  $e(t), r(t) \in \mathcal{L}_\infty$  in  $\mathcal{D}$ . Given that  $e(t), r(t) \in \mathcal{L}_\infty$ , a standard linear analysis technique can be used along with (3.19) to show that  $\dot{e}(t) \in \mathcal{L}_\infty$  in  $\mathcal{D}$ . Since  $e(t), \dot{e}(t) \in \mathcal{L}_\infty$ , (3.19) can be used along with the assumption that  $x_d(t), \dot{x}_d(t) \in \mathcal{L}_\infty$  to

prove that  $x(t), \dot{x}(t) \in \mathcal{L}_\infty$  in  $\mathcal{D}$ . Given that  $x(t), \dot{x}(t) \in \mathcal{L}_\infty$ , (3.9) can be used along with the assumption that  $g(x)$  is nonsingular to prove that the control input  $\mu(t) \in \mathcal{L}_\infty$  in  $\mathcal{D}$ . Since  $r(t) \in \mathcal{L}_\infty$ , the assumption that  $g(x)$  is nonsingular can be used along with (3.26) to prove that  $\dot{\mu}(t) \in \mathcal{L}_\infty$  in  $\mathcal{D}$ . Given that  $r(t), e(t) \in \mathcal{L}_\infty$ , the bounding inequalities in (3.23) can be used along with (3.28) to prove that  $\dot{r}(t) \in \mathcal{L}_\infty$  in  $\mathcal{D}$ . Since  $\dot{e}(t), \dot{r}(t) \in \mathcal{L}_\infty$ , (3.25) can be used to prove that  $z(t)$  is uniformly continuous in  $\mathcal{D}$ . Hence, the definitions of  $U(w)$  and  $z(t)$  can be used to prove that  $U(w)$  is uniformly continuous in  $\mathcal{D}$ .

Let  $\mathcal{S} \subset \mathcal{D}$  denote a set defined as follows:

$$\mathcal{S} \triangleq \left\{ w(t) \in \mathcal{D} \mid U(w(t)) \leq \frac{1}{2} (\rho^{-1} (2\sqrt{k_s \lambda_0}))^2 \right\}. \quad (3.45)$$

Note that, based on the definitions (3.44) and (3.45), the sets  $\mathcal{D}$  and  $\mathcal{S}$  are dependent on the initial conditions and do not depend on time 't'. Theorem 8.4 of (Khalil, 1996) can now be invoked to state that

$$c \|z(t)\|^2 \rightarrow 0 \quad \text{as} \quad t \rightarrow \infty \quad \forall w(0) \in \mathcal{S}.$$

Based on the definition of  $z(t)$ , (3.45) can be used to show that

$$\|e(t)\| \rightarrow 0 \quad \text{as} \quad t \rightarrow \infty \quad \forall w(0) \in \mathcal{S}. \quad (3.46)$$

Hence, asymptotic regulation of the flow field velocity is achieved, provided the initial conditions lie within the set  $\mathcal{S}$ , where  $\mathcal{S}$  can be made arbitrarily large by increasing the control gain  $k_s$  - a semi-global result.  $\square$

### 3.5 Simulation Results

A numerical simulation was created to demonstrate the performance of the proposed observer/control system. The simulation demonstrates the performance of the control law in (3.26) using each of the proposed observer designs in (3.15) and (3.18). For high-fidelity CFD results of an AFC system similar to the proposed AFC system, the reader is referred to (Nguyen, Golubev, Mackunis, Ramos, & Pasiliao, 2015). The objective of the simulation is to regulate the velocity of a flow field to a constant value. The simulation objective of regulating the flow field to a constant velocity profile is provided here as a proof-of-concept only. Physically, the objective of this simulation can be interpreted as suppressing the variations in the kinetic energy of the flow field over a given spatial domain. For further discussion regarding the practical motivation for this control objective, the reader is referred to (M. J. Balajewicz et al., 2013). To test the controller performance under different operating conditions, five different simulations were run using each of the two observer designs, where the initial conditions  $a_1(0)$  and  $a_2(0)$  were selected randomly in each case. The reduced-order flow dynamic model in the simulation uses two POD modes, but the proposed control design can be applied to ROM consisting of an arbitrary number of modes.

The flow system parameters utilized to create the simulated flow environment {see (2.42)-(2.44)} are  $b_1 = -5$ ,  $b_2 = 32.7$ ,  $L_{11} = 30$ ,  $L_{12} = 36.5$ ,  $L_{21} = -111.7$ ,  $L_{22} = -120.5$ ,  $Q_{112} = -45.4$ ,  $Q_{122} = 47.2$ ,  $Q_{211} = -361.1$ ,  $Q_{212} = 304$  (MacKunis et al., 2011). The remaining coefficients of  $Q_{k_{ij}}$  were taken to be zero (MacKunis et al., 2011). The control gain values were selected as  $k_s = 5$ ,  $\alpha = 3$ , and  $\beta = 15$ ; and the desired constant POD modes were selected as  $x_1 = 0.2$  and  $x_2 = 0$ . The input gain matrix  $g$  was taken to be the  $2 \times 2$  identity matrix,  $I_{2 \times 2}$ , without loss

of generality. Note that, based on (3.26), the proposed control design is applicable to reduced-order models containing any constant, nonsingular input gain matrix  $g$ . Based on the parameters described, the systems of equations in (3.9) and (3.10) are rewritten as:

$$\dot{x}_1(t) = b_1 + L_{11}x_1 + L_{12}x_2 + Q_{112}x_1x_2 + Q_{122}x_2x_2 + g_{11}\mu_1 \quad (3.47)$$

$$\dot{x}_2(t) = b_2 + L_{21}x_1 + L_{22}x_2 + Q_{212}x_1x_2 + Q_{221}x_1x_1 + g_{22}\mu_2 \quad (3.48)$$

$$y(x) = h(x) = x_1 + x_2 \quad (3.49)$$

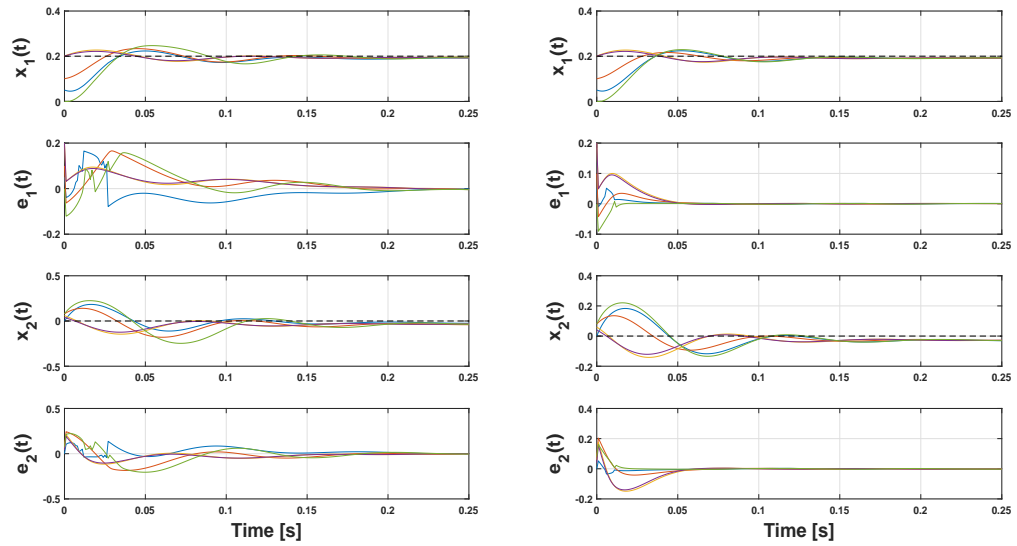


Figure 3.1: Zoomed plots magnifying the initial closed-loop transient response of the states  $x_1(t)$ ,  $x_2(t)$  and the error  $e_1(t)$ ,  $e_2(t)$  using the observers in (3.15) (left) and (3.18) (right).

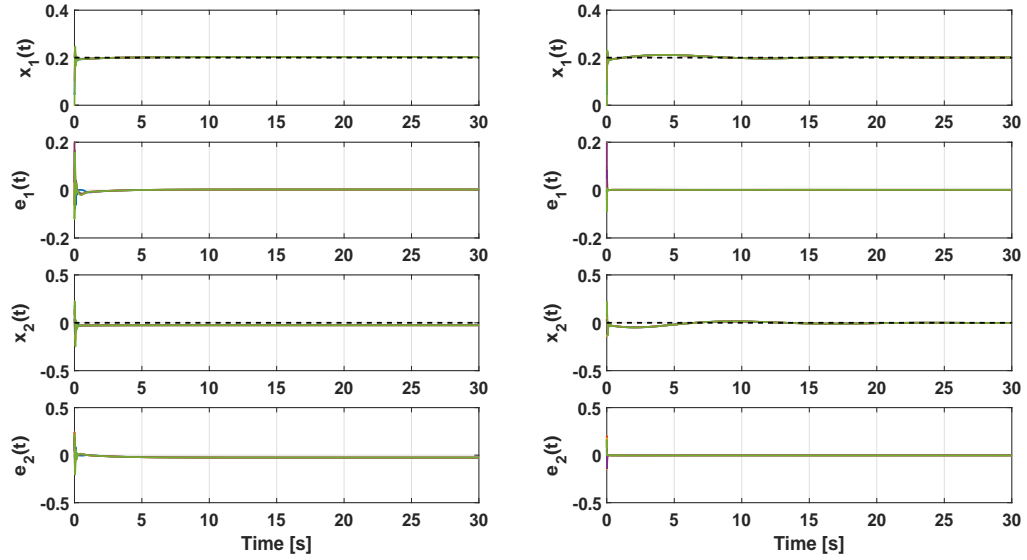


Figure 3.2: Closed-loop response of the states  $x_1(t)$ ,  $x_2(t)$  and the error  $e_1(t)$ ,  $e_2(t)$  for the total simulation time using the observers in (3.15) (left) and (3.18) (right).

The simulation results are summarized in Figs. 3.1 - 3.3. The states  $x_1(t)$  and  $x_2(t)$  and the estimates  $\hat{x}_1(t)$  and  $\hat{x}_2(t)$  converge to the desired constant values using the observer design in (3.15) and (3.18). Fig. 3.1 shows the initial transient responses of  $x_1(t)$  and  $e_1(t)$ ,  $x_2(t)$  and  $e_2(t)$  during the first 0.25 seconds of closed-loop operation using the two observer designs. The results demonstrate that a slight performance improvement is achieved by using the observer design in (3.18), which incorporates partial knowledge of the flow dynamics. The states and their estimates remain stable and convergent throughout the entire simulation duration. Fig. 3.2 shows the time response of  $x_1(t)$  and  $e_1(t)$ ,  $x_2(t)$  and  $e_2(t)$  for the total simulation time. Magnified plots of the control input showing the initial transient response are given in Fig. 3.3.



The results in Fig. 3.3 show that the closed-loop control system using observer (3.15) incurs a slightly higher control effort as compared to the system using observer (3.18). Again, this suggests that the performance of the overall closed-loop AFC system can be improved by incorporating additional knowledge of the system dynamics in the estimator design.

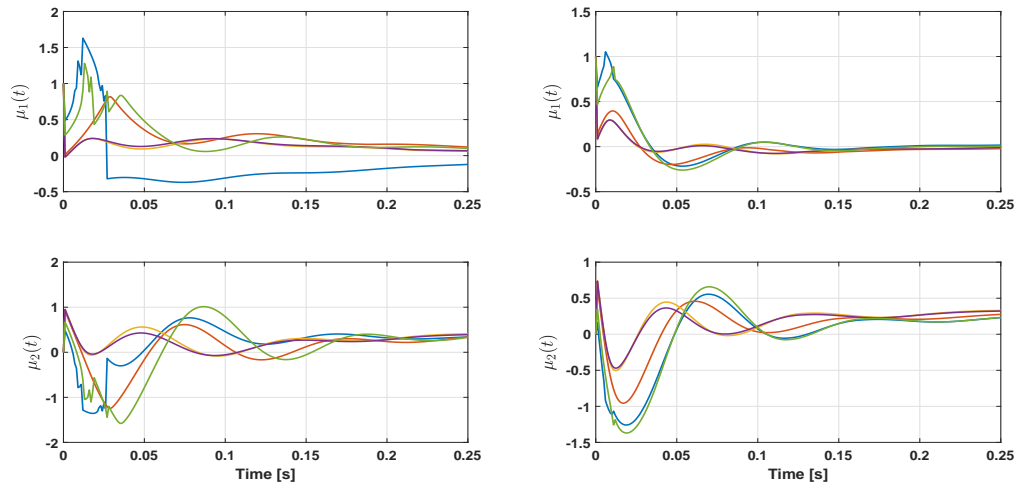


Figure 3.3: Commanded control inputs during the initial transient period of closed-loop controller operation using the observers in (3.15) (left) and (3.18) (right).

## 3.6 Conclusion

A nonlinear control method is developed, which is rigorously proven to asymptotically regulate the velocity of a fluid flow field over a given spatial domain. The control design amalgamates a SMO with a Lyapunov-based robust nonlinear control method to achieve asymptotic regulation of a flow field to a desired flow field velocity profile.

To reduce the computational burden, the proposed control law can be implemented without the use of adaptive parameter update laws, neural networks, computational fluid dynamics (CFD) calculations, or fuzzy logic rule sets. To achieve the result, a POD-based model reduction technique is utilized to recast the Navier-Stokes PDEs as a set of nonlinear ODEs in terms of the unknown, time-varying coefficients from Galerkin projection. A sliding mode observer is then designed to estimate the unknown coefficients, and the state estimates are utilized as feedback measurements in a nonlinear control law. By leveraging the finite-time estimation capability of the SMO, a rigorous Lyapunov-based stability analysis is utilized to prove that the control law drives the velocity of the flow field to a desired velocity profile over a given finite spatial domain. Numerical simulation results are provided to demonstrate the performance of the proposed control law in reliably regulating the flow field velocity using two different observer designs. Future work will focus on extending the observer and controller design to compensate for actuator uncertainty and nonlinearities in SJA-based flow control applications.

## Chapter 4

# Sliding Mode Estimation Strategy for Synthetic Jet Actuator-based Flow Control Under Actuator Uncertainty

This chapter presents a SJA-based closed-loop active flow control and estimation method, which compensates for the parametric uncertainty inherent in SJAs. A POD-based model reduction technique is first utilized to recast the Navier-Stokes partial differential equation as a set of ordinary differential equations in terms of the unknown Galerkin coefficients. The POD-based reduced-order model is then expressed in a control-oriented form, which incorporates the parametric uncertainty inherent in the SJA model. A novel sliding mode estimator is designed to estimate the unknown Galerkin coefficients in the uncertain SJA-based reduced-order model.

This is the first time that a sliding mode estimation strategy is rigorously proven to achieve finite-time state estimation for a flow system in the presence of input-multiplicative parametric uncertainty. A rigorous proof of finite time state estimation is provided, and the estimates are used in a nonlinear control law, which achieves asymptotic regulation of a fluid flow field to a desired time-varying velocity profile. A Lyapunov-based stability analysis is utilized to prove asymptotic regulation of the flow field velocity, and numerical simulation results are provided to demonstrate the performance of the proposed closed-loop active flow control system.

## 4.1 POD-based Reduced-order Model

In this section, a POD-based model reduction technique is utilized to derive a reduced-order, control-oriented model for the actuated flow dynamics.

### 4.1.1 Reduced-order Model for the Actuated Flow Dynamics

The incompressible Navier-Stokes equations are given as (Batchelor, 2000)

$$\nabla \cdot v = 0, \quad \frac{\partial v}{\partial t} = -(v \cdot \nabla)v + \frac{1}{\text{Re}} \nabla^2(v) - \nabla p \quad (4.1)$$

where  $v(s, t) : \Omega \times [0, \infty) \in R^3$  denotes the velocity of the flow field over a spatial domain  $s \in \Omega \subset \mathbb{R}^3$ ;  $p(s, t) \in \mathbb{R}^3$  is the space-and time-dependent pressure of the flow field over  $\Omega$ ; and  $\text{Re}$  denotes the Reynolds number.

In the POD-based model order reduction method, the flow velocity field  $v(s, t)$  is expanded as a weighted sum of actuated and unactuated POD modes defined in the spatial domain  $\Omega$ . The actuation effects are embedded in the coefficients of the

Galerkin system. Specifically, the actuation effects can be included in the reduced-order model by defining the modal decomposition as (Akhtar et al., 2009; Kasnakoğlu et al., 2009)

$$v(s, t) = v_0 + \sum_{i=1}^n x_i(t)\phi_i(s) + \sum_{i=1}^m \gamma_i(t)\psi_i(s) \quad (4.2)$$

In (4.2),  $\phi_i(s) \in \mathbb{R}^3$  denote the POD modes;  $x_i(t)$ ,  $i = 1, \dots, n$ , are the unknown, unmeasurable time-varying coefficients resulting from the modal decomposition; and  $v_0 \in \mathbb{R}^3$  denotes the mean flow velocity over  $\Omega$ , where  $\psi_i(s) \in \mathbb{R}$  denote the actuation modes, and  $\gamma_i(t) \in \mathbb{R}$  denote actuation values (i.e., control inputs). By leveraging an input separation method similar to that in (Kasnakoğlu et al., 2009), the actuation modes can be defined as the modes  $\psi_i(s)$  that minimize the energy not captured in the modal expansion of the actuated flow field. The subsequent simulation section assumes  $m = 4$  actuation modes, but the flow estimation and control method in this paper can easily be extended to address any number of actuation modes ( $m \geq n$ ).

#### 4.1.1.1 Actuated Dynamic Model

By substituting the actuated modal decomposition (4.2) into (4.1), and following the procedure described in Section 2.6.2, the actuated reduced-order flow dynamics can be expressed as

$$\dot{x} = f(x) + g(x)u, \quad y = h(x) \quad (4.3)$$

where  $x(t) \triangleq [x_1(t), x_2(t), \dots, x_n(t)]^T \in \mathbb{R}^n$  contains the unmeasurable coefficients resulting from POD-based model order reduction,  $g(x) \in \mathbb{R}^{n \times m}$  is an input gain matrix,  $u(t) \triangleq [u_1(t), \dots, u_m(t)] \in \mathbb{R}^m$  denotes a subsequently defined virtual control

input (e.g., resulting from  $m$  arrays of SJAs), and  $y(t) \in \mathbb{R}$  is the measurable output (e.g., sensor measurements of flow field velocity or pressure (MacKunis et al., 2011)).

**Property 2.** *If  $x(t) \in L_\infty$ , then the first and second partial derivatives of  $f(x)$ ,  $g(x)$ , and  $h(x)$  with respect to  $x(t)$  exist and are bounded. Based on the flow measurement equation and the actuated flow dynamics in (4.3),  $f(x)$  and  $h(x)$  can be expressed as  $f(x) \triangleq A(x)x$  and  $h(x) \triangleq Cx$  (explicit definitions of  $f(x)$  can be found in (MacKunis et al., 2011) and omitted here for brevity).*

## 4.2 SJA-based Control Model Derivation

In this section, the POD-based reduced-order model for the actuated flow dynamics will be augmented to include the effects of SJA actuation. To this end, a well-accepted, empirical model for the virtual surface deflection generated by SJA (Deb et al., 2008) will be utilized to represent the control actuation signal in the flow dynamics reduced-order model provided in Section 4.1.1. A series of algebraic steps will then be utilized to express the SJA-actuated flow dynamics in a control-oriented form, which explicitly includes the parametric uncertainty inherent in the SJA actuator model. The uncertain control model is a key feature of the proposed flow control design, which enables us to derive a nonlinear observer that is proven to compensate for the parametric uncertainty in the SJA actuators.

### 4.2.1 SJA Actuator Model

The virtual control surface deflection angle generated by an array of  $m$  SJAs can be expressed as (Deb et al., 2007, 2008)

$$u_i(t) = \theta_{2i}^* - \frac{\theta_{1i}^*}{v_i(t)}, \quad i = 1, 2, \dots, m. \quad (4.4)$$

In (4.4),  $v_i(t) \triangleq A_{ppi}^2(t) \in \mathbb{R}^+$  denotes a measurable input signal, where  $A_{ppi}$  represents the peak-to-peak voltage magnitude applied to the  $i^{\text{th}}$  SJA array; and  $\theta_{1i}^*$ ,  $\theta_{2i}^* \in \mathbb{R}$  are uncertain positive parameters. The SJA actuator model given in (4.4) illustrates one of the main challenges in SJA-based estimator and control design: the virtual surface deflection control input  $u_i(t)$  depends nonlinearly on the SJA voltage input signal  $v_i(t)$  and contains parametric uncertainty due to  $\theta_{1i}^*$  and  $\theta_{2i}^*$ . To address these challenges, the voltage input signal  $v_i(t)$  can be designed using the robust-inverse control structure (MacKunis et al., 10-13 Dec., 2013)

$$v_i(t) = \frac{\hat{\theta}_{1i}}{\hat{\theta}_{2i} - u_{di}(t)} \quad (4.5)$$

where,  $\hat{\theta}_{1i}, \hat{\theta}_{2i} \in \mathbb{R}^+$  are constant, *best-guess* feedforward estimates of the uncertain parameters  $\theta_{1i}^*$  and  $\theta_{2i}^*$ . In (4.5),  $u_{di}(t) \in \mathbb{R}$ , for  $i = 1, \dots, m$ , are subsequently defined auxiliary control signals.

**Remark 8. (*Singularity Avoidance*)** Note that using a singularity avoidance algorithm (Mondschein, Tao, & Burkholder, 2011) can be used to ensure that  $v_i(t)$  remains singularity-free.

After substituting (4.4), (4.5) into (4.3) the SJA-based control model can be expressed as

$$\dot{x} = f(x) + \Xi_B + \Omega u_d(t) \quad (4.6)$$

where  $u_d(t) \triangleq [u_{d1}(t), \dots, u_{dm}(t)]^T \in \mathbb{R}^m$ , and expressions for the uncertain constant

auxiliary terms  $\Xi_B \in \mathbb{R}^m$  and  $\Omega \in \mathbb{R}^{n \times m}$  can be readily obtained. To handle the uncertainty in the input-multiplicative matrix  $\Omega$  in (4.6), the auxiliary control signal  $u_d(t)$  is designed as

$$u_d(t) = \hat{\Omega}^\# \mu(t) \quad (4.7)$$

where  $\hat{\Omega} \in \mathbb{R}^{m \times n}$  denotes feedforward estimate of  $\Omega$ , and  $[\cdot]^\#$  denotes the pseudoinverse of a (nonsquare) matrix. Note that the standard matrix inverse operation could be used in place of the pseudoinverse for the case where  $n = m$ . In (4.7),  $\mu(t) \in \mathbb{R}^n$  denotes a known, nominal control input signal. After substituting (4.7) into (4.6), the open loop SJA-based system can be expressed as

$$\dot{x} = f(x) + \Xi_B + \tilde{\Omega} \mu(t) \quad (4.8)$$

where  $\tilde{\Omega} \triangleq \Omega \hat{\Omega}^\# \in \mathbb{R}^{n \times n}$ . Heuristically, the uncertain matrix  $\tilde{\Omega}$  represents the deviation between the actual SJA parameters  $\theta_{1i}^*, \theta_{2i}^*$  and their constant estimates  $\hat{\theta}_{1i}, \hat{\theta}_{2i}$ , for  $i = 1, \dots, m$ .

**Property 3.** *The uncertain matrix  $\tilde{\Omega}$  can be decomposed as*

$$\tilde{\Omega} = I_n + \Delta(t) \quad (4.9)$$

where  $I_n \in \mathbb{R}^{n \times n}$  denotes the identity matrix, and  $\Delta(t) \in \mathbb{R}^{n \times n}$  denotes uncertain “mismatch” matrix.

**Assumption 5.** *Approximate model knowledge is available such that the mismatch matrix  $\Delta$  satisfies*

$$\|\Delta(t)\|_{i\infty} < \varepsilon < 1 \quad (4.10)$$



where  $\varepsilon \in \mathbb{R}^+$  is a known bounding constant, and  $\|\cdot\|_{i\infty}$  denotes the induced infinity norm of a matrix. Heuristically, Inequality (4.10) can be interpreted as the assumption of approximate SJA model knowledge.

Preliminary results show that Assumption 5 is mild in the sense that the proposed estimation and control method performs well over a wide range of SJA parametric uncertainty.

By substituting (4.9) into (4.8), the SJA-based flow dynamic model can be expressed as

$$\dot{x} = f(x) + \Xi_B + \mu(t) + \Delta(t)\mu(t), \quad y = h(x). \quad (4.11)$$

### 4.3 Observer Design

In this section, an observer is designed, which estimates the full state  $x(t)$  of the uncertain system described in (4.11) using only measurable outputs (i.e.,  $y(t)$ ). The derivation presented here will provide the mathematical details in the non-trivial re-design of a sliding mode estimator, which compensates for the parametric uncertainty in the SJA actuator model (cf. (S. V. Drakunov, 1992)).

To facilitate the following estimator design and stability analysis, a vector of output signals is defined as

$$\begin{aligned} H(x, \mu) &\triangleq \begin{bmatrix} h_1(x) & h_2(x, \mu) & \cdots & h_n(x, \mu) \end{bmatrix}^T \\ &= \begin{bmatrix} h(x) & L_f h(x) & \cdots & L_f^{n-1} h(x) \end{bmatrix}^T \end{aligned} \quad (4.12)$$

where  $L_f^i h(x)$  denotes the  $i^{\text{th}}$  Lie derivative of the output function  $h(x)$  (Isidori, 2013),

along the direction of the vector field  $f(x, \mu)$ , where  $f(x, \mu)$  denotes the right hand side of (4.11). Note that  $h_1(x) = h(x)$  does not depend on the measurable input signal  $\mu(t)$  based on the output equation in (4.11).

**Condition 3** (Observability). *The system given in (4.11) must satisfy the observability condition*

$$\text{rank}(\mathcal{O}(x, \mu)) = n, \quad \forall x \in \mathbb{R}^n, \quad (4.13)$$

where the observability matrix  $\mathcal{O}(x, \mu) \triangleq \frac{\partial H(x, \mu)}{\partial x} \in \mathbb{R}^{n \times n}$ . Note that the observability condition given in (4.13) can be ensured through judicious sensor placement.

Provided Condition 3 is satisfied, the sliding mode observer that estimates the full state  $x(t)$  for the uncertain SJA-based dynamic system in (4.11) can be designed as

$$\dot{\hat{x}} = f(\hat{x}) + \mathcal{O}^{-1}(x, \mu) M(\hat{x}, \mu) \{ \text{sgn}(\Psi(t) - H(\hat{x})) \} + \mu(t) \quad (4.14)$$

where  $H(\cdot)$  is defined in (4.12), and  $\mathcal{O}(x, \mu)$  is introduced in (4.13). In (4.14),  $\{\text{sgn}[\cdot]\}_{eq}$  denotes a continuous “equivalent value operator” of the discontinuous signum function (S. V. Drakunov, 1992). Also, in (4.14),  $\Psi(t) = [\psi_1(t), \dots, \psi_n(t)]^T \in \mathbb{R}^n$  is defined using the modified recursive form (cf. (S. V. Drakunov, 1992))

$$\psi_1(t) = h_1(x) \quad (4.15)$$

$$\psi_{i+1}(t) = m_i \{ \text{sgn}[\psi_i(t) - h_i(\hat{x}(t))] \}_{eq} + \frac{\partial h_i(\hat{x})}{\partial x} \mu(t) \quad (4.16)$$

for  $i = 1, \dots, n - 1$ . The observer design in (4.14) will be shown to compensate for the SJA actuator parametric uncertainty through the design of the sliding gain term

$M(\hat{x}, \mu) \in \mathbb{R}^{n \times n}$ , which has the general form

$$M(\hat{x}, \mu) = \text{diag}[m_1(\hat{x}, \mu), \dots, m_n(\hat{x}, \mu)] \quad (4.17)$$

where  $m_i(\hat{x}, \mu) \in \mathbb{R}$ , for  $i = 1, \dots, n$ , denote subsequently designed observer gains. Through the appropriate design of the gain matrix  $M(\hat{x}, \mu)$ , it will be shown that the sliding mode observer in (4.14) achieves finite-time estimation of the state  $x(t)$  using only measurements of the output signal  $y(t)$ . The following theorem and stability proof will present a design for  $M(\hat{x}, \mu)$  that yields finite-time estimation for the system in (4.11), which includes parametric uncertainty in the SJA actuator model.

**Assumption 6.** *The initial conditions of the state and state estimate satisfy  $x(0) - \hat{x}(0) \leq \epsilon_0$ , where  $\epsilon_0$  is a known bounding constant.*

**Theorem 6.** *Provided the observability condition 3 is satisfied, the sliding mode observer in (4.14) achieves finite-time estimation of the state  $x(t)$  in the sense that  $\hat{x}(t) \equiv x(t)$  for  $t \geq t_n$ , where  $t_n \in \mathcal{L}_\infty$ .*

*Proof.* Based on (4.13), the observability matrix  $\mathcal{O}(x, \mu)$  is full rank, and  $\left| \det \left( \frac{\partial H(x)}{\partial x} \right) \right| \geq \epsilon > 0$ . It thus follows that the map  $H(x, \mu)$  is a diffeomorphism (i.e., there is a one to one correspondence between  $x(t)$  and  $H(x, \mu)$  for any given value of  $\mu(t)$ ). Since  $H(x, \mu)$  is a diffeomorphism, it is sufficient to prove that  $\tilde{x}(t) = H(x, \mu) - H(\hat{x}, \mu) = 0$  for  $t \geq t_n$ .

The estimation error dynamics can be obtained by taking the time derivative of  $\tilde{x}(t) = [\tilde{x}_1(t), \dots, \tilde{x}_n(t)]^T$  as

$$\dot{\tilde{x}}(t) = \frac{\partial H(x, \mu)}{\partial x} \dot{x} - \frac{\partial H(\hat{x}, \mu)}{\partial x} \dot{\hat{x}}. \quad (4.18)$$

By utilizing (4.11), (4.12), (4.14), and (4.17), the estimation error dynamics for  $\tilde{x}_1(t)$  can be expressed as

$$\begin{aligned} \dot{\tilde{x}}_1(t) = & \frac{\partial h_1(x)}{\partial x} (f(x) + \Xi_B) + \frac{\partial h_1(x)}{\partial x} \Delta\mu(t) + \left( \frac{\partial h_1(x)}{\partial x} - \frac{\partial h_1(\hat{x})}{\partial x} \right) \mu(t) \\ & - \frac{\partial h_1(\hat{x})}{\partial x} f(\hat{x}) - m_1 \{ \text{sign}(\tilde{x}_1(t)) \}_{eq} \end{aligned} \quad (4.19)$$

where the fact that  $\psi_1(t) = h_1(x) = h(x)$  was utilized. Based on (4.19) and the convergence analysis, the sliding gain term  $m_1(\hat{x}, \mu)$  is designed as

$$m_1(\hat{x}, \mu) = \beta_{1,1} + \beta_{2,1} \|\mu\| \quad (4.20)$$

where the auxiliary observer gains  $\beta_{1,1}$  and  $\beta_{2,1}$  are selected to satisfy

$$\beta_{1,1} > \left| \frac{\partial h_1(x)}{\partial x} (f(x) + \Xi_B) - \frac{\partial h_1(\hat{x})}{\partial x} f(\hat{x}) \right| \quad (4.21)$$

$$\beta_{2,1} > \left| \frac{\partial h_1(x)}{\partial x} - \frac{\partial h_1(\hat{x})}{\partial x} \right| + \varepsilon \left| \frac{\partial h_1(x)}{\partial x} \right| \quad (4.22)$$

where  $\varepsilon$  is introduced in (4.10). Provided Assumptions (5) and (6) and inequalities (4.10), (4.21), and (4.22) are satisfied, (4.19) can be upper bounded as

$$\dot{\tilde{x}}_1(t) \leq -\kappa \{ \text{sign}(\tilde{x}_1(t)) \} \Rightarrow |\tilde{x}_1(t)| \leq |\tilde{x}_1(0)| - \kappa t \quad (4.23)$$

where  $\kappa \in \mathbb{R}^+$  is a known bounding constant. Hence, (4.23) can be used to prove that sliding mode is reached, and  $\tilde{x}_1(t) \equiv 0$  after some finite time  $t = t_1$ .

To facilitate the proof of finite-time convergence for the remaining estimation error terms  $\tilde{x}_2, \dots, \tilde{x}_n$ , the expressions in (4.12), (4.14) and (4.16) will be utilized to rewrite

(4.19) as

$$\dot{\tilde{x}}_1(t) = h_2(x) - \frac{\partial h_1(\hat{x})}{\partial x} \mu(t) - m_1 \{ \text{sign}(\psi_1(t) - h_1(\hat{x})) \}_{eq} \quad (4.24)$$

where the fact that  $h_2(x) \triangleq \frac{\partial h_1(x)}{\partial x} \dot{x} = \frac{\partial h_1(x)}{\partial x} (f(x) + \Xi_B + \mu(t) + \Delta\mu(t))$  was utilized.

Given that  $\tilde{x}_1(t) \equiv 0$  for  $t \geq t_1$ , it follows that  $\dot{\tilde{x}}_1(t) \equiv 0$ , and (4.24) can be used to show that

$$h_2(x, \mu) = \frac{\partial h_1(\hat{x})}{\partial x} \mu(t) + m_1 \{ \text{sign}(\psi_1(t) - h_1(\hat{x})) \}_{eq} \quad (4.25)$$

for  $t \geq t_1$ . It follows from (4.16) and (4.25) that  $h_2(\hat{x}) = \psi_2(t)$ . The estimation error dynamics for  $\tilde{x}_2$  can be expressed as

$$\dot{\tilde{x}}_2(t) = h_3(x) - \frac{\partial h_2(\hat{x})}{\partial x} \mu(t) - m_2 \{ \text{sign}(\tilde{x}_2(t)) \}_{eq} \quad (4.26)$$

given that  $\tilde{x}_2(t) \equiv 0$  for  $t \geq t_2$ , from (4.16) and (4.26) that  $h_3(\hat{x}) = \psi_3(t)$ . In similar way,

$$\tilde{x}_i(t) \equiv 0 \Rightarrow \psi_{i+1}(t) - h_{i+1}(\hat{x}) = \tilde{x}_{i+1} \quad (4.27)$$

and the following recursion relation is obtained:

$$\dot{\tilde{x}}_i(t) = h_{i+1}(x) - \frac{\partial h_i(\hat{x})}{\partial x} \mu(t) - m_i \{ \text{sign}(\tilde{x}_i) \}_{eq}. \quad (4.28)$$

The convergence of  $\tilde{x}_2(t), \dots, \tilde{x}_n(t)$  to the corresponding sliding manifolds can be

achieved by selecting the sliding gain terms  $m_i(\hat{x}, \mu)$  to satisfy (see (4.20))

$$m_i(\hat{x}, \mu) > h_{i+1} - \frac{\partial h_i(\hat{x})}{\partial x} \mu(t) \quad (4.29)$$

for  $i = 1, \dots, n - 1$ , where the explicit design of  $m_i(\hat{x}, \mu)$  is in the form of (4.20), with observer gains  $\beta_{1,i}$  and  $\beta_{2,i}$  selected similarly as in (4.21) and (4.22) for  $i = 2, \dots, n$ . Hence, provided Assumptions (5) and (6), (4.20), (4.21), (4.22), and (4.29) are satisfied, it can be shown that the sliding manifolds  $\tilde{x}_1(t) = \tilde{x}_2(t) = \dots = \tilde{x}_n(t) = 0$  are reached in finite time. Hence,  $\hat{x}(t) \equiv x(t)$  in finite time.  $\square$

## 4.4 Control Development

In this section, the finite-time convergence property of the sliding mode observer will be leveraged to develop a feedback control law, which achieves asymptotic regulation of a fluid flow velocity profile for the flow dynamic system given in (4.11).

### 4.4.1 Control Objective

The control objective is to design the control signal  $\mu(t)$  to regulate the the state vector  $x(t)$  to a desired reference profile  $x_d(t)$ , using only state estimates  $\hat{x}(t)$  as feedback measurements. To quantify the control objective, a flow velocity profile tracking  $e(t) \in \mathbb{R}^n$  is defined as

$$e(t) = x(t) - x_d(t), \quad (4.30)$$

Thus, the control objective can be stated mathematically as

$$\|e(t)\| \rightarrow 0, \quad (4.31)$$

where  $\|\cdot\|$  in (5.12) denotes standard Euclidean norm (or 2-norm).

**Assumption 7.** *The desired flow field velocity profile  $x_d(t)$  and its first three time derivatives are bounded in the sense that  $x_d(t), \dot{x}_d(t), \ddot{x}_d(t), \dddot{x}_d(t) \in \mathcal{L}_\infty \forall t \geq 0$ .*

#### 4.4.2 Open Loop Error System

An auxiliary tracking error  $r(t) \in \mathbb{R}^n$  is defined as

$$r(t) = \dot{e} + \alpha e. \quad (4.32)$$

where  $\alpha \in \mathbb{R}^{n \times n}$  is a positive, diagonal constant control gain matrix. Note that the tracking error signal  $e(t)$  in (4.30) and auxiliary tracking error  $r(t)$  in (4.32) are not directly measurable since they depend on the state  $x(t)$ . Taking the time derivative of (4.32) and using the definition of (4.11), the open loop error dynamics can be expressed as

$$\dot{r} = \frac{\partial f(x)}{\partial x} (r - \alpha e + \dot{x}_d) + \tilde{\Omega} \dot{\mu}(t) + \dot{\Delta}(t) \mu(t) - \ddot{x}_d + \alpha(r - \alpha e). \quad (4.33)$$

The error dynamics in (4.33) can be expressed as

$$\dot{r} = \tilde{N}(t) + N_d(t) + \tilde{\Omega} \dot{\mu}(t) + \dot{\Delta}(t) \mu(t) - e, \quad (4.34)$$

where the unknown, unmeasurable auxiliary functions,  $\tilde{N}(t)$ ,  $N_d(t) \in \mathbb{R}^n$  are defined as

$$\tilde{N} = \frac{\partial f(x)}{\partial x} (r - \alpha e + \dot{x}_d) + \alpha(r - \alpha e) + e, \quad N_d = -\ddot{x}_d \quad (4.35)$$

**Assumption 8.** *Approximate model knowledge is available such that the mismatch matrix  $\dot{\Delta}(t)$  satisfies*

$$\left\| \dot{\Delta}(t) \right\|_{i\infty} < \varepsilon_1 < 1 \quad (4.36)$$

where  $\varepsilon_1 \in \mathbb{R}^+$  is a known bounding constant, and  $\|\cdot\|_{i\infty}$  denotes the induced infinity norm of a matrix.

The motivation for the separation of terms in (4.35) are based on the fact that the following inequalities can be developed

$$\|\tilde{N}\| \leq \rho(\|z\|) \|z\|, \quad \|N_d\| \leq \zeta_{N_d}, \quad \|\dot{N}_d\| \leq \zeta_{N_{d2}} \quad (4.37)$$

where  $\zeta_{N_d}, \zeta_{N_{d2}} \in \mathbb{R}^+$  are known bounding constants;  $\rho(\cdot)$  is a positive, globally invertible, non-decreasing function; and  $z(t) \in \mathbb{R}^{2n}$  is defined as

$$z(t) \triangleq \begin{bmatrix} e^T(t) & r^T(t) \end{bmatrix}^T. \quad (4.38)$$



### 4.4.3 Closed-Loop Error System

Based on the open-loop error system dynamics in (4.34), the control term  $\mu(t)$  is designed as:

$$\dot{\mu}(t) = -k_u \|\mu(t)\| \text{sgn}(\hat{r}) - (k_s + I_{n \times n})\hat{r} - \beta \text{sgn}(\hat{r}) \quad (4.39)$$

where  $k_u, k_s, \beta \in \mathbb{R}^{n \times n}$  are positive, diagonal constant control gain matrices.

In (4.39),  $\hat{e}(t), \hat{r}(t) \in \mathbb{R}^n$  are estimates of the error signals  $e(t)$  and  $r(t)$  defined as

$$\hat{e}(t) \triangleq \hat{x}(t) - x_d(t), \quad \hat{r}(t) \triangleq \dot{\hat{e}} + \alpha \hat{e}. \quad (4.40)$$

After substituting (4.39) into (4.34), the closed-loop error dynamics is obtained as

$$\dot{r} = \tilde{N} + N_d - \tilde{\Omega} k_u \|\mu(t)\| \text{sgn}(\hat{r}) - \tilde{\Omega} (k_s + I_{n \times n}) \hat{r} - \tilde{\Omega} \beta \text{sgn}(\hat{r}) + \dot{\Delta}(t) \mu(t) - e. \quad (4.41)$$

## 4.5 Stability Analysis

**Theorem 7.** *Provided Theorem 6 is satisfied, (4.14) can be used to show that  $\hat{e}(t) \equiv e(t)$  and  $\hat{r}(t) \equiv r(t)$ ; and the robust nonlinear control law given in (4.5), (4.7), and (4.39) ensures that all system signals remain bounded throughout closed-loop operation, and that the flow field velocity profile tracking error is asymptotically regulated in the sense that*

$$\|e(t)\| \rightarrow 0 \quad \text{for} \quad t \geq t_n < \infty \quad (4.42)$$

provided the control gain  $k_u, k_s$  and  $\beta$  introduced in (4.39) are selected according to the conditions

$$\lambda_{\min}(k_s) > \frac{\rho^2(\|z\|)}{4\varepsilon\lambda_{\min}(\alpha, \epsilon)}, \quad \lambda_{\min}(k_u) \geq \frac{\varepsilon_1}{\varepsilon}, \quad \lambda_{\min}(\beta) \geq \frac{\zeta_{N_d}}{\varepsilon}. \quad (4.43)$$

*Proof.* (See Theorem 7) Let  $V(z, t) : \mathbb{R}^{2n} \times [0, \infty) \rightarrow \mathbb{R}$  be a nonnegative function defined as

$$V = \frac{1}{2}e^T e + \frac{1}{2}r^T r \quad (4.44)$$

After taking the time derivative of (4.44) and using (4.9), (4.32) and (4.41),  $\dot{V}(z, t)$  can be expressed as

$$\begin{aligned} \dot{V}(z, t) = & -\alpha e^T e + r^T \tilde{N} + r^T N_d - r^T (I_{n \times n} + \Delta)k_u \|\mu(t)\| \operatorname{sgn}(\hat{r}) \\ & - r^T (I_{n \times n} + \Delta)(k_s + I_{n \times n})\hat{r} - r^T (I_{n \times n} + \Delta)\beta \operatorname{sgn}(\hat{r}) + r^T \dot{\Delta}(t)\mu(t). \end{aligned} \quad (4.45)$$

By using the bounding inequalities in (4.35) and Assumptions 5 and 8 the above expression can be upper bounded as

$$\begin{aligned} \dot{V}(z, t) \leq & -\alpha \|e^2\| + \|r\|\rho(\|z\|)\|z\| + \zeta_{N_d}\|r\| - \varepsilon\lambda_{\min}(k_s + 1)\|r^2\| \\ & - \varepsilon\lambda_{\min}(k_u)\|r\|\|\mu\| - \varepsilon\lambda_{\min}(\beta)\|r\| + \varepsilon_1\|r\|\|\mu\| \end{aligned} \quad (4.46)$$

$$\begin{aligned} \dot{V}(z, t) \leq & -\alpha \|e^2\| - \varepsilon\|r^2\| - \varepsilon\lambda_{\min}(k_s)\|r^2\| + \rho(\|z\|)\|z\|\|r\| \\ & - [\varepsilon\lambda_{\min}(k_u) - \varepsilon_1]\|r\|\|\mu\| - [\varepsilon\lambda_{\min}(\beta) - \zeta_{N_d}]\|r\|. \end{aligned} \quad (4.47)$$

If the gains  $k_u$  and  $\beta$  satisfy the sufficient gain condition in (4.43), the bracketed terms are positive and by completing the squares the upper bound in (4.47) can be

expressed as

$$\dot{V}(z, t) \leq -\alpha\|e^2\| - \varepsilon\|r^2\| - \varepsilon\lambda_{\min}(k_s) \left[ \|r\| - \frac{\rho(\|r\|)}{2\varepsilon\lambda_{\min}(k_s)}\|z\| \right]^2 + \frac{\rho^2(\|z\|)}{4\varepsilon\lambda_{\min}(k_s)}\|z^2\| \quad (4.48)$$

$$\dot{V}(z, t) \leq - \left( \min(\alpha, \varepsilon) - \frac{\rho^2(\|z\|)}{4\varepsilon\lambda_{\min}(k_s)} \right) \|z^2\| \quad (4.49)$$

Provided the gain condition in (4.43) is satisfied, (4.44) and (4.49) can be used to show that  $V(t) \in \mathcal{L}_\infty$ ; hence,  $e(t), r(t) \in \mathcal{L}_\infty$ . Given that  $e(t), r(t) \in \mathcal{L}_\infty$ , a standard linear analysis technique can be used along with (4.30) to show that  $\dot{e}(t) \in \mathcal{L}_\infty$ . Since  $e(t), \dot{e}(t) \in \mathcal{L}_\infty$ , (4.30) can be used along with the assumption that  $x_d(t), \dot{x}_d(t) \in \mathcal{L}_\infty$  to prove that  $x(t), \dot{x}(t) \in \mathcal{L}_\infty$ . Given that  $x(t), \dot{x}(t) \in \mathcal{L}_\infty$ , (4.3) can be used along with the Assumption 5 to prove that the control input  $\mu(t) \in \mathcal{L}_\infty$ . Since  $r(t) \in \mathcal{L}_\infty$ , Assumption 5 can be used along with (4.39) to prove that  $\dot{\mu}(t) \in \mathcal{L}_\infty$ .

The definition of  $V(z, t)$  in (4.44) can be used along with the inequality (4.49) to show that  $V(z, t)$  can be upper-bounded as

$$\dot{V}(z, t) \leq -cV(z, t) \quad (4.50)$$

provided the sufficient condition in (4.43) is satisfied. The differential inequality in (4.50) can be expressed as

$$V(z, t) \leq V(z(0))e^{-ct}. \quad (4.51)$$

Hence, (4.38),(4.44) and (4.50) can be used to conclude that

$$\|e(t)\| \leq \|z(0)\|e^{-\frac{c}{2}t} \quad \forall t \in [0, \infty). \quad (4.52)$$

□

## 4.6 Simulation Results

A numerical simulation was created to test the performance of the proposed SMO. The simulation demonstrates the performance of the control law in (4.39) using the proposed observer design in (4.14). The objective of the simulation is to regulate the flow field velocity to a desired constant value. The proposed controller design is compared with a controller that does not account for uncertainty compensation (Kidambi, MacKunis, Ramos-Pedroza, & Drakunov, 2017). The results show an improvement in performance of the proposed closed-loop observer/controller system. The reduced-order flow dynamic model in the simulation uses four POD modes, but the proposed control design can be applied to ROM consisting of an arbitrary number of modes.

The flow field dynamic reduced-order model in this simulation can be expressed as (S. V. Gordeyev & Thomas, 2013)

$$\begin{aligned}
 \dot{x}_1 &= b_1 + L_{11}x_1 + Q_{141}x_1x_4 + Q_{111}x_1^2 + Q_{121}x_1x_2 + Q_{131}x_1x_3 + \mu_1 & (4.53) \\
 \dot{x}_2 &= b_2 + [L_{22} + t_2(x_2^2 + x_3^2)]x_2 + L_{23}x_3 + Q_{121}x_1x_2 + \mu_2 \\
 \dot{x}_3 &= b_3 + L_{32}x_2 + [L_{33} + t_3(x_2^2 + x_3^2)]x_3 + Q_{313}x_1x_3 + Q_{314}x_1x_4 + \mu_3 \\
 \dot{x}_4 &= b_4 + L_{41}x_1 + L_{44}x_4 + Q_{444}x_4^2 + Q_{414}x_1x_4 + Q_{424}x_2x_4 + Q_{434}x_3x_4 + \mu_4
 \end{aligned}$$

with a measurement (i.e., output) equation given by

$$y = \sum_{i=1}^4 c_i x_i \quad (4.54)$$

where,  $c_i, i = 1, \dots, 4$  are the coefficients of the output matrix and without loss of generality are assumed to be 1. Thus, based on (4.53) and (4.54), the simulation plant model is in the form of (4.11), where  $x : [0, \infty) \rightarrow \mathbb{R}^4$  and  $y : \mathbb{R}^4 \rightarrow \mathbb{R}$ . For completeness in defining the simulation plant model, the values of the constant parameters  $b_i, L_{ij}, Q_{ijk}$  for  $i, j, k = 1, \dots, 4$  are provided in Table 4.3. The initial conditions of the states and estimates are provided in Table 4.2. The observer gains (see (4.21), (4.22) and (4.29))  $\beta_{1,i}$  and  $\beta_{2,i}$ , where  $i = 1, 2, 3, 4$  denotes the POD mode are provided in Table 4.4. The control gain values (see 4.39) were selected as  $k_s = 29$ ,  $k_u = 3$ ,  $\alpha = 20$ , and  $\beta = 16$ ; and the desired constant POD modes were chosen as  $x_1 = 10$ ,  $x_2 = 8$ ,  $x_3 = -1$  and  $x_4 = -2$ . The input gain matrix  $g$  was taken to be the  $4 \times 4$  identity matrix,  $I_{4 \times 4}$ , without loss of generality. Note that, based on (4.39), the proposed control design is applicable to reduced-order models containing any constant, nonsingular input gain matrix  $g$ .

Table 4.1: SJA parameters and their estimates for all three cases

Nominal Values	$\hat{\theta}_{1i}$	32.9, 29.8, 26.7, 24.0	$\hat{\theta}_{2i}$	14.7, 13.8, 12.8, 11.7
Case 1	$\theta_{1i}^*$	32.6, 27.3, 17.1, 20.9	$\theta_{2i}^*$	13.4, 11.8, 10.6, 8.0
Case 2	$\theta_{1i}^*$	31.4, 26.4, 19.5, 21.8	$\theta_{2i}^*$	13.4, 11.7, 10.5, 10.6
Case 3	$\theta_{1i}^*$	27.1, 28.3, 22.1, 21.2	$\theta_{2i}^*$	13.2, 12.1, 10.1, 10.2

Table 4.2: Initial Conditions of the states and Estimates

States ( $x(t)$ )	10	9	6	5
Estimates ( $\hat{x}(t)$ )	8	6	3	2

Table 4.3: Parameters Used in the Simulation Plant Model

Linear Terms		Quadratic and Cubic Terms	
$b_1 = 557.7$	$L_{11} = -86.1$	$Q_{111} = 1.8$	$Q_{414} = 2.9$
$b_2 = 1016.9$	$L_{22} = -392.4$	$Q_{121} = -2.2$	$Q_{424} = -9.8$
$b_3 = 41.0$	$L_{23} = 263.9$	$Q_{131} = -2.3$	$Q_{434} = 6.3$
$b_4 = -628.9$	$L_{32} = -218.3$	$Q_{141} = -6.8$	$Q_{444} = -7.3$
	$L_{33} = -7.6$	$Q_{212} = 75.0$	
	$L_{41} = 43.4$	$Q_{313} = 5.0$	$t_2 = -2.5$
	$L_{44} = -113.5$	$Q_{314} = 3.9$	$t_3 = -0.2$

Table 4.4: Observer gains used in the simulation

$\beta_{11} = 5$	$\beta_{12} = 2$	$\beta_{13} = 3$	$\beta_{14} = 3$
$\beta_{21} = 0.1$	$\beta_{22} = 0.1$	$\beta_{23} = 0.1$	$\beta_{24} = 0.1$

To test the performance of the closed-loop system to compensate for SJA uncertainty, a Monte Carlo-type simulation was created, which shows the results of the closed-loop AFC system under three different sets of values for the uncertain SJA parameters  $\theta_{1i}^*, \theta_{2i}^*$ . Specifically, the results were obtained using randomly selected values

of the SJA parameters that deviate from nominal by up to 36%. Table 4.1 shows the deviation of each SJA parameter from its nominal value and the percentage of uncertainty associated with it. The simulation results are summarized in Fig. 4.1 - 4.7. The states  $x_1(t)$ ,  $x_2(t)$ ,  $x_3(t)$  and  $x_4(t)$  and the estimates  $\hat{x}_1(t)$ ,  $\hat{x}_2(t)$ ,  $\hat{x}_3(t)$  and  $\hat{x}_4(t)$  are shown to effectively converge to the desired constant values using the proposed estimation and control method in (6.19) and (5.20). Fig. 4.1 shows the SMO reliably estimating the true states, even under the highly oscillatory open loop state response. Fig. 4.2 shows the zoomed-in initial transient response of the SMO in the open loop. Fig. 4.3 shows the closed-loop response of the true states with and without the uncertainty compensation elements in the observer and controller structure, and Fig. 4.4 is a zoomed plot that magnifies the initial transient response. The results in Figs. 4.3 and 4.4 clearly demonstrate the improvement in closed-loop performance that is achieved by incorporating the proposed input uncertainty compensation elements in the estimation and control system. Fig. 4.5 shows the commanded control signals during closed-loop operation. Based on the reduced-order model definitions in (4.2) - (4.5), the units of the actuation signals are approximations of the SJA input voltages in [Volts](Krishnappa, 2016; Tantaroudas & Da Ronch, 2017). The experimental SJA studies in (Krishnappa, 2016) show that the commanded SJA input voltages remain well within reasonable limits throughout closed-loop operation. Fig. 4.6 and 4.7 show the Monte Carlo closed-loop response of the true states and estimates under three different uncertain SJA parameters, respectively. The results demonstrate the capability of our SMO and control method to compensate for significant SJA parametric uncertainty and to regulate the states of the reduced-order flow dynamic model to a desired profile. Physically, this can be interpreted as driving the flow field to a desired

velocity profile.

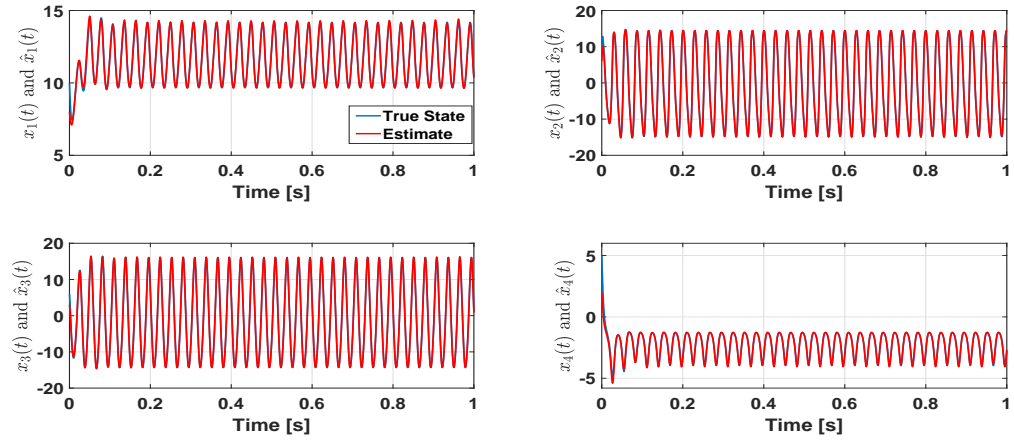


Figure 4.1: Time Evolution of the states for open-loop (uncontrolled) configuration

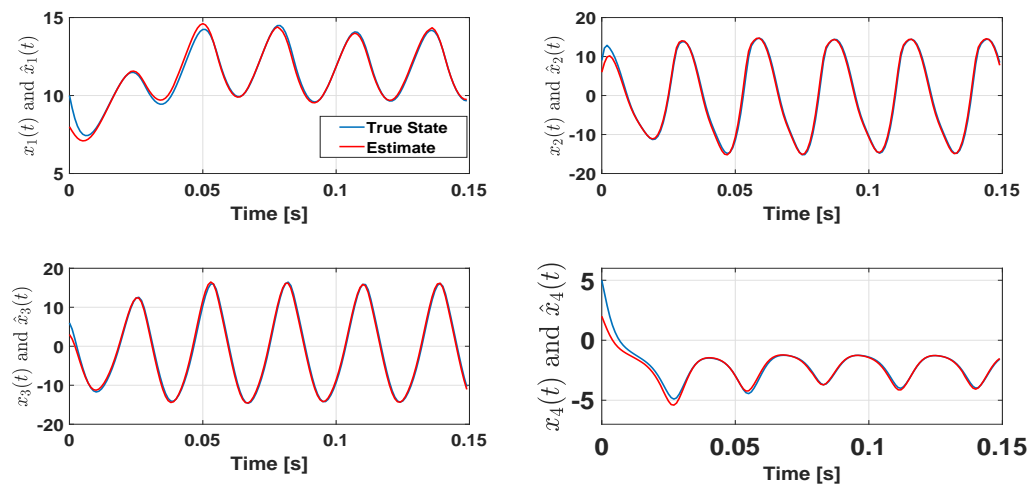


Figure 4.2: Zoomed-in plots showing the initial convergence phase of the states (blue) and the estimates (red) using the observer in (4.14).



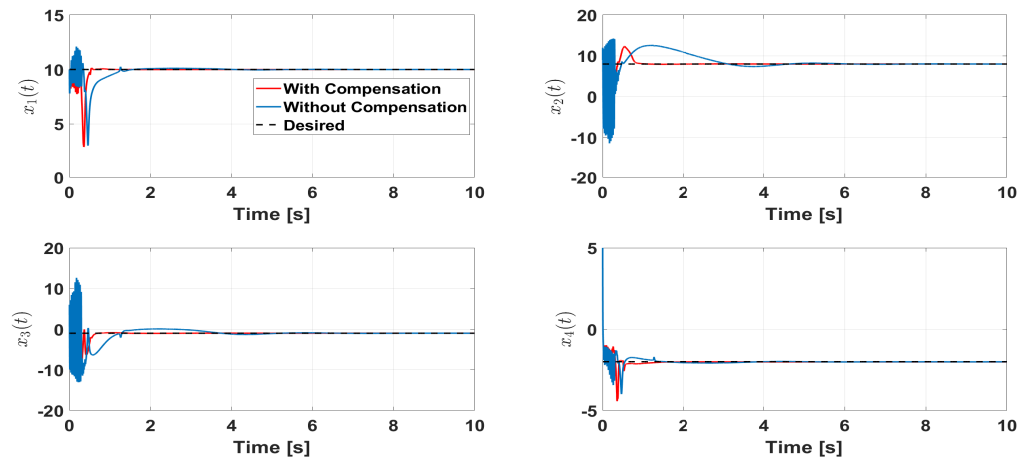


Figure 4.3: Closed-loop response of true states with and without compensation for uncertainty

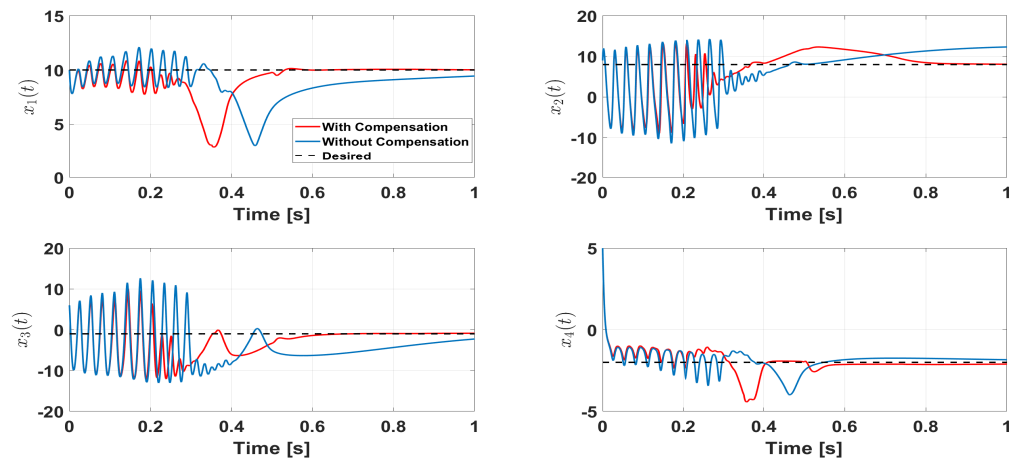


Figure 4.4: Zoomed-in plots showing the initial transient response of the closed-loop system for case 1, with (red) and without (blue) compensation for uncertainty

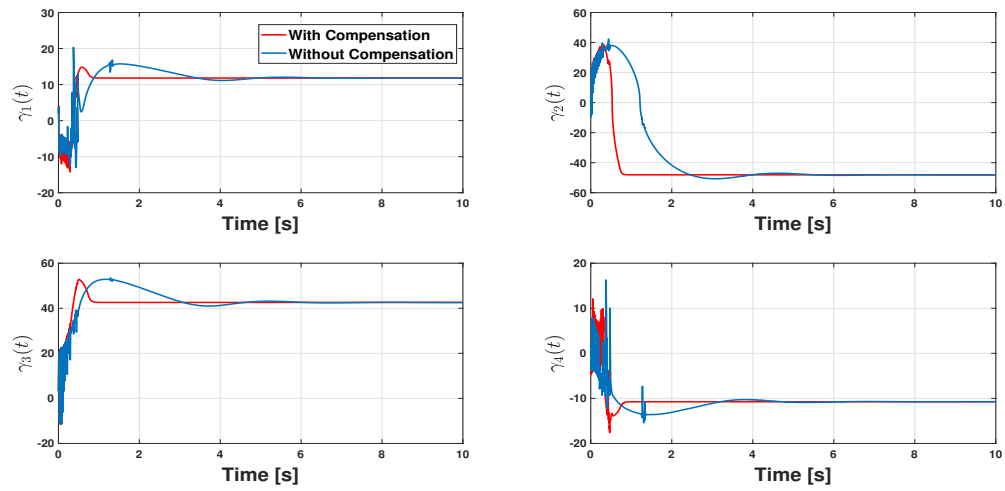


Figure 4.5: Closed-loop response of the control signal  $\gamma(t)$

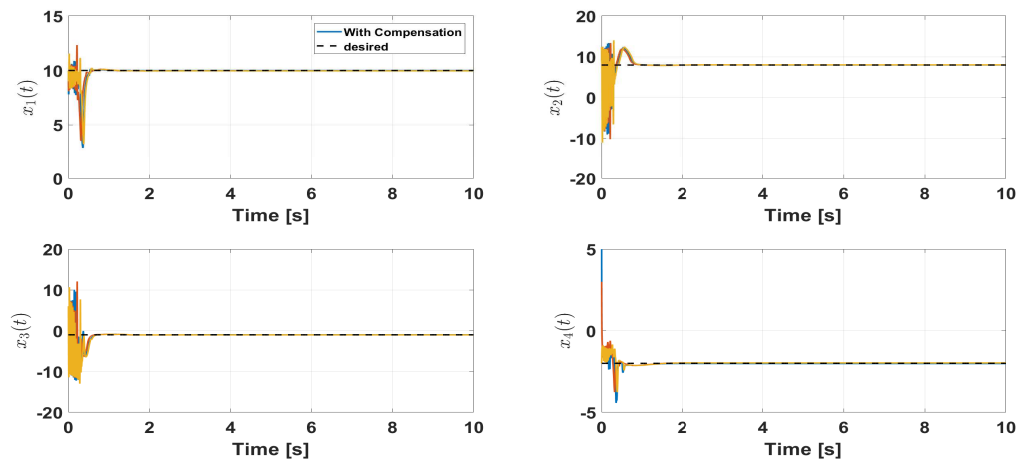


Figure 4.6: Monte Carlo-Type simulation results for three different sets of uncertain SJA parameters for actual states

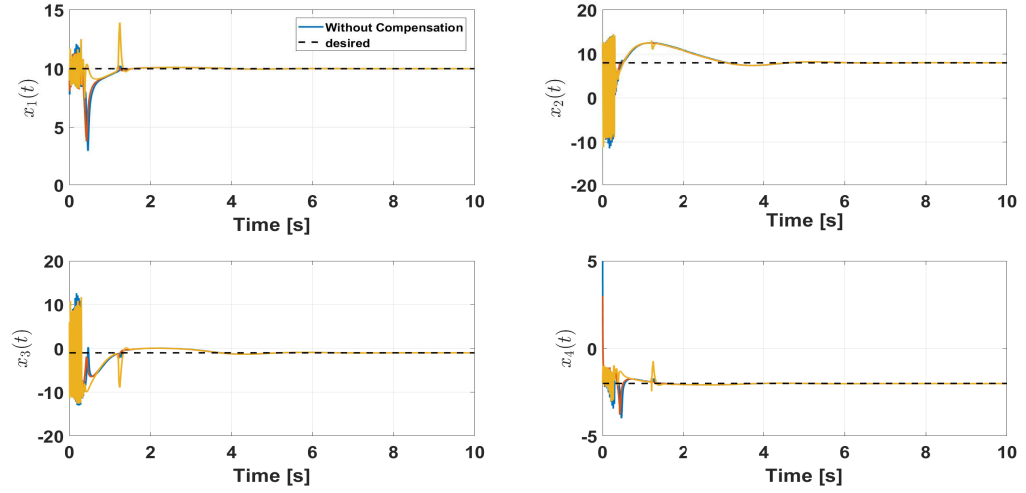


Figure 4.7: Monte Carlo-Type simulation results for three different sets of uncertain SJA parameters for estimated states

## 4.7 Conclusion

A SJA-based closed-loop active flow control system is presented, which compensates for the parametric uncertainty inherent in SJAs. To achieve the result a POD-based reduced-order model is utilized to recast the Navier-Stokes partial differential equations as a finite set of ordinary differential equations in terms of the unknown Galerkin coefficients. A sliding mode estimator is designed to estimate the unknown Galerkin coefficients in the uncertain SJA-based reduced-order model in the presence of input-multiplicative parametric uncertainty in the SJA actuator model. To the best of the authors' knowledge, this is the first time that a sliding mode estimation strategy is rigorously proven to achieve finite-time state estimation for a flow system in the pres-

ence of input-multiplicative parametric uncertainty. A rigorous proof of finite-time state estimation is provided, and the estimates are used in a nonlinear control law, which achieves asymptotic regulation of a fluid flow field to a desired time-varying velocity profile. A Lyapunov-based stability analysis is utilized to prove asymptotic regulation of the flow field velocity, and numerical simulation results are provided, which demonstrate the capability of the SJA-based closed-loop active flow control system to achieve asymptotic regulation of a fluid flow field in the presence of significant uncertainty in SJA.

# Chapter 5

## Limit Cycle Oscillation

## Suppression Using a Closed-loop

## Nonlinear Active Flow Control

## Technique

This chapter presents a nonlinear control method, which achieves simultaneous fluid flow velocity control and LCO suppression in a flexible airfoil. The proposed control design is based on a dynamic model that incorporates the fluid structure interactions (FSI) in the airfoil. The FSI describe how the flow field velocity at the surface of a flexible structure gives rise to fluid forces acting on the structure. In the proposed control method, the LCO are controlled via control of the flow field velocity near the surface of the airfoil using surface-embedded SJAs. Specifically, the flow field velocity profile is driven to a desired time-varying profile, which results in a LCO-stabilizing

fluid forcing function acting on the airfoil. A Lyapunov-based stability analysis is used to prove that the active flow control system asymptotically converges to the LCO-stabilizing forcing function that suppresses the LCO. Numerical simulation results are provided to demonstrate the performance of the proposed active flow-and-LCO suppression method.

## 5.1 Mathematical Model

In this section, the mathematical model of LCO dynamics in an airfoil and the flow field dynamics based on the Navier-Stokes equations are presented. Section 5.1.1 describes the LCO dynamics of a foil in the presence of fluid forces. In 5.1.2, a detailed description of the fluid flow model using the incompressible Navier-Stokes equations is presented and POD-based model reduction technique is utilized to recast the incompressible Navier-Stokes equations as a finite set of nonlinear ODEs. A reduced-order model for the actuated flow dynamics is presented in section 5.1.3, which will be utilized to develop the proposed closed-loop system. Fig. 5.1 shows the block diagram of the proposed closed-loop system.

### 5.1.1 LCO Dynamic Model

The equation of motion describing the LCO dynamics, in the presence of a fluid forcing function are expressed as (Torrielli, Tubino, & Solari, 2010)

$$M(s)\ddot{h}(s, t) + C(s)\dot{h}(s, t) + \kappa(s)h(s, t) = F_{fluid}(s, t) \quad (5.1)$$



(Torrielli et al., 2010)

$$F_{fluid}(s, t) = b(s)u(s, t) \quad (5.2)$$

In (5.2) the fluid forcing function is directly dependent on the fluid flow velocity field  $u(s, t)$  near the surface of the wing. The goal is to drive the flow field velocity  $u(s, t)$  to a desired time varying profiles that result in desirable fluid forcing function that suppress large LCO on a wing. The positive definite function  $b(s)$  in the fluid forcing function  $F(s, t)$  is given as

$$b(s) = \rho b c_d U(s) \quad (5.3)$$

where  $\rho$  being the density of the air/fluid,  $b$  is the cross-section characteristic size and  $c_d$  the drag coefficient. The mean wind velocity  $U(s)$  is assumed to have aligned with a symmetric axis of the structural cross-section.

**Remark 9.** *The fluid forcing function  $F_{fluid}(s, t)$  in (5.1) can be viewed as a virtual control input, which can be designed to drive the LCO to a desired state that minimizes the oscillations. In this paper, closed-loop active flow control methods will be used to drive the fluid flow dynamics (i.e, velocity) to states that produce forcing functions  $F_{fluid}(s, t)$  with desirable performance characteristics.*

### 5.1.2 Flow Dynamics Reduced-order Model

In this section, a POD-based model reduction technique is utilized to recast the incompressible Navier-Stokes equations as a finite set of nonlinear ODEs. By expressing the Navier-Stokes PDEs as a set of ODEs, an approximate dynamic model for the flow dynamics will be obtained, which is more amenable to control design.



The incompressible Navier-Stokes equations are given as (Batchelor, 2000)

$$\nabla \cdot u = 0, \quad \frac{\partial u}{\partial t} = -(u \cdot \nabla)u + \nu \nabla^2(u) - \nabla p, \quad (5.4)$$

where  $u(s, t) : \Omega \times [0, \infty) \rightarrow \mathbb{R}^3$  denotes the velocity of the flow field over a spatial domain  $s \in \Omega$ ;  $p(s, t) \in \mathbb{R}^3$  is the space- and time-dependent pressure of the flow field over  $\Omega$ ; and  $\nu \triangleq \frac{1}{\text{Re}}$  is the kinematic viscosity, where  $\text{Re}$  denotes the Reynolds number.

POD, which is often referred to as Karhunen-Loève expansion or principal component analysis, is used to obtain lower-dimensional dynamic models for fluid flow. Specifically, POD is utilized to develop a set of basis functions (POD modes) that approximates the original infinite-dimensional flow dynamic model as a finite-dimensional model in terms of the POD modes. In the POD-based model order reduction method, the flow velocity field  $u(s, t)$  is expanded as a weighted sum of actuated and unactuated POD modes defined in the spatial domain  $\Omega$ . The actuation effects are embedded in the coefficients of the Galerkin system. Specifically, the actuation effects can be included in the reduced-order model by defining the modal decomposition as (Akhtar et al., 2009; Kasnakoglu et al., 2009)

$$u(s, t) = u_0 + \sum_{i=1}^n x_i(t)\phi_i(s) + \sum_{i=1}^m \gamma_i(t)\psi_i(s) \quad (5.5)$$

In (5.5),  $\phi_i(s) \in \mathbb{R}^3$  denote the POD modes;  $x_i(t)$ ,  $i = 1, \dots, n$ , are time-varying coefficients resulting from the modal decomposition; and  $u_0 \in \mathbb{R}^3$  denotes the mean flow velocity over  $\Omega$ , where  $\psi_i(s) \in \mathbb{R}$  denote the actuation modes, and  $\gamma_i(t) \in \mathbb{R}$  denote actuation values (i.e., control inputs). Physically, the actuation values could

represent voltage input signals to SJAs, for example (MacKunis et al., 10-13 Dec., 2013). By leveraging an input separation method similar to that in (Kasnakoglu et al., 2009), the actuation modes can be defined as the modes  $\psi_i(s)$  that minimize the energy not captured in the modal expansion of the actuated flow field.

### 5.1.3 Reduced-order Model for the Actuated Flow

By substituting the actuated modal decomposition in (5.5) into (5.4), and following the procedure described in Section 2.6.2, the actuated reduced-order flow dynamics can be expressed as

$$\dot{x} = f(x) + g(x)\mu, \quad y = h(x) \quad (5.6)$$

where  $x(t) \triangleq [x_1(t), x_2(t), \dots, x_n(t)]^T \in \mathbb{R}^n$  contains the unmeasurable coefficients resulting from POD-based model order reduction,  $g(x) \in \mathbb{R}^{n \times m}$  is an input gain matrix,  $\mu(t) \triangleq [\mu_1(t), \dots, \mu_m(t)] \in \mathbb{R}^m$  denotes a subsequently defined virtual control input (e.g., resulting from  $m$  arrays of SJAs), and  $y(t) \in \mathbb{R}^p$  is the measurable output (e.g., sensor measurements of flow field velocity or pressure (MacKunis et al., 2011)). The equation in (5.6), contains the time derivative of the control signal  $\gamma$ . A detailed derivation of actuated reduced-order model in (5.6) can be found in (Lewin & Haj-Hariri, 2005; Kasnakoglu et al., 2009) and is omitted here for brevity. In the subsequent AFC design and analysis, the controller development will be presented using a virtual control signal  $\mu(t) \in \mathbb{R}^m$ , which is defined via the parameterization

$$g(x)\mu = Q_{ain}(x, \gamma) + Q_{in}(\gamma, \gamma). \quad (5.7)$$

**Remark 10.** In (5.7), the terms  $Q_{ain}(x, \gamma)$ ,  $Q_{in}(\gamma, \gamma) \in \mathbb{R}^n$  are quadratic in their

respective arguments. Since the  $\gamma(t)$  dependence is quadratic in this case, the mapping between  $\gamma(t)$  and  $\mu(t)$  will not be unique in general; but the subsequent discussion is based on the assumption that the desired, commanded control input can be delivered by the virtual control signal.

**Remark 11.** *In the current closed-loop control development, the only requirement is that the number of inputs is greater than or equal to number of outputs (i.e  $m \geq p$ ). The subsequent stability analysis and simulation section is based on a single-input single-output case where  $m = p = 1$  without loss of generality.*

**Property 4.** *If  $x(t) \in L_\infty$ , then  $f(x), g(x), h(x)$  and the first and second partial derivatives of  $f(x), g(x)$ , and  $h(x)$  with respect to  $x(t)$  exist and are bounded. Explicit definitions of  $f(x)$  and  $h(x)$  can be found in (Kidambi, Ramos-Pedroza, MacKunis, & Drakunov, 2019) and are omitted here for brevity.*

## 5.2 SJA-based Control Model Derivation

In this section, the POD-based reduced-order model for the actuated flow dynamics will be augmented to include the effects of SJA actuation. By following a similar procedure described in Section 4.2, the SJA-based flow dynamic model can be expressed as

$$\dot{x} = f(x) + \Xi_B + \mu(t) + \Delta(t)\mu(t), \quad y = Cx, \quad (5.8)$$

where the output matrix  $C \in \mathbb{R}^{1 \times n}$  for the single output case.

**Remark 12. (SJA in Flow Control)** *The actuation term  $\mu(t)$  in the flow dynamics in (5.6) is assumed to be generated by means of the virtual deflection angle*

resulting from a single SJA or an array of SJAs. The main contribution presented in this paper is the rigorous stability analysis that proves how a SJA-based closed-loop control system can be designed to achieve asymptotic regulation of a fluid forcing function in the presence of parametric uncertainty in the SJA actuator model. For further details on the use of SJA in flow control applications, the reader is referred to (Deb et al., 2008).

**Remark 13.** The control objective in this paper is based on driving the fluid forcing function to a desired fluid forcing function, which is designed in a separate step based on the objective of regulating LCO. The fluid forcing function in (5.2) can be approximated using POD as

$$F_{fluid} = b(s)u(s, t) \simeq b(s)y(t) = b(s)Cx(t), \quad (5.9)$$

where  $y(t)$  is the output of the flow dynamic model described in (5.8). The approximation accuracy can be made arbitrarily accurate by adjusting the number of POD modes which are defined in (5.5).

## 5.3 Control Development

The control objective is to design the control signal  $\mu(t)$  to regulate the fluid forcing function  $F_{fluid}(s, t)$  defined in (5.9) to a desired fluid forcing function  $F_{fluid,des}(s, t)$ , which is defined as

$$F_{fluid,des}(s, t) = b(s)y_d(t) \quad (5.10)$$

where  $y_d(t)$  is the approximate desired flow field velocity response that suppresses LCO. To quantify the control objective, a tracking error  $e(t) \in \mathbb{R}$  and an auxiliary tracking error  $r(t) \in \mathbb{R}$  are defined as

$$e(t) = F_{fluid} - F_{fluid,des}, \quad r(t) = \dot{e} + \alpha e, \quad (5.11)$$

where  $\alpha \in \mathbb{R}$  is a positive, constant control gain. Thus, the control objective can be stated mathematically as

$$e(t) \rightarrow 0. \quad (5.12)$$

### 5.3.1 Open Loop Error System

Taking the time derivative of  $r(t)$  and using the definition of (5.11), the open loop error dynamics can be expressed as

$$\dot{r} = b(s)C \left[ \frac{\partial f(x)}{\partial x} \dot{x} + \tilde{\Omega} \dot{\mu}(t) + \dot{\Delta}(t) \mu(t) \right] - \ddot{F}_{fluid,des} + \alpha(r - \alpha e), \quad (5.13)$$

where the constant uncertain matrix  $\tilde{\Omega}$  is defined in (4.9).

The error dynamics in (5.13) can be rewritten as

$$\dot{r} = \tilde{N}(t) + N_d(t) + \tilde{\Omega}_1 \dot{\mu}(t) + b(s)C \dot{\Delta}(t) \mu(t) - e, \quad (5.14)$$

where  $\tilde{\Omega}_1 \triangleq b(s)C\tilde{\Omega}$  and the unknown, unmeasurable auxiliary functions,  $\tilde{N}(t)$ ,

$N_d(t) \in \mathbb{R}$  are defined as

$$\tilde{N} = b(s)C \frac{\partial f(x)}{\partial x} \dot{x} + \alpha(r - \alpha e) + e, \quad (5.15)$$

$$N_d = -\ddot{F}_{fluid,des} \quad (5.16)$$

**Assumption 10.** *Approximate model knowledge is available such that the mismatch matrix  $\dot{\Delta}(t)$  satisfies*

$$b(s)C \left\| \dot{\Delta}(t) \right\|_{i\infty} < \varepsilon_1 < 1 \quad (5.17)$$

where  $\varepsilon_1 \in \mathbb{R}^+$  is a known bounding constant, and  $\|\cdot\|_{i\infty}$  denotes the induced infinity norm of a matrix.

The motivation for the separation of terms in (5.14), (5.15) and (5.16) is based on the fact that the following inequalities can be developed

$$\|\tilde{N}\| \leq \rho(\|z\|) \|z\|, \quad \|N_d\| \leq \zeta_{N_d}, \quad \|\dot{N}_d\| \leq \zeta_{\dot{N}_d}, \quad (5.18)$$

where  $\rho(\cdot)$  is a positive, globally invertible non-decreasing function; and  $\zeta_{N_d}, \zeta_{\dot{N}_d} \in \mathbb{R}^+$  are known bounding constants; and  $z(t) \in \mathbb{R}^2$  is defined as

$$z(t) \triangleq \begin{bmatrix} e(t) & r(t) \end{bmatrix}^T. \quad (5.19)$$

### 5.3.2 Closed-Loop Error System

Based on the open-loop error system dynamics in (5.14), the control  $\mu(t)$  is designed via

$$\dot{\mu}(t) = -k_u \|\mu(t)\| \operatorname{sgn}(r) - (k_s + 1)r - \beta \operatorname{sgn}(r) \quad (5.20)$$

where  $k_u, k_s, \beta \in \mathbb{R}$  are positive, constant control gains. After substituting (5.20) into (5.14), the closed-loop error dynamics are obtained as

$$\begin{aligned} \dot{r} = & \tilde{N} + N_d - \tilde{\Omega}_1 k_u \|\mu(t)\| \operatorname{sgn}(r) - \tilde{\Omega}_1 (k_s + 1)r \\ & - \tilde{\Omega}_1 \beta \operatorname{sgn}(r) + b(s)C\dot{\Delta}(t)\mu(t) - e. \end{aligned} \quad (5.21)$$

## 5.4 Stability Analysis

**Theorem 8.** *The robust nonlinear control law given in (4.5), (4.7), and (5.20) ensures that all system signals remain bounded throughout closed-loop operation, and that the fluid forcing function tracking error is asymptotically regulated in the sense that*

$$\|e(t)\| \rightarrow 0 \quad \text{as} \quad t \rightarrow \infty, \quad (5.22)$$

*provided the control gain  $k_u, k_s$  and  $\beta$  introduced in (5.20) are selected according to the conditions*

$$k_s > \frac{\rho^2(\|z\|)}{4\epsilon \min(\alpha, \epsilon)}, \quad k_u \geq \frac{\epsilon_1}{\epsilon}, \quad \beta \geq \frac{\zeta_{N_d}}{\epsilon}. \quad (5.23)$$

*Proof.* Let  $V(z, t) : \mathbb{R}^2 \rightarrow \mathbb{R}$  be a non-negative function defined as

$$V = \frac{1}{2}e^2 + \frac{1}{2}r^2 \quad (5.24)$$

After taking the time derivative of (5.24) and using (4.9), (5.11) and (5.21),  $\dot{V}(z, t)$  can be expressed as

$$\begin{aligned} \dot{V}(z, t) = & -\alpha e^2 + r\tilde{N} + rN_d - r\tilde{\Omega}_1 k_u \|\mu(t)\| \operatorname{sgn}(r) \\ & - r\tilde{\Omega}_1(k_s + 1)r - r\tilde{\Omega}_1 \beta \operatorname{sgn}(r) + b(s)Cr\dot{\Delta}(t)\mu(t). \end{aligned} \quad (5.25)$$

By using the bounding inequalities in (5.17), (5.18) and Assumptions 5, 10 and Property 3, the expression in (5.25) can be upper bounded as

$$\begin{aligned} \dot{V}(z, t) \leq & -\alpha|e|^2 + |r|\rho(|z|)|z| + \zeta_{N_d}|r| - \varepsilon(k_s + 1)|r|^2 \\ & - \varepsilon k_u |r||\mu| - \varepsilon\beta|r| + \varepsilon_1|r||\mu| \end{aligned} \quad (5.26)$$

$$\begin{aligned} \dot{V}(z, t) \leq & -\alpha|e|^2 - \varepsilon|r|^2 - \varepsilon(k_s)|r|^2 + \rho(|z|)|z||r| \\ & - [\varepsilon k_u - \varepsilon_1]|r||\mu| - [\varepsilon\beta - \zeta_{N_d}]|r|. \end{aligned} \quad (5.27)$$

If the gains  $k_u$  and  $\beta$  satisfy the sufficient gain conditions in (5.23), the bracketed terms are positive, and by completing the squares the upper bound in (5.27) can be expressed as

$$\dot{V}(z, t) \leq -\alpha|e|^2 - \varepsilon|r|^2 - \varepsilon k_s \left[ |r| - \frac{\rho(|z|)}{2\varepsilon k_s} |z| \right]^2 + \frac{\rho^2(|z|)}{4\varepsilon k_s} |z|^2 \quad (5.28)$$



$$\dot{V}(z, t) \leq - \left[ \min(\alpha, \epsilon) - \frac{\rho^2(\|z\|)}{4\varepsilon(k_s)} \right] \|z\|^2 \quad (5.29)$$

Provided the  $k_s$  gain condition in (5.23) is satisfied, (5.24) and (5.29) can be used to show that  $V(t) \in \mathcal{L}_\infty$ ; hence,  $e(t), r(t) \in \mathcal{L}_\infty$ . Given that  $e(t), r(t) \in \mathcal{L}_\infty$ , a standard linear analysis technique can be used along with (5.11) to show that  $\dot{e}(t) \in \mathcal{L}_\infty$ . Since  $e(t), \dot{e}(t) \in \mathcal{L}_\infty$ , (5.9), (5.10) and (5.11) can be used along with the assumption that  $y_d(t), \dot{y}_d(t) \in \mathcal{L}_\infty$  to prove that  $y(t), \dot{y}(t) \in \mathcal{L}_\infty$ . Given that  $y(t), \dot{y}(t) \in \mathcal{L}_\infty$ , (5.6) and Condition 2 can be used to prove that  $x(t), \dot{x}(t) \in \mathcal{L}_\infty$ . Since  $x(t), \dot{x}(t) \in \mathcal{L}_\infty$ , (5.6) can be used along with Property 4 to prove that the control input  $\mu(t) \in \mathcal{L}_\infty$ . Given that  $r(t), \mu(t) \in \mathcal{L}_\infty$ , (5.20) can be used to prove that  $\dot{\mu}(t) \in \mathcal{L}_\infty$ .

The definition of  $V(z, t)$  in (5.24) can be used along with the inequality (5.29) to show that  $V(z, t)$  can be upper-bounded as

$$\dot{V}(z, t) \leq -cV(z, t) \quad (5.30)$$

provided the sufficient condition in (5.23) is satisfied. The differential inequality in (5.30) can be solved as

$$V(z, t) \leq V(z(0))e^{-ct}. \quad (5.31)$$

Hence, (5.31) can be used to conclude that

$$\|e(t)\| \leq \|z(0)\|e^{-\frac{c}{2}t} \quad \forall t \in [0, \infty). \quad (5.32)$$

□

## 5.5 Simulation Results

A numerical simulation was performed to demonstrate the performance of the proposed control law. The simulation tests the capability of the proposed controller design in (5.20) to regulate fluid forcing function in (5.2) to desired fluid forcing function that suppresses the plunging LCO. Even though the closed-loop stability analysis proposed here is for a general case, the simulation presented in this section is for a specific case where  $p = m = 1$ , without loss of generality.

### 5.5.1 Flow parameters

The system parameters and the flow field dynamic reduced-order model equations utilized for the simulated flow environment are summarized in section 4.6.

The control gain values were selected as  $k_s = 25$ ,  $k_u = 8$ ,  $\alpha = 10$ , and  $\beta = 15$ . Fig. 5.2 shows the open-loop plunging response of the LCO and Fig. 5.3 shows the closed-loop regulation of plunging LCO using the proposed control law. Fig. 5.4 shows the control magnitude during the closed-loop operation. Future work will address the chattering in the control response.

### 5.5.2 LCO parameters

The details of the LCO dynamic model utilized in the simulation are summarized in (Ramos-Pedroza et al., 2017). Table 5.1 summarizes the physical parameters used in the LCO dynamic model.

Table 5.1: Dynamic parameters and geometric dimensions of the LCO Model

$\rho = 1.225 \text{ kg/m}^3$	$a = -0.6$	$c_{m_\alpha} = -0.635$
$m = 12.387 \text{ kg}$	$b = 0.125 \text{ m}$	$v = 13 \text{ m/s}$
$C_\alpha = 0.036 \text{ kg} \cdot \text{m}^2/\text{s}$	$c_{l_\beta} = 3.358$	$s_p = 0.6 \text{ m}$
$I_\alpha = 0.065 \text{ kg} \cdot \text{m}$	$C_h = 27.43 \text{ kg/s}$	$c_{l_\alpha} = 6.28$
$K_h = 2844.4 \text{ N/m}$	$c_{m_\beta} = -0.635$	$x_a = 0.2847$

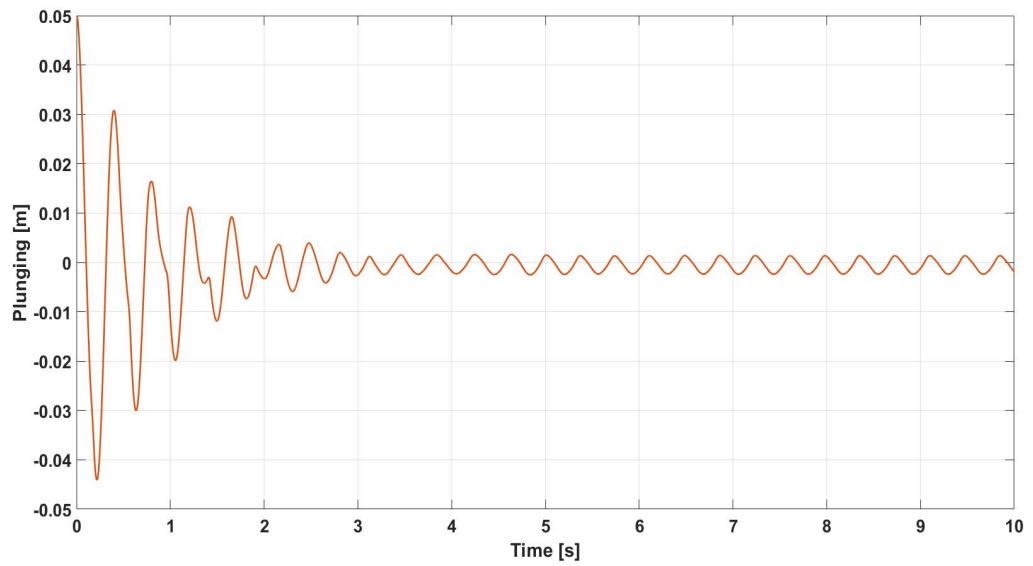


Figure 5.2: Open-loop plunging time response of the LCO simulated system

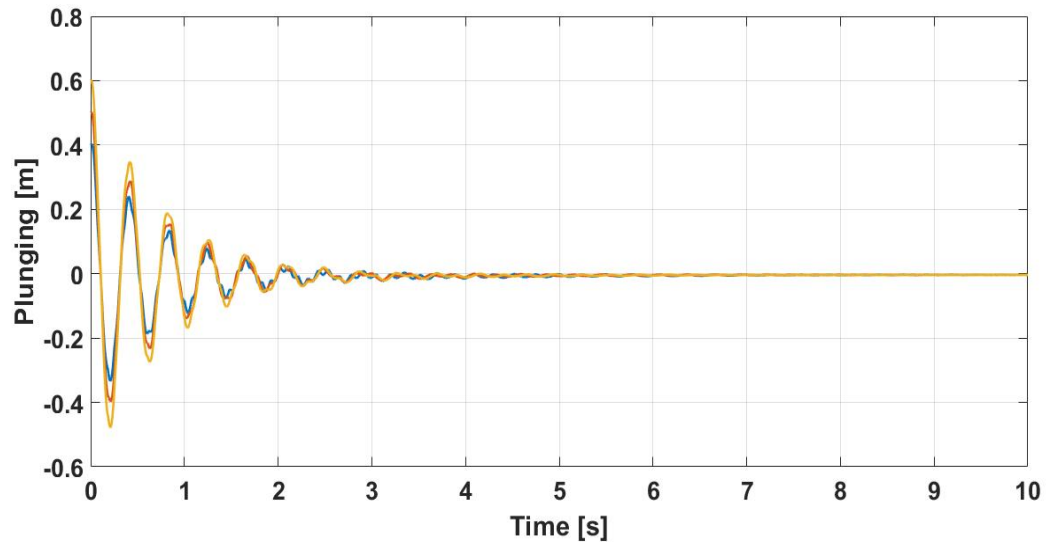


Figure 5.3: Closed-loop time response of LCO plunging with different initial conditions

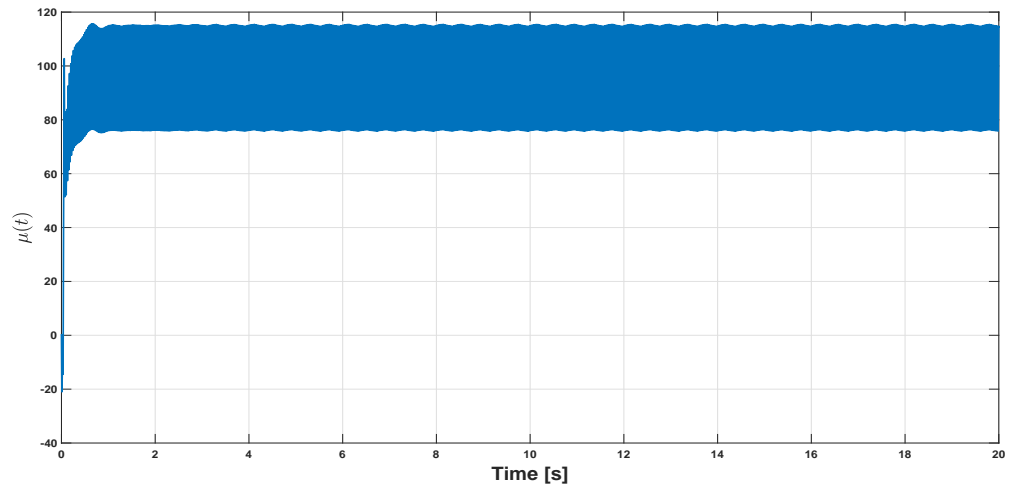


Figure 5.4: Control magnitude during closed-loop operation

## 5.6 Conclusion

A nonlinear control method is developed, which is rigorously proven to asymptotically regulate the velocity of a fluid flow field to a desired velocity profile, that results in generating the desired fluid forcing function to suppress LCO in an airfoil. To achieve the result, a LCO dynamic model is utilized along with a FSI model and a reduced order flow model. The reduced order flow model is obtained by POD-based model reduction technique, in which the Navier-Stokes PDEs are recast as a set of nonlinear ODEs. A Lyapunov-based stability analysis is utilized to prove asymptotic regulation of the fluid forcing function that drives LCO suppression. Numerical simulation results are provided, which demonstrate the capability of the proposed control algorithm to achieve asymptotic regulation of LCO.

## Chapter 6

# A Hierarchical Sliding Mode Estimation Method Using a Differential Inclusions-based Analysis

In this chapter, a sliding mode observer (SMO) design and convergence analysis are presented in this paper, which includes a rigorous treatment to address multiple discontinuities in the resulting estimation error dynamics. In an extension of our previous SMO results, the current work provides a non-trivial reworking of the SMO estimation error system development and stability analysis that incorporates differential inclusions. The specific contributions presented in this paper beyond the previous work include: **1)** A differential inclusions-based analysis of the SMO, which incorporates the set-valued definition of the discontinuous signum function; **2)** An ex-

panded derivation of the estimation error dynamics, which emphasizes advantageous properties particular to our SMO structure; **3)** A Lyapunov-based stability analysis of the SMO, that rigorously incorporates the multiple discontinuities in the estimation error dynamics. The Lyapunov-based stability analysis proves that the SMO achieves finite-time estimation of the complete state vector, where the output equation is in a nonstandard mathematical form. To test the performance of the SMO, numerical simulation results are also provided, which demonstrate the capability of the SMO to estimate the state of a fluid flow dynamic system using only a single sensor measurement of the flow field velocity.

## 6.1 Preliminaries

In this section, we provide background on the mathematical tools utilized to address the challenges involved in analyzing the behavior of differential equations with discontinuous RHS. While the generalized solutions of differential equations with continuous RHS are well known, the presence of discontinuities necessitates modified mathematical approaches to obtain the solutions. In this paper, we utilize *differential inclusions* to handle the challenge of analyzing the stability of a SMO method, where the equations of the error dynamics contain discontinuities.

### 6.1.1 Mathematical Definitions

Consider a nonlinear system defined as

$$\dot{x} = f(x, t) \tag{6.1}$$

where  $x(t) \in \mathcal{X} \subset \mathbb{R}^n$  denotes the state vector,  $f : \mathcal{X} \times [0, \infty) \rightarrow \mathbb{R}^n$  is Lebesgue measurable and essentially locally bounded, uniformly in  $t$ ; and  $\mathcal{X}$  is an open and connected set. The definition of a solution to (6.1) is well established for the case where  $f$  is Lipschitz continuous; however, this basic definition is not applicable if there exists a discontinuity in  $f$  at any point in  $\mathcal{X}$ . To address the case where  $f$  contains discontinuities, differential inclusions can be utilized to obtain the generalized solution of (6.1) at a point of discontinuity by analyzing the behavior of the derivative of  $f$  at neighboring points (Filippov, 1988; Krasovskii, 1963).

**Remark 14.** (Stability of Systems with Discontinuous RHS) *The stability of closed-loop systems in the form of (6.1) with continuous right-hand sides can be analyzed using existing Lyapunov theory (Khalil, 1996; Slotine & Li, 1991). However, these theorems must be modified to analyze systems with discontinuous RHS (Fischer et al., 2013; Guo & Huang, 2009). The differences between Lyapunov analyses for systems with continuous and discontinuous systems include: differential equations are replaced with differential inclusions, points are replaced with sets, and gradients are replaced by generalized gradients.*

The following definitions are provided to facilitate the subsequent analysis.

**Definition 5.** (Filippov Solution) *(Filippov, 1988; Shevitz & Paden, 1994) A function  $x(t)$  is called a solution to (1) on the interval  $[0, \infty)$  if  $x(t)$  is absolutely continuous and for almost all  $t \in [0, \infty)$*

$$\dot{x} = K[f](x(t), t) \tag{6.2}$$

where  $K[f](x(t), t)$  denotes an upper semi-continuous, nonempty, compact and convex



valued map on  $\mathcal{X}$ , defined as

$$K[f](x(t), t) \triangleq \bigcap_{\epsilon > 0} \bigcap_{\mu N = 0} \overline{\text{co}} f(B(x(t), \epsilon) - N, t) \quad (6.3)$$

where  $\bigcap_{\mu N = 0}$  denotes the intersection over sets  $N$  of Lebesgue measure zero, and  $\overline{\text{co}}$  denotes convex closure. In (6.3),  $B(x(t), \epsilon)$  is the open set defined as

$$B(x(t), \epsilon) \triangleq \{v \in \mathbb{R}^n \mid \|x(t) - v\| < \epsilon\}. \quad (6.4)$$

A simple example to illustrate the definitions in (6.2) - (6.4) is provided in the subsequent Section 6.1.2.

**Definition 6.** (Directional Derivative) (*Kaplan, 1991*) The right directional derivative of a function  $f : R^m \rightarrow R^n$ , at  $x \in \mathbb{R}^m$  in the direction of  $v \in R^m$  is defined as

$$f'(x, v) = \lim_{t \rightarrow 0^+} \frac{f(x + tv) - f(x)}{t}. \quad (6.5)$$

The generalized directional derivative of  $f$  at  $x$  in the direction of  $v$  is defined as

$$f^0(x, v) = \lim_{y \rightarrow x} \sup_{t \rightarrow 0^+} \frac{f(y + tv) - f(y)}{t}. \quad (6.6)$$

**Definition 7.** (Regular Function) (*Clarke, 1983*) A function  $f : R^m \rightarrow R^n$  is regular at  $x \in R^m$ , if the right directional derivative of  $f$  at  $x$  in the direction of  $v$  exists  $\forall v \in R^m$ , and  $f'(x, v) = f^0(x, v)$ .

**Definition 8.** (Clarke's Generalized Gradient) (*Clarke, 1983*) Given a function  $V : \mathbb{R}^n \times [0, \infty) \rightarrow \mathbb{R}$ , where  $V(x, t)$  is locally Lipschitz in  $(x, t)$ , the generalized gradient

of  $V$  at  $(x, t)$  is defined as

$$\partial V(x, t) = \overline{\text{co}} \{ \lim \nabla V(x_i, t_i) \mid (x_i, t_i) \rightarrow (x, t), (x_i, t_i) \notin \Omega_V \} \quad (6.7)$$

where  $\Omega_V$  denotes the set of measure zero where the gradient of  $V$  is not defined.

**Lemma 2.** (Chain Rule) (*Paden & Sastry, 1987; Shevitz & Paden, 1994*) Let  $V : \mathbb{R}^n \times [0, \infty) \rightarrow \mathbb{R}$  be a regular, Lipschitz function. If  $x(t)$  a Filippov solution of  $\dot{x} = f(x, t)$ , then  $\frac{d}{dt}V(x(t), t)$  exists almost everywhere (a.e.) for  $t \geq 0$ , and  $\dot{V}(x(t), t) \stackrel{\text{a.e.}}{\in} \dot{\hat{V}}(x(t), t)$  where

$$\dot{\hat{V}}(x(t), t) \triangleq \bigcap_{\xi \in \partial V(x(t), t)} \xi^T \begin{bmatrix} K[f](x(t), t) \\ 1 \end{bmatrix}. \quad (6.8)$$

*Proof of Lemma 2 can be found in (Shevitz & Paden, 1994) and (Paden & Sastry, 1987) and is omitted for brevity.*

### 6.1.2 Simple Example of Differential Inclusion

The concept of Filippov's solution is illustrated using a simple scalar differential equation (Paden & Sastry, 1987)

$$\dot{x} = -\text{sgn}(x); \quad x(0) = 1. \quad (6.9)$$

The state is 1 at time 0 and moves at constant velocity -1 until it reaches 0 and remains at the point of discontinuity in the right hand side of (6.9). In fact, this is Filippov's solution to (6.9). Since  $B(0, \epsilon)$ ,  $\epsilon > 0$ , an open interval containing the origin, intersects both  $(-\infty, 0)$  and  $(0, \infty)$  on the sets of positive measure, we have

that  $K[-sgn](0) = \overline{co}\{-1, 1\} = [-1, 1]$ . For general  $x$ , the differential inclusion (6.2) and (6.4) becomes

$$\dot{x} \in -SGN(x) \quad (6.10)$$

where  $SGN$  is the set-valued sign function defined as (Paden & Sastry, 1987)

$$SGN(x) \triangleq \begin{cases} \{1\} & \text{if } x > 0 \\ [-1, 1] & \text{if } x = 0 \\ \{-1\} & \text{if } x < 0 \end{cases} \cdot \quad (6.11)$$

## 6.2 Observer Design

This section presents a SMO design for a class of autonomous, nonlinear systems. Specifically, a rigorous analysis is utilized to derive a set of estimation error dynamic equations, the right-hand side of which contains discontinuities resulting from the use of the  $sgn(\cdot)$  function in the SMO equation. A detailed analysis is also provided to define the sets within which discontinuities exist.

### 6.2.1 Dynamic Model and Properties

Consider a class of nonlinear systems given by

$$\dot{x} = f(x) \quad (6.12)$$

$$y = h(x) \quad (6.13)$$

where  $x : [0, \infty) \rightarrow \mathbb{R}^n$  denotes the state vector, and  $y : \mathbb{R}^n \rightarrow \mathbb{R}$  is the system output (e.g., sensor measurement). In (6.12) and (6.13),  $f : \mathbb{R}^n \rightarrow \mathbb{R}^n$  and  $h : \mathbb{R}^n \rightarrow \mathbb{R}$  are

sufficiently smooth vector functions as described in the subsequent Assumption 11.

To facilitate the subsequent observer design and convergence analysis, an auxiliary measurement vector  $H : \mathbb{R}^n \rightarrow \mathbb{R}^n$  is defined as (S. V. Drakunov, 1992; Kidambi, Ramos-Pedroza, MacKunis, & Drakunov, 2016; Kidambi et al., 2017, 2019)

$$H(x) \triangleq \begin{bmatrix} h_1(x) & \cdots & h_n(x) \end{bmatrix}^T \quad (6.14)$$

where

$$h_1(x) = h(x) \quad (6.15)$$

$$h_{i+1}(x) = \frac{\partial h_i(x)}{\partial x} f(x). \quad (6.16)$$

The function  $h_{i+1}(x)$  is the  $i^{\text{th}}$  Lie (directional) derivative of  $h(x)$  along the trajectories of the system described in (6.12). Thus, the elements of  $H(x)$  can be expressed as

$$h_i(x) = L_f^{i-1} h(x) \quad (6.17)$$

Based on (6.12) and (6.15) it follows that, if  $x$  is a solution of (6.12), then

$$\frac{d}{dt} h_i(x) = h_{i+1}(x) \quad (6.18)$$

**Assumption 11.** *If  $x(t) \in \mathcal{L}_\infty$ , the first  $n - 1$  partial derivatives of  $f(x)$  and first  $n$  partial derivatives of  $h(x)$  exist and are bounded in the sense that  $\frac{\partial^{n-1} f(x)}{\partial x^{n-1}} \in \mathcal{L}_\infty$  and  $\frac{\partial^n h(x)}{\partial x^n} \in \mathcal{L}_\infty$ .*

The differentiability requirements described in Assumption 11 stem from the use of repeated Lie derivatives in the observer structure as defined explicitly in Equations

(6.15) - (6.18), along with the subsequent bounding conditions in Inequality (6.33). Although Assumption 11 is fairly restrictive, our subsequent Simulation Results section presents an example of a practical system (i.e., reduced-order fluid flow dynamic model) which satisfies Assumption 11. Future work will investigate extensions of the current observer design, in which Assumption 11 can be relaxed or eliminated.

**Assumption 12.** *For a given domain  $\mathcal{X}_0 \subset \mathbb{R}^n$  of initial conditions of the system (6.12), all solutions of (6.12) belong to the open one-component domain  $\mathcal{X} \subset \mathbb{R}^n$ , for all  $t \in [0, \infty)$ .*

**Condition 4 (Observability).** *The Jacobian  $\mathcal{O} \triangleq \frac{\partial H(x)}{\partial x}$  of the continuous map  $H(x)$  is nondegenerating in  $\mathcal{X}$  in the sense that*

$$|\det \mathcal{O}| \geq \delta > 0$$

*for some  $\delta$  and for every  $x \in \mathcal{X}$ .*

From Condition 4, the Jacobian matrix  $\mathcal{O}$  is invertible. This fact will be utilized in the subsequent SMO design.

### 6.2.2 Observer Design

Under Condition 4, an observer that estimates the full state  $x$  of the system in (6.12) using only output measurements  $y$  can be designed as

$$\dot{\hat{x}} = \mathcal{O}^{-1}(\hat{x}) M(\hat{x}) \operatorname{sgn}(\Phi(t) - H(\hat{x})) \quad (6.19)$$

where  $\mathcal{O}(\cdot)$  is introduced in Condition 4, and  $\hat{x} : [0, \infty) \rightarrow \mathbb{R}^n$  denotes the estimate of the state  $x$  in (6.12). In (6.19)  $\text{sgn}(\cdot)$  operates element-wise on the vector argument so that  $\text{sgn}(\zeta) \triangleq [\text{sgn}(\zeta_1) \text{sgn}(\zeta_2) \cdots \text{sgn}(\zeta_n)]^T \forall \zeta \in \mathbb{R}^n$ . Also in (6.19),  $M : \mathbb{R}^n \rightarrow \mathbb{R}^{n \times n}$  denotes a diagonal matrix with positive elements defined as

$$M(\hat{x}) = \text{diag}(m_1(\hat{x}), \dots, m_n(\hat{x})) \quad (6.20)$$

where  $m_i : \mathbb{R}^n \rightarrow \mathbb{R}^+$ , for  $i = 1, \dots, n$ , denote control gains, which could be constant or could depend on  $\hat{x}$  in general. In (6.19),  $\Phi : [0, \infty) \rightarrow \mathbb{R}^n$  is defined as

$$\Phi(t) = [\phi_1(t), \dots, \phi_n(t)]^T \quad (6.21)$$

where the elements  $\phi_i(t)$  are defined via the recursive relationship

$$\phi_1(t) = y(t) \quad (6.22)$$

$$\phi_{i+1}(t) = m_i(\hat{x}) \text{sgn}(\phi_i(t) - h_i(\hat{x})) \quad (6.23)$$

for  $i = 1, \dots, n - 1$ .

**Remark 15.** (Measurable Auxiliary Signals) *Based on (6.22),  $\phi_1(t)$  is simply the measurable output of the system in (6.12) and (6.13). Further, the recursion relation in (6.23) ensures that the auxiliary signals  $\phi_2(t), \phi_3(t), \dots, \phi_n(t)$  are also measurable throughout observer operation. Indeed, it follows from (6.23) that the auxiliary signals depend only on  $y(t)$  and  $\hat{x}(t)$ .*

Through judicious design of the gain matrix  $M$ , it can be shown that the observer

in (6.19) estimates the state  $x(t)$  in a finite time interval. The choice of  $M$  is based on the region  $\mathcal{X}_0$  of initial conditions for the system (6.12) and on the upper bounds of  $h_i(x)$ . This proof is provided via Lyapunov-based stability analysis in the subsequent Section 6.4.

## 6.3 SMO Estimation Error Dynamics

### 6.3.1 Objective

Under Condition 4, the map  $H$  in (6.14) is a diffeomorphism (i.e., there is a one-to-one correspondence between  $x$  and  $H$ ). Since  $H$  is a diffeomorphism, it follows that  $H(x) - H(\hat{x}) \rightarrow 0 \Rightarrow x - \hat{x} \rightarrow 0$ . Thus, to quantify the estimation objective, it is sufficient to define the estimation error as

$$e(t) = H(x) - H(\hat{x}) \tag{6.24}$$

where  $e(t) \triangleq [e_1(t) \cdots e_n(t)]^T$  represents the estimation error. The estimation objective can therefore be mathematically stated as

$$\|e(t)\| \rightarrow 0, \tag{6.25}$$

where  $\|\cdot\|$  in (6.25) denotes the standard Euclidean norm (or 2-norm). Note that the choice to use the 2-norm is arbitrary, and the subsequent stability analysis could be used to prove convergence of the observer error using the p-norm definition in general.

### 6.3.2 Estimation Error Dynamics

The estimation error dynamics can be obtained by taking the time derivative of (6.24) as

$$\dot{e}(t) = \frac{\partial H(x)}{\partial x} \dot{x} - \frac{\partial H(\hat{x})}{\partial x} \dot{\hat{x}}. \quad (6.26)$$

After using (6.1) and (6.19), the estimation error dynamics can be expressed as

$$\dot{e}(t) = \frac{\partial H(x)}{\partial x} f(x) - M(\hat{x}) \operatorname{sgn}(\Phi(t) - H(\hat{x})) \quad (6.27)$$

where the fact that  $\mathcal{O}(\hat{x}) = \left. \frac{\partial H(x)}{\partial x} \right|_{x=\hat{x}}$  was utilized.

**Remark 16.** *Note that the estimation error dynamic equation in (6.27) is in the form of (6.1), where the RHS includes discontinuities resulting from the use of the sliding mode observer introduced in (6.19). The use of differential inclusions provides for existence of solutions, and the subsequent estimator convergence analysis will be provided utilizing the definition of the Filippov solution presented in Section 6.1.*

To facilitate the subsequent Lyapunov-based stability analysis, the definitions in (6.15) and (6.16) will be used to rewrite the error dynamics in (6.27) as

$$\begin{bmatrix} \dot{e}_1(t) \\ \dot{e}_2(t) \\ \vdots \\ \dot{e}_n(t) \end{bmatrix} = \begin{bmatrix} h_2(x) \\ h_3(x) \\ \vdots \\ h_{n+1}(x) \end{bmatrix} - \begin{bmatrix} m_1(\hat{x}) \operatorname{sgn}(\sigma_1) \\ m_2(\hat{x}) \operatorname{sgn}(\sigma_2) \\ \vdots \\ m_n(\hat{x}) \operatorname{sgn}(\sigma_n) \end{bmatrix} \quad (6.28)$$

where  $\sigma_i : \mathbb{R}^n \rightarrow \mathbb{R}$  denote sliding surfaces for the  $i^{\text{th}}$  estimation error that are defined



explicitly as

$$\sigma_i \triangleq \phi_i(t) - h_i(\hat{x}) \quad (6.29)$$

for  $i = 1, \dots, n$ , where  $\phi_i(t)$  are defined in (6.22) and (6.23). The estimation error dynamic equations in (6.28) can be rewritten in the compact form

$$\dot{e}_i(t) = h_{i+1}(x) - m_i(\hat{x}) \operatorname{sgn}(\sigma_i) \quad (6.30)$$

for  $i = 1, \dots, n$ .

**Property 5.** (Sliding Surface Definition) *Based on the definitions in (6.13), (6.15), (6.22) and (6.29), it follows by definition that*

$$\sigma_1(t) = e_1(t). \quad (6.31)$$

Property 5 will be utilized in the subsequent convergence analysis of the proposed SMO.

### 6.3.3 Hierarchical Analysis of Estimation Error Dynamics

The motivation for expressing the estimation error dynamics in the forms given in (6.28) and (6.30) is based on the recursive structure of the auxiliary signals in (6.22) and (6.23). The decoupling between the individual elements of the estimation error dynamics for  $e_i(t)$ , for  $i = 1, \dots, n$ , is highlighted in (6.30) to facilitate the hierarchical strategy of the convergence analysis in the subsequent Stability Analysis Section.

**Theorem 9.** (Sliding Surface Convergence) *The hierarchical definition of the auxiliary signals  $\phi_i(t)$ , for  $i = 1, \dots, n$ , in (6.22) and (6.23) can be used along with (6.29)*

and (6.30) to show that

$$e_i(t) = 0 \Rightarrow \sigma_{i+1}(t) = e_{i+1}(t) \quad (6.32)$$

for  $i = 1, \dots, n$ , provided the observer gains  $m_i(\hat{x})$ , for  $i = 1, \dots, n$ , are selected to satisfy the sufficient condition

$$m_i(\hat{x}) > |h_{i+1}(x)|. \quad (6.33)$$

*Proof.* By using (6.30), the following can be obtained immediately:

$$e_i(t) = 0 \Rightarrow \dot{e}_i(t) = 0 \Rightarrow \quad (6.34)$$

$$h_{i+1}(x) = m_i(\hat{x}) \operatorname{sgn}(\sigma_i). \quad (6.35)$$

Based on the recursive definition of  $\phi_i(t)$  in (6.23), it follows from (6.35) that  $\phi_{i+1}(t) = h_{i+1}(x)$ . Thus,  $\sigma_{i+1}(t) = h_{i+1}(x) - h_{i+1}(\hat{x})$  from (6.29). Hence, (6.32) can be obtained from (6.24). This proves Theorem 9.  $\square$

## 6.4 Stability Analysis

**Theorem 10** (Observer Convergence). *For the class of nonlinear systems described by Equations (6.12) and (6.13), the observer described in (6.14), (6.19)-(6.21) ensures that all system states and estimates remain bounded and that finite-time estimation*

of the complete system state  $x(t)$  is achieved in the sense that

$$\|e(t)\| \equiv 0 \quad \text{for} \quad t \geq t_n < \infty \quad (6.36)$$

using only measurements  $y(t)$ , provided the observer gains  $m_i$ , for  $i = 1, \dots, n$ , are selected to satisfy Inequality (6.33), and where  $t_n \in \mathcal{L}_\infty$  are (finite) calculable time instants that are explicitly derived in the appendix.

*Proof.* Let  $V_i : \mathbb{R} \times [0, \infty) \rightarrow \mathbb{R}$ , for  $i = 1, \dots, n$ , be locally Lipschitz, positive definite, Lyapunov candidate functions defined as

$$V_i = \frac{1}{2}e_i^2. \quad (6.37)$$

After taking the time derivative of (6.37),  $\dot{V}_i(e_i) \stackrel{a.e.}{\in} \dot{\check{V}}_i(e_i)$  and

$$\dot{\check{V}}_i(e_i, t) \triangleq \bigcap_{\xi_i \in \partial V_i(e_i, t)} \xi_i^T K \begin{bmatrix} \dot{e}_i \\ 1 \end{bmatrix} (e_i, t). \quad (6.38)$$

Given that the Lyapunov candidate function in (6.37) is continuously differentiable, the generalized gradient reduces to the standard gradient (Fischer et al., 2013), and thus, (6.38) can be expressed as

$$\dot{\check{V}}_i \subset \nabla_i V_i^T K[\dot{e}_i](e_i) \subset e_i^T K[\dot{e}_i] \quad (6.39)$$

where  $\nabla_i \triangleq \partial/\partial e_i$ , for  $i = 1, \dots, n$ . By using (6.30), the equation in (6.39) can be rewritten as

$$\dot{\check{V}}_i \subset e_i^T (h_{i+1}(x) - m_i(\hat{x})K[\text{sgn}(\sigma_i(t))]) \quad (6.40)$$

for  $i = 1, \dots, n$ , where  $K[\text{sgn}(\cdot)] = \text{SGN}(\cdot)$  denotes the set-valued signum function defined in (6.11).

To complete the stability proof, Property 5 and Theorem 9 will be leveraged, and the proof will be carried out sequentially. To this end, consider the case where  $i = 1$ , for which the expression in (6.40) becomes

$$\dot{\tilde{V}}_1 \subset e_1^T (h_2(x) - m_1(\hat{x})\text{SGN}(e_1)) \quad (6.41)$$

where the definition in (6.31) was utilized. The scalar inequality in (6.41) can be reduced and upper bounded as

$$\dot{\tilde{V}}_1 \leq -(m_1(\hat{x}) - |h_2(x)|) |e_1|. \quad (6.42)$$

The reduction of the set in (6.41) to the scalar inequality in (6.42) results from the fact that the set-defined term  $K[\text{sgn}(e_1)]$  is multiplied by  $e_1$ . Thus, when  $e_1 = 0$ , it follows that

$$(0) \text{SGN}(0) = \{0\}. \quad (6.43)$$

By selecting the gain  $m_1(\hat{x})$  according to the sufficient condition in (6.33), the upper bound in (6.42) can be expressed as

$$\dot{\tilde{V}}_1 \leq -\kappa_1 |e_1| \quad (6.44)$$

where  $\kappa_1 \in \mathbb{R}^+$  is a known bounding constant. Inequality (6.44) can now be used

along with (6.37) to prove finite-time convergence of  $e_1(t)$  in the sense that

$$|e_1| \equiv 0, \quad \text{for } t \geq t_1$$

where  $t_1 \in \mathcal{L}_\infty$  can be computed.

Given that  $e_1(t) \equiv 0$  for  $t \geq t_1$ , (6.32) can be used to show that  $\sigma_2(t) = e_2(t)$ , and thus, the set (6.40) for  $i = 2$  can be expressed as

$$\dot{\tilde{V}}_2 \subset e_2^T (h_3(x) - m_2(\hat{x})SGN(e_2)). \quad (6.45)$$

The scalar inequality in (6.45) then reduces to

$$\dot{\tilde{V}}_2 \leq -(m_2(\hat{x}) - |h_3(x)|)|e_2|. \quad (6.46)$$

By again using the sufficient gain condition in (6.33), (6.46) can be expressed as

$$\dot{\tilde{V}}_2 \leq -\kappa_2 |e_2| \quad (6.47)$$

where  $\kappa_2 \in \mathbb{R}^+$  is a known bounding constant. The inequality in (6.47) can be used along with (6.37) (for  $i = 2$ ) to prove that

$$|e_2| \equiv 0, \quad \text{for } t \geq t_2$$

where  $t_2 \in \mathcal{L}_\infty$  is calculable. Continuing in this sequential manner, and leveraging Theorem 9, it follows that

$$|e_i| \equiv 0, \quad \text{for } t \geq t_i$$

for  $i = 3, \dots, n$ , provided the sufficient condition in (6.33) is satisfied. Thus, the objective in (6.36) of Theorem 10 is proved.  $\square$

**Remark 17.** (Implementation of the SMO) *It should be noted that, although the convergence proof of the proposed SMO was provided in a sequential manner, the SMO implementation does not require any special treatment. The sequential analysis used for the proof in this section was provided for clarity of the presentation only. Indeed, the simulation results in the following section were obtained by implementing the estimator with a single fixed set of observer gains  $m_i$ , for  $i = 1, \dots, n$ , which was selected a single time at observer initialization.*

## 6.5 Simulation Study: Flow Field Velocity Estimation

A numerical simulation was created to test the performance of the proposed SMO. The simulation is based on the observer design described in (6.19) - (6.23). The simulation tests the capability of the proposed SMO to estimate the complete state of a fluid flow dynamic system using only sensor measurements of the flow field velocity.

### 6.5.1 Reduced-order Model Derivation

A challenge in designing an observer for such systems is that fluid flow dynamics are governed by complex models such as the Burgers' equations or Navier-Stokes equations, which are partial differential equations (PDEs). In this example, we will

consider the Navier-Stokes equations, which can be expressed as

$$\nabla \cdot v = 0, \quad \frac{\partial v}{\partial t} = -(v \cdot \nabla)v + \frac{1}{Re} \nabla^2(v) - \nabla p, \quad (6.48)$$

where  $v(s, t) : \Omega \times [0, \infty) \in \mathbb{R}^3$  denotes the velocity of the flow field over a spatial domain  $s \in \Omega \subset \mathbb{R}^3$ , where  $\frac{1}{Re}$  is kinematic viscosity.

POD-based model order reduction is utilized to recast the PDE dynamic model into a finite set of ordinary differential equations (ODEs). In the POD modal decomposition technique, the flow field velocity  $v(s, t)$  is expanded as a weighted sum of POD modes defined in the spatial domain  $\Omega$  as

$$v(s, t) = v_0 + \sum_{i=1}^n x_i(t) \psi_i(s). \quad (6.49)$$

In (6.49),  $\psi_i(s) \in \mathbb{R}^3$ , denote the POD modes and  $x_i(t)$ ,  $i = 1, \dots, n$ , denote unknown, time-varying coefficients resulting from the modal decomposition. By substituting the velocity field expansion (6.49) into (6.48), the POD-based reduced-order model of the Navier-Stokes equations is obtained as

$$\dot{x}_k(t) = L_k x(t) + x^T(t) Q_k x(t) + b_k, \quad k = 1, \dots, n \quad (6.50)$$

$L_k(s) \in \mathbb{R}^{1 \times n}$ ,  $Q_k(s) \in \mathbb{R}^{n \times n}$ , and  $b_k \in \mathbb{R}$ , denote constant parameter matrices, which can be explicitly obtained from a given set of experimental or high-fidelity simulation data. The expression in (6.50) represents a system of nonlinear ordinary differential equations resulting from POD-based model order reduction. The system of ODEs in (6.50) can be expressed in the general form given in (6.12). For additional details on

POD-based model order reduction, readers are referred to (Holmes, 2012; Chatterjee, 2000; MacKunis et al., 2011). Further details on the POD-based modal decomposition from (6.48)  $\rightarrow$  (6.50) can be found in (Kidambi et al., 2019; MacKunis et al., 2011). The reduced-order model resulting from POD contains an unmeasurable state vector containing the time-varying coefficients from Galerkin projection.

The flow field observer design presented here is based on the standard assumption that one or more sensor measurements are available. By using the similar POD modal decomposition analysis the output measurement equation can be expressed as (Holmes, 2012; Chatterjee, 2000)

$$y(t) = Cx(t), \tag{6.51}$$

where  $y(t) \in \mathbb{R}$ , and  $C \in \mathbb{R}^{1 \times n}$  is a vector of known constants, and  $x(t) = [x_1(t), x_2(t), \dots, x_n(t)]^T$  is introduced in (6.50). Physically, the expression in (6.51) can be interpreted as the measured velocity at a predefined location as approximated in terms of the POD modes. Specifically, the plant model in (6.50) and the output equation in (6.51) can be expressed in the form given in (6.12) and (6.13).



## 6.5.2 Simulation Results

The flow field dynamic reduced-order model with a measurement (i.e., output) equation in this simulation can be expressed as (S. V. Gordeyev & Thomas, 2013)

$$\begin{aligned}
 \dot{x}_1 &= b_1 + L_{11}x_1 + Q_{141}x_1x_4 + Q_{111}x_1^2 + Q_{121}x_1x_2 + Q_{131}x_1x_3 & (6.52) \\
 \dot{x}_2 &= b_2 + [L_{22} + t_2(x_2^2 + x_3^2)]x_2 + L_{23}x_3 + Q_{121}x_1x_2 \\
 \dot{x}_3 &= b_3 + L_{32}x_2 + [L_{33} + t_3(x_2^2 + x_3^2)]x_3 + Q_{313}x_1x_3 + Q_{314}x_1x_4 \\
 \dot{x}_4 &= b_4 + L_{41}x_1 + L_{44}x_4 + Q_{444}x_4^2 + Q_{414}x_1x_4 + Q_{424}x_2x_4 + Q_{434}x_3x_4 \\
 y &= x_1 + x_2 + x_3 + x_4. & (6.53)
 \end{aligned}$$

Thus, based on (6.52) and (6.53), the simulation plant model is in the form of (6.12) and (6.13), where  $x : [0, \infty) \rightarrow \mathbb{R}^4$  and  $y : \mathbb{R}^4 \rightarrow \mathbb{R}$ . For completeness in defining the simulation plant model, the values of the constant parameters  $b_i$ ,  $L_{ij}$ ,  $Q_{ijk}$  for  $i, j, k = 1, \dots, 4$  are provided in Table I.

The initial values for the states and estimates were selected as

$$\begin{aligned}
 x_1 = 0.01, \quad x_2 = 0.5, \quad x_3 = 0.1, \quad x_4 = 0.1 \\
 \hat{x}_1 = 0, \quad \hat{x}_2 = 0, \quad \hat{x}_3 = 0, \quad \hat{x}_4 = 0
 \end{aligned}$$

Figures 6.5.2 and 6.5.2 show the observer performance for estimator gains selected as (see (6.19) and (6.20))

$$m_1 = 7, \quad m_2 = 7, \quad m_3 = 7, \quad m_4 = 2.$$

Table 6.1: Parameters Used in the Simulation Plant Model

Linear Terms		Quadratic and Cubic Terms	
$b_1 = 557.7$	$L_{11} = -86.1$	$Q_{111} = 1.8$	$Q_{414} = 2.9$
$b_2 = 1016.9$	$L_{22} = -392.4$	$Q_{121} = -2.2$	$Q_{424} = -9.8$
$b_3 = 41.0$	$L_{23} = 263.9$	$Q_{131} = -2.3$	$Q_{434} = 6.3$
$b_4 = -628.9$	$L_{32} = -218.3$	$Q_{141} = -6.8$	$Q_{444} = -7.3$
	$L_{33} = -7.6$	$Q_{212} = 75.0$	
	$L_{41} = 43.4$	$Q_{313} = 5.0$	$t_2 = -2.5$
	$L_{44} = -113.5$	$Q_{314} = 3.9$	$t_3 = -0.2$

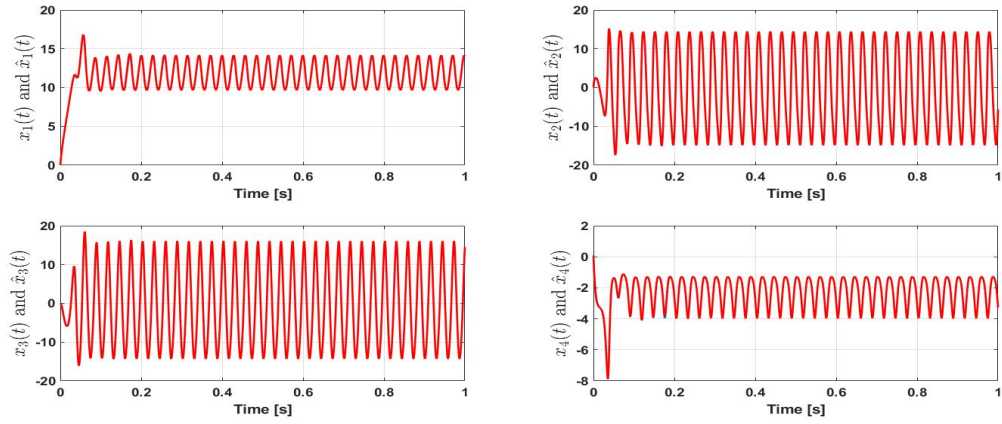


Figure 6.1: Time evolution of the states (blue) and the estimates (red) using the observer in (6.19)

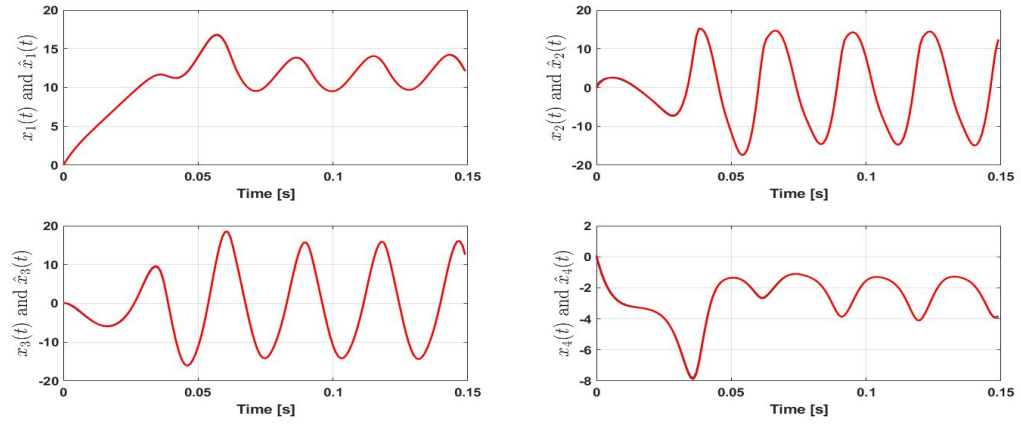


Figure 6.2: Zoomed plots showing the initial convergence phase of the states (blue) and the estimates (red) using the observer in (6.19)

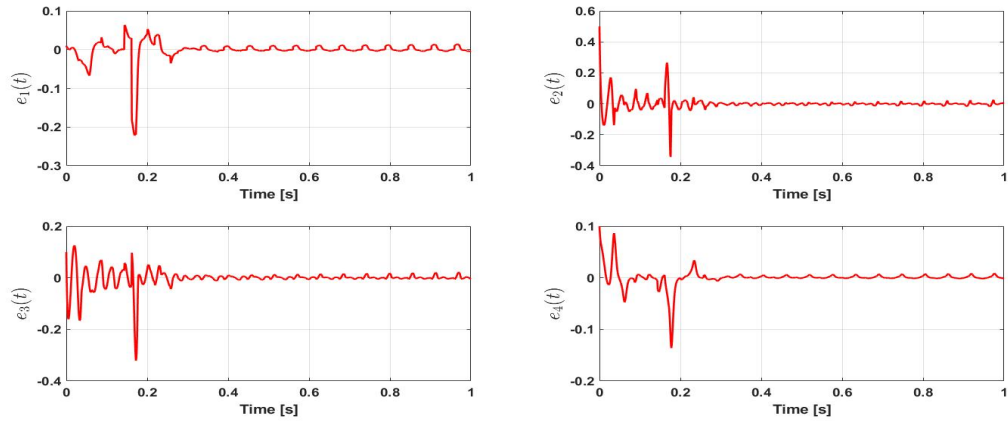


Figure 6.3: Time evolution of the error in each state over the entire simulation time

Figure 6.5.2 shows that the SMO reliably estimates the true states, even under the highly oscillatory state response. To clarify the results, Figure 6.5.2 shows the

initial transient response of SMO system. The results demonstrate the capability of the proposed SMO design to reliably estimate the unmeasurable state of the system.

## 6.6 Conclusion

A rigorous error system development and stability analysis are presented, which are based on a hierarchical SMO strategy containing multiple discontinuities. The hierarchical structure of the SMO is shown to achieve finite-time estimation of the complete state vector using a single scalar measurement, which could be a nonlinear function of the state in general. The challenge involved in analyzing the convergence behavior of the estimation error dynamic equations with discontinuous RHS is addressed through the use of differential inclusions in a Lyapunov-based framework. The result is a Lyapunov-based stability analysis that proves finite-time state estimation, while also incorporating a formal treatment of the multiple discontinuities inherent in the SMO design. Numerical simulation results are provided to demonstrate the capability of the SMO to estimate the full state of a fluid flow dynamic system using only a single available sensor measurement. Future work will address a rigorous analysis of the SMO as part of a closed-loop nonlinear control system under model uncertainty.

# Chapter 7

## Conclusion and Future Work

In this dissertation, a closed-loop active flow control method along with a sliding mode estimator is presented to regulate the fluid flow velocity field. A POD-based model order reduction technique has been applied to reduce the Navier-Stokes PDE to a finite dimensional nonlinear ODE. A rigorous Lyapunov-based stability analysis is used to prove that the closed-loop active flow control system asymptotically tracks a desired flow field velocity profile over a given spatial domain.

This initial result was extended to include actuator dynamics in the flow dynamic model. A POD-based model order reduction is also developed with the effects of actuation embedded in the reduced-order model. SJAs have been used due their advantages, the major challenge in using SJAs in closed-loop control design is the presence of parametric uncertainty inherent in the SJA actuator model. A novel sliding mode estimator and robust control technique is developed, so that the states of the ROM achieve asymptotic regulation and tracking of desired value in presence of parametric uncertainty.

The proposed closed-loop active flow control result is used along with FSI model that results in generating the desired fluid forcing function to suppress LCO in an airfoil. A Lyapunov-based stability analysis is utilized to prove asymptotic regulation of the fluid forcing function that drives LCO suppression.

Finally, the challenge involved in analyzing the convergence behavior of the estimation error dynamic equations with discontinuous RHS is addressed through the use of differential inclusions in a Lyapunov-based framework. The result is a Lyapunov-based stability analysis that proves finite-time state estimation, while also incorporating a formal treatment of the multiple discontinuities inherent in the SMO design.

## 7.1 Future Work

Future work relating to this research could include

1. Looking at the effects on the closed-loop response using other model order reduction techniques such as balanced POD (or) dynamic mode decomposition (DMD).
2. Examining the performance of the sliding mode estimation and control algorithm in the presence of disturbances.
3. Analyzing the effect of closed-loop control on the development of sliding mode estimation using differential inclusions-based analysis.

# Appendix A

## Proof of Lemma 1

This appendix provides a detailed derivation of Lemma 1 in Section 3.4. By integrating (3.32) on both sides,

$$\int_0^t L(\tau) d\tau = \int_0^t r^T(\tau)(N_d(\tau) - \beta \text{sgn}(e(\tau)))d\tau \quad (\text{A.1})$$

By substituting the value of  $r(t)$  from (3.19) into (A.1), it can be written as:

$$\int_0^t L(\tau) d\tau = \int_0^t (\dot{e} + \alpha e)(N_d(\tau) - \beta \text{sgn}(e(\tau)))d\tau \quad (\text{A.2})$$

$$\begin{aligned} &= \int_0^t \frac{\partial e^T(\tau)}{\partial \tau}(N_d(\tau) - \beta \text{sgn}(e(\tau)))d\tau \\ &\quad + \int_0^t \alpha e^T(\tau)(N_d(\tau) - \beta \text{sgn}(e(\tau)))d\tau \end{aligned} \quad (\text{A.3})$$

$$\begin{aligned} &= \int_0^t \frac{\partial e^T(\tau)}{\partial \tau}(N_d(\tau))d\tau - \int_0^t \frac{\partial e^T(\tau)}{\partial \tau}(\beta \text{sgn}(e(\tau)))d\tau \\ &\quad + \int_0^t \alpha e^T(\tau)(N_d(\tau) - \beta \text{sgn}(e(\tau)))d\tau \end{aligned} \quad (\text{A.4})$$

---


$$\begin{aligned}
&= N_d(t)e^T(t) - N_d(0)e^T(0) - \beta |e(t)| + \beta |e(0)| \\
&\quad + \int_0^t \alpha e^T(\tau) \left( N_d(\tau) + \frac{N_d(\tau)}{\alpha} - \beta \operatorname{sgn}(e(\tau)) \right) d\tau
\end{aligned} \tag{A.5}$$

Selecting  $\beta$  sufficiently large based on the condition given in (3.29) the sufficient condition in (3.33) is satisfied.



# Appendix B

## Proof of Theorem 10

This appendix provides a detailed derivation of the time instants  $t_n$  for  $i = 1, \dots, n$ , which are introduced in (6.36) of Theorem 10.

The Lyapunov candidate function defined in (6.37) is given as

$$V_i = \frac{1}{2}e_i^2 \Rightarrow |e_i| = \sqrt{2V_i} \quad (\text{B.1})$$

By generalizing the expression in (6.44),  $\forall i = 1, 2, \dots, n$ , which is given as

$$\dot{V}_i \leq -\kappa_i |e_i| \quad (\text{B.2})$$

$$dV_i \leq \kappa_i |e_i| dt, \quad (\text{B.3})$$

---

integrating on both sides, by using (B.1 )

$$\int_{V_i(0)}^{V_i(t)} \frac{1}{\sqrt{2V_i}} dV_i \leq \int_0^{t_i} \kappa_i dt \quad (\text{B.4})$$

$$\frac{1}{\sqrt{2}} \left[ 2\sqrt{V_i(t)} - 2\sqrt{V_i(0)} \right] \leq -\kappa_i [t_i - 0] \quad (\text{B.5})$$

$$\sqrt{2V_i(t)} \leq \kappa_i t_i + \sqrt{2V_i(0)} \quad (\text{B.6})$$

$$|e_i(t)| \leq |e_i(0)| - \kappa_i t_i \quad (\text{B.7})$$

$$t_i = \frac{|e_i(0)|}{\kappa_i}, \text{ for } i = 1, \dots, n. \quad (\text{B.8})$$

# References

- Ahuja, S., & Rowley, C. W. (2010). Feedback control of unstable steady states of flow past a flat plate using reduced-order estimators. *Journal of fluid mechanics*, *645*, 447–478.
- Akhtar, I., Nayfeh, A. H., & Ribbens, C. J. (2009). On the stability and extension of reduced-order galerkin models in incompressible flows. *Theoretical and Computational Fluid Dynamics*, *23*(3), 213–237.
- Amitay, M., Smith, D. R., Kibens, V., Parekh, D. E., & Glezer, A. (2001). Aerodynamic flow control over an unconventional airfoil using synthetic jet actuators. *AIAA journal*, *39*(3), 361–370.
- Andino, M. Y., Wallace, R. D., Glauser, M. N., Camphouse, R. C., Schmit, R. F., & Myatt, J. H. (2011). Boundary feedback flow control: proportional control with potential application to aero-optics. *AIAA journal*, *49*(1), 32.
- Annoni, J., & Seiler, P. (2017). A method to construct reduced-order parameter-varying models. *International Journal of Robust and Nonlinear Control*, *27*(4), 582–597.
- Bakewell Jr, H. P., & Lumley, J. L. (1967). Viscous sublayer and adjacent wall region in turbulent pipe flow. *The Physics of Fluids*, *10*(9), 1880–1889.

- Balajewicz, M., & Dowell, E. (2012). Reduced-order modeling of flutter and limit-cycle oscillations using the sparse volterra series. *Journal of Aircraft*, *49*(6), 1803–1812.
- Balajewicz, M. J., Dowell, E. H., & Noack, B. R. (2013). Low-dimensional modelling of high-reynolds-number shear flows incorporating constraints from the navier-stokes equation. *Journal of Fluid Mechanics*, *729*, 285–308.
- Batchelor, G. K. (2000). *Turbulence, coherent structures, dynamical system, and symmetry*. Cambridge, United Kingdom: Cambridge University Press.
- Brogia, R., Choi, K.-S., Houston, P., Pasquale, L., & Zanchetta, P. (2018). Output feedback control of flow separation over an aerofoil using plasma actuators. *International Journal of Numerical Analysis and Modeling*.
- Cadirci, S., Gunes, H., & Rist, U. (2013). Active flow control applications with a jet and vortex actuator in a laminar cross flow. *International Journal of Heat and Fluid Flow*, *39*, 146–159.
- Cai, Z., de Queiroz, M. S., & Dawson, D. M. (2006). Robust adaptive asymptotic tracking of nonlinear systems with additive disturbance. *IEEE Transactions on Automatic Control*, *51*(3), 524–529.
- Caraballo, E., Little, J., Debiasi, M., & Samimy, M. (2007). Development and implementation of an experimental-based reduced-order model for feedback control of subsonic cavity flows. *Journal of Fluids Engineering*, *129*(7), 813–824.
- Cattafesta III, L. N., & Sheplak, M. (2011). Actuators for active flow control. *Annual Review of Fluid Mechanics*, *43*, 247–272.
- Chatterjee, A. (2000, April). An introduction to the proper orthogonal decomposition. *Current Science*, *78*(7), 808–817.

- Chaturantabut, S. (Sep., 2017). Temporal localized nonlinear model reduction with a priori error estimate. *Applied Numerical Mathematics*, 119, 225-238.
- Clarke, F. (1983). *Optimization and nonsmooth analysis*. Reading, MA: Addison-Wesley.
- Couchot, J.-F., Deschinkel, K., & Salomon, M. (2013). Active mems-based flow control using artificial neural network. *Mechatronics*, 23(7), 898-905.
- Deb, D., Tao, G., Burkholder, J. O., & Smith, D. R. (2007). Adaptive compensation control of synthetic jet actuator arrays for airfoil virtual shaping. *Journal of Aircraft*, 44(2), 616-626.
- Deb, D., Tao, G., Burkholder, J. O., & Smith, D. R. (2008). Adaptive synthetic jet actuator compensation for a nonlinear aircraft model at low angles of attack. *IEEE Transactions on Control Systems Technology*, 16(5), 983-995.
- Debiasi, M., & Samimy, M. (2004). Logic-based active control of subsonic cavity flow resonance. *AIAA journal*, 42(9), 1901-1909.
- De Giorgi, M., De Luca, C., Ficarella, A., & Marra, F. (2015). Comparison between synthetic jets and continuous jets for active flow control: application on a naca 0015 and a compressor stator cascade. *Aerospace Science and Technology*, 43, 256-280.
- Dinh, H. T., Kamalapurkar, R., Bhasin, S., & Dixon, W. E. (2014). Dynamic neural network-based robust observers for uncertain nonlinear systems. *Neural Networks*, 60, 44-52.
- Drakunov, S., & Utkin, V. (1992). Sliding mode control in dynamic systems. *International Journal of Control*, 55(4), 1029-1037.
- Drakunov, S. V. (1992). Sliding-mode observers based on equivalent control method.

- In [1992] *proceedings of the 31st ieee conference on decision and control* (pp. 2368–2369).
- Drakunov, S. V., & Reyhanoglu, M. (2011). Hierarchical sliding mode observers for distributed parameter systems. *Journal of Vibration and Control*, 17(10), 1441–1453.
- Filippov, A. F. (1988). *Differential equations with discontinuous right-hand sides*. Norwell, MA: Kluwer.
- Fischer, N., Kamalapurkar, R., & Dixon, W. E. (2013). Lasalle-yoshizawa corollaries for nonsmooth systems. *IEEE Transactions on Automatic Control*, 58(9), 2333–2338.
- Fisher, R., Nishino, T., & Savill, M. (2017). Numerical analysis of a bidirectional synthetic jet for active flow control. *AIAA Journal*, 55(3), 1064–1069.
- Gad-el Hak, M. (2006). *flow control: passive, active, and reactive flow management*. Cambridge university press.
- Gantmakher, F. R. (2000). *The theory of matrices* (Vol. 131). American Mathematical Soc.
- Gordeyev, S., & Thomas, F. O. (2013). A temporal proper orthogonal decomposition (tpod) method for closed-loop flow control. *Experiments in Fluids*, 54, p.1477.
- Gordeyev, S. V., & Thomas, F. O. (2013). A temporal proper decomposition (tpod) for closed-loop flow control. *Experiments in fluids*, 54(3), 1477.
- Guay, M., & Hariharan, N. (June 11-13, 2008). Airflow velocity estimation in building systems. Seattle, WA, USA.
- Guo, Z., & Huang, L. (2009). Generalized lyapunov method for discontinuous systems. *Nonlinear Analysis: Theory, Methods & Applications*, 71(7-8), 3083–3092.

- Heller, H. H., & Bliss, D. B. (1976). Flow-induced pressure fluctuations in cavities and concepts for their suppression. *Aeroacoustics: STOL Noise; Airframe and Airfoil Noise*, 45, 281–296.
- Holmes, P. (2012). *Turbulence, coherent structures, dynamical systems and symmetry*. Cambridge university press.
- Isidori, A. (2013). *Nonlinear control systems*. Springer Science & Business Media.
- Ito, K., & Ravindran, S. (1998). A reduced-order method for simulation and control of fluid flows. *Journal of computational physics*, 143(2), 403–425.
- Jiang, T., Huang, C., & Guo, L. (2015). Control of uncertain nonlinear systems based on observers and estimators. *Automatica*, 59, 35–47.
- John, T., Guay, M., & Hariharan, N. (June 10-12, 2009). Pod based observer for contaminant flow estimation in building systems. St. Louis, MO, USA.
- Kalashnikova, I., & Barone, M. (2012). Efficient non-linear proper orthogonal decomposition/galerkin reduced order models with stable penalty enforcement of boundary conditions. *International Journal for Numerical Methods in Engineering*, 90(11), 1337–1362.
- Kaplan, W. (1991). *Advanced calculus*. Reading, MA: Addison-Wesley.
- Kasnakoğlu, C., Camphouse, R. C., & Serrani, A. (2009). Reduced-order model-based feedback control of flow over an obstacle using center manifold methods. *Journal of Dynamic Systems, Measurement, and Control*, 131(1), 011011.
- Kasnakoğlu, C., Serrani, A., & Efe, M. Ö. (2008). Control input separation by actuation mode expansion for flow control problems. *International Journal of Control*, 81(9), 1475–1492.
- Khalil, H. K. (1996). Nonlinear systems. *Prentice-Hall, New Jersey*, 2(5), 5–1.

- 
- Kidambi, K. B., MacKunis, W., Ramos-Pedroza, N., & Drakunov, S. V. (2017). Active flow control under actuator uncertainty using a sliding mode estimation strategy. In *2017 IEEE Conference on Control Technology and Applications (CCTA)* (pp. 7–12).
- Kidambi, K. B., Ramos-Pedroza, N., MacKunis, W., & Drakunov, S. V. (2016). Robust nonlinear estimation and control of fluid flow velocity fields. In *Decision and Control (CDC), 2016 IEEE 55th Conference on* (pp. 6727–6732).
- Kidambi, K. B., Ramos-Pedroza, N., MacKunis, W., & Drakunov, S. V. (2019). A closed-loop nonlinear control and sliding mode estimation strategy for fluid flow regulation. *International Journal of Robust and Nonlinear Control*, *29*(3), 779–792.
- Krasovskii, N. N. (1963). *Stability of motion*. Stanford, CA: Stanford University Press.
- Krishnappa, S. (2016). *An experimental study of synthetic jet actuators with applications in airfoil lco control* (Unpublished master’s thesis). Embry-Riddle Aeronautical University, FL, USA.
- Kurowski, M. (2017). Numerical simulation of a synthetic jet actuator for active flow control. In *Recent progress in flow control for practical flows* (pp. 203–221). Springer.
- Lall, S., Marsden, J. E., & Glavaški, S. (2002). A subspace approach to balanced truncation for model reduction of nonlinear control systems. *International journal of robust and nonlinear control*, *12*(6), 519–535.
- Lewin, G., & Haj-Hariri, H. (2005). Reduced-order modeling of a heaving airfoil. *AIAA journal*, *43*(2), 270–283.



- Lin, J., Howard, F., & Selby, G. (1989). Turbulent flow separation control through passive techniques. In *2nd shear flow conference* (p. 976).
- Lyapunov, A. M. (1992). The general problem of the stability of motion. *International journal of control*, *55*(3), 531–534.
- MacKunis, W., Drakunov, S. V., Reyhanoglu, M., & Ukeiley, L. (2011). Nonlinear estimation of fluid flow velocity fields. In *2011 50th ieee conference on decision and control and european control conference* (pp. 6931–6935).
- MacKunis, W., Subramanian, S., Mehta, S., Ton, C., Curtis, J. W., & Reyhanoglu, M. (10-13 Dec., 2013). Robust nonlinear aircraft tracking control using synthetic jet actuators. Florence, Italy.
- Mohseni, K., & Mittal, R. (2014). *Synthetic jets: fundamentals and applications*. CRC Press.
- Mondschein, S. T., Tao, G., & Burkholder, J. O. (2011). Adaptive actuator nonlinearity compensation and disturbance rejection with an aircraft application. In *American control conference (acc), 2011* (pp. 2951–2956).
- Nagarajan, K. K., Cordier, L., & Airiau, C. (2013). Development and application of a reduced order model for the control of self-sustained instabilities in cavity flows. *Communications in Computational Physics*, *14*(1), 186–218.
- Nguyen, L. D., Golubev, V. V., Mackunis, W., Ramos, N., & Pasiliao, C. L. (2015). High-accuracy simulations of robust lco control using synthetic jet actuators. In (p. pp.01-03). Kissimmee, FL, USA.
- Paden, B., & Sastry, S. (1987). A calculus for computing flippov’s differential inclusion with application to the variable structure control of robot manipulators. *IEEE transactions on circuits and systems*, *34*(1), 73–82.

- Park, D., & Guay, M. (2015). Distributed estimation for a class of nonlinear systems with application to navier-stokes flow estimation. *The Canadian Journal of Chemical Engineering*, *93*(4), 678–688.
- Park, H., & Lee, M. (1998). An efficient method of solving the navier–stokes equations for flow control. *International Journal for Numerical Methods in Engineering*, *41*(6), 1133–1151.
- Patre, P. M., MacKunis, W., Kaiser, K., & Dixon, W. E. (2008). Asymptotic tracking for uncertain dynamic systems via a multilayer neural network feedforward and rise feedback control structure. *IEEE Transactions on Automatic Control*, *53*(9), 2180–2185.
- Pedroza, N. R. (2018). Robust nonlinear estimation and control applications using synthetic jet actuators.
- Pinier, J. T., Ausseur, J. M., Glauser, M. N., & Higuchi, H. (2007). Proportional closed-loop feedback control of flow separation. *AIAA journal*, *45*(1), 181–190.
- Ramos-Pedroza, N., MacKunis, W., & Golubev, V. (2017). A robust nonlinear output feedback control method for limit cycle oscillation suppression using synthetic jet actuators. *Aerospace Science and Technology*, *64*, 16–23.
- Richards John, A., & Xiuping, J. (1999). *Remote sensing digital image analysis: an introduction*. Springer-Verlag, Berlin.
- Rowley, C. W. (2005). Model reduction for fluids, using balanced proper orthogonal decomposition. *International Journal of Bifurcation and Chaos*, *15*(03), 997–1013.
- Rowley, C. W., Colonius, T., & Murray, R. M. (2004). Model reduction for compressible flows using pod and galerkin projection. *Physica D: Nonlinear Phenomena*,

- 189(1), 115–129.
- Rowley, C. W., & Juttijudata, V. (2005). Model-based control and estimation of cavity flow oscillations. In *Proceedings of the 44th IEEE conference on decision and control* (pp. 512–517).
- Rowley, C. W., & Williams, D. R. (2006). Dynamics and control of high-reynolds-number flow over open cavities. *Annu. Rev. Fluid Mech.*, 38, 251–276.
- Saha, P., Biswas, G., Mandal, A., & Sarkar, S. (2017). Investigation of coherent structures in a turbulent channel with built-in longitudinal vortex generators. *International Journal of Heat and Mass Transfer*, 104, 178–198.
- Sánchez-Torres, J. D., Loukianov, A. G., Moreno, J. A., & Drakunov, S. V. (27-29 June, 2012). An equivalent control based sliding mode observer using high order uniform robust sliding operators. Montreal, QC, Canada.
- Shaw, L. L. (1979). Suppression of aerodynamically induced cavity pressure oscillations. *The Journal of the Acoustical Society of America*, 66(3), 880–884.
- Shevitz, D., & Paden, B. (1994, Sep). Lyapunov stability theory of nonsmooth systems. *IEEE Transactions on Automatic Control*, 39(9), 1910–1914.
- Siegel, S., Cohen, K., & McLaughlin, T. (2006). Numerical simulations of a feedback-controlled circular cylinder wake. *AIAA journal*, 44(6), 1266.
- Singh, S. N., Myatt, J. H., Addington, G. A., Banda, S., & Hall, J. K. (2001). Optimal feedback control of vortex shedding using proper orthogonal decomposition models. *Journal of fluids engineering*, 123(3), 612–618.
- Slotine, J. J. E., & Li, W. (1991). *Applied nonlinear control*. Prentice Hall, Inc, Englewood Cliff, NJ.
- Sohankar, A., Khodadadi, M., & Rangraz, E. (2015). Control of fluid flow and

- heat transfer around a square cylinder by uniform suction and blowing at low reynolds numbers. *Computers & Fluids*, 109, 155–167.
- Tang, H., Salunkhe, P., Zheng, Y., Du, J., & Wu, Y. (2014). On the use of synthetic jet actuator arrays for active flow separation control. *Experimental Thermal and Fluid Science*, 57, 1–10.
- Tantaroudas, N. D., & Da Ronch, A. (2017). Nonlinear reduced-order aeroservoelastic analysis of very flexible aircraft. *Advanced UAV Aerodynamics, Flight Stability and Control: Novel Concepts, Theory and Applications*, 143.
- Torrielli, A., Tubino, F., & Solari, G. (2010). Effective wind actions on ideal and real structures. *Journal of Wind Engineering and Industrial Aerodynamics*, 98(8-9), 417–428.
- Utkin, V. I. (2013). *Sliding modes in control and optimization*. Springer Science & Business Media.
- Wallace, R., Shea, P., Glauser, M., Thirunavukkarasu, V., & Carlson, H. (2012). Simulation-guided, model-based feedback flow control for a pitching turret. *AIAA journal*, 50(8), 1685–1696.
- Wang, L., Luo, Z., Xia, Z., Liu, B., & Deng, X. (2012). Review of actuators for high speed active flow control. *Science China Technological Sciences*, 55(8), 2225–2240.
- Wilcox, Z., MacKunis, W., Bhat, S., Lind, R., & Dixon, W. (2010). Lyapunov-based exponential tracking control of a hypersonic aircraft with aerothermoelastic effects. *Journal of guidance, control, and dynamics*, 33(4), 1213.
- Xian, B., Dawson, D. M., de Queiroz, M. S., Chen, J., et al. (2004). A continuous asymptotic tracking control strategy for uncertain nonlinear systems. *IEEE*

*Transactions on Automatic Control*, 49(7), 1206–1211.

Zhang, Z., & Xu, S. (2015). Observer design for uncertain nonlinear systems with unmodeled dynamics. *Automatica*, 51, 80–84.

Zhao, G., Zhao, Q., Gu, Y., & Chen, X. (2016a). Experimental investigations for parametric effects of dual synthetic jets on delaying stall of a thick airfoil. *Chinese Journal of Aeronautics*, 29(2), 346–357.

Zhao, G., Zhao, Q., Gu, Y., & Chen, X. (2016b). Experimental investigations for parametric effects of dual synthetic jets on delaying stall of a thick airfoil. *Chinese Journal of Aeronautics*, 29(2), 346–357.